TET2 repression by androgen hormone regulates global hydroxymethylation status and prostate cancer progression

Ken-ichi Takayama[*1, 2], Aya Misawa[*1], Takashi Suzuki[3], Kiyoshi Takagi[3], Yoshihide Hayashizaki[4, 5], Tetsuya Fujimura[6], Yukio Homma[6], Satoru Takahashi[7], Tomohiko Urano[1, 2], Satoshi Inoue[1, 2, 8]

[1]Department of Anti-Aging Medicine, [2]Department of Geriatric Medicine, Graduate School of Medicine, The University of Tokyo, Bunkyo-ku, Tokyo 113-8655, Japan

[3]Department of Pathology, Tohoku University Graduate School of Medicine, Sendai, Miyagi, 980-8575, Japan

[4]RIKEN Omics Science Center (OSC), RIKEN Yokohama Institute, Yokohama, Kanagawa, 230-0045, Japan

[5]RIKEN Preventive Medicine & Diagnosis Innovation Program, Wako, Saitama, 351-0198, Japan

[6]Department of Urology, Graduate School of Medicine, The University of Tokyo, Japan

[7]Department of Urology, Nihon University School of Medicine, Itabashi-ku, Tokyo, 173-0032, Japan

[8] Division of Gene Regulation and Signal Transduction, Research Center for Genomic Medicine, Saitama Medical University, Hidaka, Saitama, 350-1241, Japan

* : These authors contributed equally to this work.

Corresponding Author: Satoshi Inoue, Department of Anti-Aging Medicine, Graduate School of Medicine, The University of Tokyo, Bunkyo-ku, Tokyo 113-8655, Japan. Phone: 81-3-5800-8834; Fax: 81-3-5800-9126; E-mail: INOUE-GER@h.u-tokyo.ac.jp.

Abstract

Modulation of epigenetic patterns has promising efficacy for treating cancer. 5-Hydroxymethylated cytosine (5-hmC) is an epigenetic mark potentially important in cancer. Here we report that 5-hmC is an epigenetic hallmark of prostate cancer (PCa) progression. A member of the ten-eleven translocation (TET) proteins, which catalyze the oxidation of methylated cytosine (5-mC) to 5-hmC, TET2, is repressed by androgens in PCa. Androgen receptor (AR)-mediated induction of the miR-29 family, which targets TET2, are markedly enhanced in hormone-refractory PCa (HRPC) and its high expression predicts poor outcome of PCa patients. Furthermore, decreased expression of miR-29b results in reduced tumor growth and increased TET2 expression in an animal model of HRPC. Interestingly, global 5-hmC modification regulated by miR-29b represses FOXA1 activity. A reduction in 5-hmC activates PCa-related key pathways such as *mTOR* and *AR*. Thus, DNA modification directly links the TET2-dependent epigenetic pathway regulated by AR to 5-hmC-mediated tumor progression.

Introduction

Epigenetic processes regulate gene expression by altering the binding of transcription factors[1]. The DNA methylation pattern is an epigenetic code that defines the global gene regulatory state[2]. The resultant regulation of gene expression is thought to govern various biological phenomena, including cancer progression. 5-Hydroxymethylation of cytosine bases (5-hmC) is a newly identified epigenetic marker; this nontraditional DNA modification involves methylation of cytosine bases (5-mC) in CpG dinucleotide sequences[2–3] and their oxidation by the ten-eleven translocation (TET) family of proteins. While 5-hmC is a potentially useful indicator of disease states such as cancer[4–8], the mechanisms controlling its abundance in tumors and its impact on gene expression and cancer cell fate are unclear.

Androgen receptor (AR) signaling is crucial for prostate tumor growth[9–13]. When bound to androgens, ARs translocate to the nucleus and transactivate target genes by interacting with other transcription factors such as forkhead-box A1 (FOXA1) [10]. Although the molecular mechanisms underlying prostate cancer progression to lethal hormone-refractory prostate cancer (HRPC) [9–13] are incompletely understood, activation of downstream signals by hypersensitive or overexpressed ARs is considered to be important. The epigenetic status of prostate cancer cells is modulated by AR binding and the subsequent recruitment

of coactivators or co-repressors[14–18]. Acetylation, methylation, phosphorylation, ubiquitylation, and ADP ribosylation of histones critically affect transcriptional regulation by ARs[19–21]. The main epigenetic mechanism that controls AR binding to DNA in prostate cancer is histone modification by histone acetyltransferases (HATs), histone methyltransferases (HMTs), and protein kinases at AR binding sites (ARBSs) [20, 21]. Specific epigenetic codes modulate opening of chromatin to induce or repress the expression of protein-encoding genes and non-coding RNAs[11]. The relationship between AR activity and DNA modifications, particularly 5-mC hydroxylation, has not been described previously, and the role of androgen-targeted non-coding RNAs such as micro RNAs (miRNAs) in global epigenetic control is largely unknown.

Here we report that 5-hmC is an epigenetic hallmark of prostate cancer inversely associated with disease progression. We show that AR-induced miRNA represses the expression of a member of the TET family, TET2, and that low expression levels of TET2 are correlated with low 5-hmC levels in advanced clinical tumors. Global mapping indicated that hydroxylation of 5-mC suppressed FOXA1 enhancer activity and impacted on prostate cancer-related pathways such as the *AR* pathway. Our findings suggest that AR-modulated TET2 pathways form the basis of a new treatment strategy for advanced, HRPCs.

Results

TET2 is repressed by androgens in prostate cancer cells

We established bicalutamide (AR antagonist)-resistant prostate cancer (BicR) cells derived from an AR-positive, bicalutamide-sensitive LNCaP prostate cancer cell line (Supplementary Fig. 1a). We first examined the androgen-regulated signals in both BicR and LNCaP cells, and the differences between them using AR ChIP-sequence (ChIP-seq) and Cap analysis of gene expression (CAGE) [22, 23], a powerful tool for analyzing global transcriptome. Interestingly, AR binding sites (ARBSs) obtained by bicalutamide treatment in BicR cells overlap with those by AR agonist, dihydrotestosterone (DHT), treatment, suggesting that bicalutamide mediates AR recruitment to the genomic regions (Supplementary Fig. 1b). In addition, we also explored androgen-induced miRNAs by sequence analysis of comprehensive short RNA profiles (Supplementary Table 1, Supplementary Fig. 2a) to analyze the role of miRNA in prostate cancer progression. In LNCaP cells, a total of 44 miRNAs were significantly induced by DHT (>1.2-fold), including representative AR-regulated miRNAs such as miR-125b[24], miR-21[25], and miR-148a[26], while 30 miRNAs were induced by DHT (>1.2-fold) in BicR cells. The members of the miR-29 family and miR-22 were the most responsive to androgen treatment in BicR cells compared with parental LNCaP cells. Our *in silico* analysis of their

direct target raised the possibility that both miRNAs target *TET2*, one of the key epigenetic regulatory factors (Supplementary Fig. 2b).

Next, our investigation of R1881 (AR agonist)-regulated genes in LNCaP cells (Fig. 1a) using CAGE showed that *TET2* was repressed by androgen treatment (Fig. 1b). To further investigate the androgen signaling during prostate cancer progression, we also performed CAGE in both LNCaP and BicR cells treated with vehicle, DHT or bicalutamide. We identified 243 and 256 promoters that were upregulated by more than 2-fold by DHT in LNCaP and BicR cells, respectively. Among these promoters, 66 were commonly regulated in both cell lines, while the others were cell-type specific (Supplementary Fig. 1c). LNCaP-specific promoters were upregulated without DHT treatment in BicR cells, indicating androgen hypersensitivity in these cells (Supplementary Fig. 1d). In BicR-specific promoters, androgen-dependent activation is more evident in BicR cells than in LNCaP cells (Supplementary Fig. 1e). We then found that negative regulation of *TET2* by DHT and bicalutamide was more evident in BicR cells than in LNCaP cells (Fig. 1c). TET2 was upregulated by bicalutamide treatment and downregulated by DHT treatment in LNCaP cells, while it was downregulated by both DHT and bicalutamide in BicR cells (Figs. 1d, e and Supplementary Fig. 3a).

TET2 is a key target gene of androgen-regulated miRNAs

To examine the roles of the androgen-regulated miRNAs in TET2 regulation, we transfected the cells with miRNA mimics and a luciferase vector containing the 3′-untranslated region (UTR) sequence of *TET2*. Consequently, miR-125b, miR-22, miR-30a, miR-200a, and miR-29a/b were found to repress the luciferase activity, suggesting the possibility of TET2 repression by androgen-regulated miRNAs (Fig. 2a). Notably, among all androgen-regulated miRNAs tested, miR-29a/b repressed the luciferase activity most strikingly. As suggested by the sequence analysis, miR-29a/b was markedly overexpressed and highly responsive to androgen in BicR cells compared with LNCaP cells (Fig. 2b). We observed that *primary miR-29a/b1* transcript was induced by DHT, although *pri-miR-29b2* was not (Supplementary Fig. 3b). Then ARBSs were found around the *miR-29a/b1* locus by AR ChIP-seq analysis in LNCaP and BicR cells (Fig. 2c and Supplementary Fig. 3c). Using bioinformatics, we identified the enrichment of four potential miR-29 family binding sites in the 3′-UTR sequence of TET2 (Fig. 2a). We also demonstrated that the repression of TET2 by miR-29a/b is dependent on these sites (Fig. 2d and Supplementary Fig. 3d) while the downregulation of miR-29a/b enhances the expression level of the TET2 protein (Fig. 2e, Supplementary Figs. 3e and f). Conversely, the overexpression of miR-29a/b was found to repress TET2 expression (Fig. 2f). In

addition, the gain and loss of miR-29a/b expression are associated with the level of 5-hmC, but not 5-mC, in prostate cancer cells (Supplementary Figs. 3g and 4a). Although most AR-positive castration-resistant prostate cancer (CRPC) cell lines such as long term androgen deprivation (LTAD) cells exhibit low levels of TET2 expression, the inhibition of miR-29a/b by anti-miR-29a/b transfection increased the TET2 expression and reversed DHT-mediated TET2 repression (Supplementary Figs. 4b-d).

AR directly represses TET2 enhancer activity in HRPC

To elucidate the mechanism of TET2 repression by bicalutamide in BicR cells, we examined the possibility that TET2 is directly regulated by AR. Using ChIP-seq analysis, we found that AR was recruited to the distal enhancer region of *TET2* by DHT treatment in both cell lines. Interestingly, after bicalutamide treatment, AR binding could be detected in the enhancer region only in BicR cells (Fig. 2g and Supplementary Fig. 4e). Unlike typical ARBSs, this locus does not mediate positive transcriptional activity in response to DHT treatment. Moreover, the bicalutamide-mediated repression of the enhancer activity in BicR cells is dependent on androgen-response elements (AREs) in the middle of the ARBS (Figs. 2h and 2i). ChIP analysis indicated that this enhancer is directly repressed by repressive histone modification (increased levels of histone H3K9 methylation) in the

antagonist-bound condition (Fig. 2j and Supplementary Fig. 4f). In addition, chromatin conformational capture (3C) assay was performed to show the physical interaction of promoter/enhancer in the *TET2* locus (Supplementary Fig. 5). We found that the long range interaction was significantly enhanced in BicR cells compared with LNCaP cells. In addition, 3C-ChIP products were immunoprecipitated by AR antibody, showing that the chromatin conformation at the *TET2* locus was changed by the complex, including AR. This result is compatible with our other analyses suggesting the direct regulation of TET2 by AR in BicR. Thus, in bicalutamide-treated HRPC cells, both indirect miR-dependent regulation and direct AR-mediated repression are important in TET2 repression.

Clinical significance of TET2 repression in prostate cancer

To investigate the role of TET2 and its associated epigenetic marker, 5-hmC, in prostate cancer progression, we evaluated the levels of TET2 and 5-hmC in clinical tumor samples by immunohistochemistry (Fig. 3a). Strong nuclear 5-hmC staining was observed in benign prostate tissues surrounding the tumors, whereas partial or complete reduction of 5-hmC staining was observed in a subset of tumor samples. Interestingly, decreased expression of TET2 and 5-hmC could be a prognostic factor predicting the survival of patients after surgery (Figs. 3b and 3c). Low expression level of TET2 is not associated

with Gleason scores, but with metastasis or advanced stages of cancer (Supplementary Table 2). Importantly, we found that TET2 repression is an independent prognostic factor by multivariate analysis (Supplementary Table 3). Using publicly available microarray datasets (GSE3325, GSE6919, GSE35988) of prostate cancer clinical samples, we confirmed that TET2 expression is significantly repressed in metastatic prostate cancer compared with localized tumors (Supplementary Fig. 7a). Thus, these results indicate that *TET2* repression is associated with disease progression, in particular, metastasis. In contrast, strong 5-mC staining is present in both the cancerous and normal prostate tissues (Supplementary Fig. 6a). We also confirmed the positive correlation of TET2 expression with 5-hmC but not 5-mC (Figs 3d and 3e). These findings suggest that deceased expression of both 5-hmC and TET2 represent a new epigenetic marker associated with survival rate and tumor progression of prostate cancer patients.

Using *in situ* hybridization (ISH), we demonstrated that miR-29a/b expression in clinical prostate cancer tissues (Fig. 3f and Supplementary Fig. 6b) is associated with poor prognosis (Fig. 3g and Supplementary Fig. 6c). We also observed that the expression of the miR-29 family is negatively correlated with that of TET2 and 5-hmC (Fig. 3h). Furthermore, qRT-PCR analysis of miR-29b and TET2 expression in clinical samples of prostate cancer obtained by laser capture microdisection (LCM) is in line with ISH results

(Supplementary Figs. 6d and 6e). Furthermore, in a public microarray dataset (GSE21036, GSE21034), we found that upregulation of miR-29a/b and repression of *TET2* in advanced prostate cancer samples (Supplementary Fig. 7b-d). In other cohorts (GSE45604, GSE23022, GSE46738), we also observed that high miR-29a/b expressions are associated with high Gleason scores, as observed in our ISH study (Supplementary Figs. 7e, 7f, Supplementary Tables 4 and 5). Taken together, our results suggest that miR-29-mediated TET2 repression for 5-hmC inhibition is a mechanism involved in prostate cancer progression.

Modulation of TET2-related pathway promotes tumor growth

We next determined whether TET2 repression is associated with tumor growth. We first performed proliferation assays in LNCaP and BicR cells and demonstrated that the overexpression and knockdown of miR-29a/b increased and decreased the proliferation of LNCaP cells, respectively (Supplementary Figs. 8a-c). Importantly, inhibition of cell growth by anti-miR-29a/b was significant in antagonist-treated BicR cells (Fig. 4a). To investigate whether this effect of miRNA is mediated by TET2 repression, we overexpressed TET2 in VCaP cells and knocked down TET2 expression in LNCaP cells by transfections with a TET expression vector or short interfering RNA (siRNA) targeting

TET2, respectively (Fig. 4b). The gain or loss of TET2 expression had a significant effect on cell proliferation (Figs. 4c and 4d), demonstrating the growth-inhibitory effect of TET2 in prostate cancer. We also demonstrated that TET2 growth inhibitory ability was associated with the C-terminal domain important for its enzymatic activity[27] (Supplementary Fig. 9). In addition, miR-29b-mediated induction of cell proliferation was abrogated by the rescue of TET2 expression (Fig. 4e), while anti-miR-29b-mediated inhibition of cell growth was relieved by *TET2* knockdown (Fig. 4f). Moreover, miR-29a/b was positively regulated by AR and promoted cell growth in other prostate cancer cells (DU145 and VCaP cells; Supplementary Figs. 8d-i). To examine the role of miR-29a/b and TET2 in castration-resistance, we also transfected CRPC-cell lines with anti-miR29a/b and observed a repression of castration-resistant cell growth (Supplementary Fig. 10). Notably, cell migration was markedly enhanced in BicR cells compared with parental LNCaP cells (Supplementary Fig. 11a). Transfection of the BicR cells with anti-miR-29b reduced cell migration, suggesting that miR-29b induction promotes BicR cell migration by repressing TET2 (Fig. 4g). Taken together, these results indicate that the miR-29 family has a tumor-promoting effect in prostate cancer.

We further analyzed the downstream signals of miR-29b and TET2 in LNCaP cells. The overexpression of miR-29b and knockdown of *TET2* induced the expression of 495

genes, suggesting that these genes are putative targets of TET2 (Supplementary Fig. 12a). Gene ontology (GO) term analysis for these genes showed that they are significantly involved in cell migration (Supplementary Fig. 12b). In addition to the TET2 downstream signaling, microarray and GO term analysis suggested that miR-29b significantly induces cell cycle related pathway such as *Aurora kinase A (AURKA)*, which is involved in the miR-29a/b-mediated growth promotion (Supplementary Figs. 12c, 13a, 13b and 13d-g). Furthermore, although our comprehensive analysis of miR-29a/b targets revealed that TET2 is the primary target of miR-29a/b in prostate cancer cells (Supplementary Fig. 12d, e), *HMG-box transcription factor 1 (HBP1)*, a tumor suppressor gene[28], was identified as another miR-29b direct target in LNCaP cells for cell proliferation (Supplementary Figs. 13c, 13h and 13i). Thus, although TET2 is the major determinant of miR-29 downstream signaling, cooperative functions of these activated pathways or target genes would be associated with miR-29b-mediated growth promotion.

Next, we examined the roles of miR-29b and TET2 in tumor progression using *in vivo* xenograft assays. Nude mice were injected with LNCaP or BicR cells and monitored for tumor growth. Oral bicalutamide treatment inhibited LNCaP tumor growth (Supplementary Fig. 11b), but not BicR tumor growth. However, anti-miR-29b injections (three times a week) into the BicR tumors significantly inhibited the tumor growth (Figs. 5a and 5b).

Importantly, TET2 expression was higher in the tumors treated with anti-miR-29b than in the control BicR tumors, even in the presence of bicalutamide (Figs. 5c and 5d). Furthermore, we also demonstrated that repression of miR-29a/b inhibited castration-resistant tumor growth in xenografts of CRPC cell lines (22Rv1 and LTAD cells; Supplementary Fig. 14). Taken together, these data highlight a potential role of increased miR-29-family-mediated TET2 repression in the progression of prostate cancer to HRPC.

5-hmC plays a critical role in FOXA1 enhancer activity

We next explored whether loss of 5-hmC in prostate cancer is genome wide or locus specific using chemical labeling (biotinylation) of 5-hmC and subsequent immunoprecipitation with streptavidin beads (5-hmC collector)[29]. We coupled this approach with deep sequencing using a ChIP-seq protocol. This assay permits quantitative comparisons of genome-wide changes in 5-hmC levels between cell lines. Using MACS[30] , we determined global 5-hmC regions (P-value < 10^{-5}, Poisson distribution, false discovery rate < 0.01; Fig. 6a) in prostate cancer cells. Interestingly, although the number of 5-hmC sites was reduced in BicR cells compared with LNCaP cells, as expected from the decrease of TET2 expression, the inhibition of miR-29b markedly increased the number of 5-hmC sites (Fig. 6a, top panel). We also performed another assay, hMed-IP, and confirmed that

5-hmC levels were repressed in BicR cells compared with LNCaP cells (Fig. 6b). Moreover, the 5-hmC regions appeared to overlap with the 5-mC regions, due to the generation of 5-hmC by the oxidation of 5-mC (Fig. 6c).

Surprisingly, we found that the FOXA1 motif was predominantly enriched in the 5-hmC regions (Fig. 6d). FOXA1, a central transcription factor of prostate cancer biology, coordinates AR binding and promotes tumor progression[31, 32]. We observed a significant overlap of the 5-hmC regions with FOXA1 binding regions and K4me1-modified regions (Fig. 6e and Supplementary Fig. 15a). Furthermore, the 5-hmC regions obtained by miR-29b knockdown overlapped with ARBSs throughout the genome (Supplementary Fig. 15b). TET2 ChIP-seq signals were observed in the vicinity of 5-hmC sites in LNCaP cells; these were also validated by ChIP analysis (Supplementary Figs. 16a-e). Moreover, we demonstrated that TET2 interacts with FOXA1 (Fig. 6f and Supplementary Fig. 17). For example, in the genomic locus of NK3 homeobox 1 (*NKX3.1*), an AR collaborative factor[33], we detected decreased 5-hmC levels in BicR cells and increased 5-hmC levels following anti-miR-29b transfection around FOXA1-bound enhancer region (Fig. 6g). Although ChIP analysis revealed that miR-29b inhibition decreases FOXA1 binding, subsequent AR recruitment, and enhancer activity, this inhibition was reversed by *TET2* knockdown, suggesting the positive and negative roles of miR-29b and TET2 in FOXA1 enhancer

activity, respectively (Fig. 6h). Conversely, we also observed a positive effect of miR-29b on FOXA1 binding by the addition of miR-29 (Supplementary Fig. 18a-c). We also examined whether 5-hmC modifications modify FOXA1 DNA binding ability. In gel shift assay, FOXA1 interact with DNA probe including FOXA1 binding sequence identified by ChIP-seq in *MTOR* locus (Supplementary Fig. 18d). We observed 5-hmC modification reduced FOXA1 binding *in vitro*. Thus, 5-hmC modulation could be a crucial epigenetic marker for the negative regulation of AR recruitment or FOXA1 enhancer activity.

Impact of 5-hmC modification on global gene regulation

We evaluated the effects of 5-hmC on gene regulation by directional RNA sequencing. RefSeq genes associated with 5-hmC are significantly included among those genes upregulated in BicR cells compared with LNCaP cells, suggesting a negative role of 5-hmC in gene expression (Figs. 7a and 7b). Kyoto Encyclopedia of Genes and Genomes (KEGG) pathway enrichment analysis of the upregulated genes revealed that they are associated with various prostate cancer-related pathways such as *AR*, mammalian target of rapamycin (*mTOR*), Signal Tranducer and Activator of Transcription 3 (*STAT3*), and cell migration (Fig. 7c), which are involved in HRPC progression. Interestingly, androgen-mediated regulation of *NKX3.1* is enhanced in BicR cells, suggesting AR

hypersensitivity, because NKX3.1 is a positive regulator for AR binding (Fig. 7a). We found that *mTOR*[34] is the most enriched signaling pathway among these 5-hmC-regulated genes in AR-positive HRPC cell line (Figs. 7c and 7d). The androgen-mediated induction of *MTOR* and *NKX3-1* genes was inhibited by anti-miR-29b (Fig. 7e), indicating that 5-hmC could be an epigenetic marker associated with the repression of the transcriptional activity of AR. Furthermore, androgen-mediated enhancer activity caused by FOXA1-binding was negatively regulated by miR-29b knockdown and reversed by *TET2* knockdown (Fig. 7f). Furthermore, enhanced mTOR activation at the protein level in BicR or VCaP cells was dependent on miR-29a/b (Fig. 7g and Supplementary Fig. 19a).

Microarray analysis in LNCaP cells demonstrated that a greater number of 5-hmC-associated genes were significantly upregulated than downregulated by si*TET2* (Fig. 8a) when compared with the background, suggesting that TET2 is mainly involved in the gene repression. By combining these results with the RNA-seq analysis, 281 genes were induced by si*TET2* and upregulated in BicR, while, 83 genes were repressed (Supplementary Fig. 20a). Interestingly, sequences surrounding both the upregulated and downregulated genes presented significant enrichment of FOXA1 and AR binding sites, suggesting the role of FOXA1 and AR for positive and negative gene regulation caused by TET2 (Supplementary Fig. 20b, c). The inhibition or addition of TET2 led to the

upregulation or repression of FOXA1-associated androgen-regulated genes, respectively, indicating a negative role of 5-mC hydroxylation in FOXA1-driven enhancer and promoter activity (Fig. 8b and 8c). Importantly, anti-miR-29b-mediated transcriptional repression of androgen-regulated genes was relieved by *TET2* knockdown (Figs. 8d and e).

Furthermore, CDK1, a 5-hmC regulated gene, is involved in AR phosphorylation (Ser81) in response to DHT stimulation[35]. The *CDK1* is upregulated in BicR cells and repressed by the inhibition of miR-29a/b (Supplementary Figs. 19b and 19c). Consistent with this result, a high p-AR (Ser81) level was observed in BicR cells without DHT, and this level was dependent on the miR-29a/b expression (Figs. 8f and 8g). Moreover, bicalutamide-dependent repression of p-AR observed in LNCaP cells is found to be diminished in BicR cells (Supplementary Fig. 19d). We found that the p-AR enhancement in BicR tumors with bicalutamide or in other AR-positive cell lines is inhibited by miR-29a/b knockdown (Fig. 8h and Supplementary Figs. 19e-g). Taken together, our results suggest that miR-29-mediated TET2 repression activated 5-hmC targeting AR-regulators such as CDK1 and then increase AR sensitivity.

The present study establishes a genome-wide map of the 5-hydroxymethylome in prostate cancer cells and reveals the oncogenic role of decreased 5-hmC levels in the comprehensive modulation of signaling pathways involved in prostate cancer progression

(Fig. 8i).

Discussion

In the present study, we demonstrate that TET2 is repressed by androgen using CAGE. We also present a novel mechanism that TET2 repression by androgen is mediated by miRNA induction. In addition, AR ChIP-seq analysis in HRPC cells indicates that antagonist-bound AR directly represses the *TET2*-enhancer activity by modifying histones. Short RNA sequence analysis revealed a strong androgen-mediated induction of members of the miR-29 family, which in turn repress the expression of TET2 to promote prostate tumor growth. We also found that the androgen antagonist, bicalutamide, differentially regulates TET2 expression in hormone-dependent and HRPC cells, suggesting a possible involvement of TET2 in anti-androgen withdrawal syndrome, a frequent clinical complication[36].

Recent research demonstrates that the dysregulation of miRNA expression profiles contributes to the pathogenesis of human malignancies[37-40]. Because the expression of the miR-29 family is reduced in several cancer tissues as compared to normal tissues, the role of the miR-29 family in cancer is controversial[41, 42]. While the precise role of the miR-29 family members in cancer is still unclear, they are known to promote metastasis in breast cancer[43, 44]. Importantly, our clinical study of prostate cancer samples demonstrates that miR-29 is negatively correlated with TET2 and highly expressed in cancers with poor

prognoses. We have shown, using both *in vitro* and *in vivo* studies, that the miR-29 family is a key determinant of the progression of prostate cancer to HRPC. *In vitro*, miR-29 family members promote the cell proliferation and migration of HRPC cells by activating cell motility and cell cycle-associated gene expression. Furthermore, miR-29a/b depletion enhanced the TET2 expression and repressed castration-resistant cell growth. *In vivo*, the miR-29 family members enhance AR antagonist- or castration resistant tumor growth. These results denote a significant oncogenic role of miR-29 in prostate cancer progression.

Our findings indicate a novel epigenetic role of AR-dependent TET2 repression in the FOXA1-cistrome. We demonstrated that 5-hmC modifications are enriched among global FOXA1 binding sites and inhibit FOXA1 binding at specific loci. However, it would be important to confirm genome-wide FOXA1 binding sites were modulated by miR-29a/b or TET2 by ChIP-seq in the future study. In addition, this research highlights the importance of global gene regulation by the miR-29 family in determining cancer cell fate. Identification of the signaling pathways regulated by 5-hmC would facilitate the elucidation of the mechanisms responsible for prostate cancer progression. We show that the hydroxylation of 5-mC inhibits the expression of p-AR, *mTOR*, and oncogenic proteins such as *STAT*[45] and *Wnt*[46], which are involved in the signaling pathways that govern the progression of prostate cancer to HRPC. Collectively, our results identify

5-hydroxymethylation, rather than methylation alone, as the primary target of the miR-29 family members in prostate cancer cells.

Interestingly, genes in the mTOR-related pathway were most enriched in areas encoding the components of 5-hmC-regulated signaling pathways. We identified the *MTOR* gene as a typical example of such a gene cluster and as a novel androgen target, particularly in HRPC. Several AR and FOXA1 binding sites were identified in the intron region of *MTOR* via ChIP-seq. The hydroxylation of 5-mC at ARBSs was repressed in HRPC cells and enhanced by inhibition of miR-29 expression. Our results indicate that loss of 5-hmC at ARBSs increased FOXA1 enhancer activity for *MTOR* induction by androgen. Recent studies have demonstrated the importance of mTOR in prostate cancer metastasis and its potential use as a target for HRPC therapy[34, 47].

Our results raise the possibility that acquired AR hypersensitivity could promote HRPC tumor growth. The hydroxylation of 5-mC by inhibition of miR-29 expression suppressed AR-dependent gene expression, and TET2 inhibition reversed the effect of miR-29 inhibition on AR signaling and cell growth. Mechanistically, the modulation of FOXA1 enhancer activity by TET2 repression could promote AR recruitments. We also found the expression level of one AR-collaborating factor, NKX3-1, which is encoded by a highly androgen-sensitive gene, was also affected by 5-hmC. Moreover, we showed that CDK1 is

one of the 5-hmC-targeted genes in prostate cancer cells and is upregulated in HRPC cells. We also noted that phosphorylation of AR at serine 81 is promoted by miR-29 induction in HRPC cells. Phosphorylation of AR at serine 81 by CDK1 has been reported to increase AR sensitivity by promoting AR binding to specific ARBSs[35]. Thus, based on the results of our clinical and biological experiments, we demonstrate the significance of TET regulation for the progression to HRPC by activating AR sensitivity.

In conclusion, our results indicate that TET2 signaling play an important role in the FOXA1-cistrome transcriptional network by controlling the global epigenetic code, 5-hmC, during prostate cancer progression. This finding highlights the importance of 5-hmC as a key epigenetic marker that regulates the steroid hormone activity by modulating FOXA1 binding. In addition, we also revealed a novel divergent function of miR-29 as a crucial epigenetic regulator that represses TET2 in cancer progression. Thus, developing novel epigenetic approaches for inhibiting miR-29 or modifying TET2-mediated pathway may have important implications for treating advanced prostate cancer.

Methods

HeliScope CAGE

The majority of transcriptome protocols running on second-generation sequencing platforms have relied on two PCR steps, one for pre-amplification of cDNA and the other for clonal amplification of templates on the flow cell prior to sequencing. In order to avoid any potential bias in the identification and quantification of RNA molecules, we used single-molecule sequencers for CAGE (cap analysis gene expression) to identify and quantify the 5' ends of capped RNAs based on cap trapping. Known genes and alternative promoters were determined after genome mapping. HeliScope CAGE quantifies gene expression with the least variability suggesting its reproducibility[22, 23] .

Total RNA was extracted from LNCaP and BicR cells using ISOGEN (Nippon Gene, Tokyo, Japan). The quality of the total RNA was determined using an Agilent Bioanalyzer, and the RNA integrity number (RIN) was confirmed to be 9.0 or higher. First-strand cDNA synthesis was performed using SuperscriptIII (Lifetechnologies) and random primer. Oxidized cDNA/RNA hybrids were biotinylated for Cap-trapping. After poly(dA) tailing, sequencing with the HeliScope Single Molecule Sequencer was performed according to the manufacturer's manual.[22]. Gene expression was measured with the number of reads aligned within a 500 bp distance from the RefSeq transcript 5′ ends, where their genomic

coordinates were downloaded from the UCSC Genome Browser database. The read counts were normalized to tags per million (tpm) based on the total number of aligned reads in the human genome reference. All CAGE tags with one or more overlapping base pair were grouped on the same strand into a single tag cluster (TC).

To analyze the androgen-regulated transcriptional program, we prepared total RNA extracted from LNCaP cell lines treated with 10 nM R1881 at 7 time points in each biological duplicate. In contrast to previous CAGE studies by the Genome sequencer FLX system (454)[48], we observed 57% of the signals within 500 bp of the 5' ends of mRNAs based on the genomic coordinates of the reference full length transcripts of RefSeq. We aggregated neighboring CAGE tags on the genome into TCs and obtained 19644 TCs. Of these, 8309 (43%), fell outside of the RefSeq gene promoters. By analyzing gene expression at each time point, we identified sets of genes regulated by androgen treatment using strict threshold for significance (*P*-value < 0.01, Fisher's exact test, Q-value < 0.01).

RNA sequencing

RNA sequencing (RNA-seq) library construction and sequencing was performed according to the manufacturer's protocol for the Applied Biosystems SOLiD 3 Plus System (Applied Biosystems). The library was sequenced using SOLiD Opti Fragment Library Sequencing

kit Master Mix 50 chemistry (Applied Biosystems), which gives 50 bp readings. The RNA-seq readings were analyzed using whole transcriptome software tools from Applied Biosystems. Matching locations were subsequently used to generate counts for annotated features, exons, transcripts or genes using RefSeq Genes to determine the exons genomic locations of known transcripts or coverage files (wiggle format). Finally, genes expression was determined as the number of reads per kilobase of exon model per million mapped reads (PRKM).

Genome-wide methylation and 5-hydroxymethylation analysis

Enrichment of methylated DNA (5-mC) was performed using a Methyl Collector Ultra kit (Active Motif). Briefly, genomic DNA was sheared by sonication. The sheared DNA was incubated with a His-tagged recombinant MBD2b/MBD3L1 protein complex. These protein-DNA complexes were captured with nickel-coated magnetic beads. Enrichment of 5-hydroxymethylated DNA (5-hmC) was performed using a Hydroxymethyl Collector kit (Active Motif), which utilizes a β-glucosyltransferase enzyme to transfer a modified glucose moiety to 5-hydroxymethylcytosine residues in double-stranded DNA. This modified glucose was then used to chemically attach a biotin conjugate to facilitate capture

and enrichment with streptavidin magnetic beads. Enriched double-stranded DNA was sequenced by a Hiseq 2000 Genome Analyzer (Illumina) applying the ChIP-seq method. Sequence readings were mapped onto the human genome (hg18) using the CASAVA software. The 5-mC and 5-hmC-enriched regions were identified by calculating *P*- value and false discovery rate (FDR) using model-based analysis of ChIP-seq (MACS[30]) and the threshold was $P < 10^{-5}$ and FDR (false discovery rate) < 0.01. The 5-hmC peaks were annotated to human RefSeq genes and the genes with 5-hmC peaks in the promoter or gene-body regions were chosen for further analysis.

ChIP sequencing (ChIP-seq)

AR and TET2 ChIP-seq was performed using an Illumina Genome Analyzer (Illumina, San Diego, CA). Libraries were prepared according to the manufacturer's instructions. Unfiltered 36 bp sequence readings were aligned to the human reference genome (hg18) using CASAVA v1.7 (Illumina). Signal scores and *P*-value for AR binding sites was calculated by MACS. The threshold of binding sites was *P*-value < 10^{-5}. Integrative genomic viewer version 2.2 was used for visualization.

hMeDIP

hMeDIP analysis was performed using a hMeDIP kit (Active Motif) according to the manufacturer's instructions. Briefly, genomic DNA was sonicated by a Bioruptor sonicator (Cosmobio). The sonicated DNA fragments (1 μg of each sample, length < 500 bp) were denatured and diluted by the immunoprecipitation buffer. The diluted DNA was incubated with 4 μL of anti-5-hmC antibody (Active Motif) at 4°C overnight. Antibody–DNA complexes were captured by protein A/G beads, and the enriched 5-hmC-containing DNA fragments were purified. We quantified the enrichment of 5-hmC by qPCR.

DNA dot blot analysis

Genomic DNA was extracted from cells using a DNeasy kit (Qiagen). Denatured DNA was spotted on a nitrocellulose membrane (Waterman) and cross-linked by UV irradiation. Briefly, the membrane was first blocked with 5% milk in TBS-Tween 20 for 1 h and then incubated with an anti-5-hmC or 5-mC antibody (1:10000) (Active Motif) for 1 h. Following which, the membrane was incubated with a horseradish peroxidase (HRP)-conjugated anti-rabbit IgG antibody (Beyond Time) for 1 h at room temperature, washed three times with TBS-Tween 20, and finally the DNA was visualized using enhanced chemiluminescence kit (GE-Healthcare).

Immunohistochemistry

Formalin-fixed tissues were embedded in paraffin and sectioned. A Histofine kit (Nichirei, Tokyo, Japan), which employs the streptavidin-biotin amplification method, was used for immunohistochemical analysis of TET2, 5-mC, and 5-hmC. The antigen-antibody complex was visualized with a 3,3'-diaminobenzidine solution (1 mM 3,3'-diaminobenzidine, 50 mM Tris-HCl buffer [pH 7.6], and 0.006% H_2O_2). During immunohistochemical analysis, immunoreactivity was evaluated in more than 1000 carcinoma cells in each case, and the percentage of immunoreactivity (labeling index (LI)) was determined by certified pathologists. Cases with the LI of more than 10% were considered TET2-, 5-mC-, or 5-hmC-positive carcinoma in this study.

miRNA *in situ* hybridization (ISH)

MicroRNA ISH Buffer and Controls kit (Exiqon, Woburn, MA) was used for ISH in this study according to manufacturer's protocol. Briefly, tissue specimens were fixed with 10% formalin and embedded in paraffin. Slides were deparaffinized and incubated with proteinase-K (10 μg mL^{-1}) for 10 min at 37°C. The hybridization mixture, containing 20 nM double-DIG LNA microRNA probe for miR-29a, miR-29b, or scramble-miR (Exiqon),

was applied and hybridized for 1 h at 60°C. The probe sequences used in this study were, miR-29a, TAACCGATTTCAGATGGTGCTA; mR-29b, AACACTGATTTCAAATGGTGCTA; and scramble-miR, GTGTAACACGTCTATACGCCCA. Slides were incubated with RNase (20 μg mL^{-1}, Wako Pure Chemical Industries, Osaka, Japan) for 30 min at 37°C, and Anti-digoxigenin-AP Fab fragments (1:1000, Roche) were applied as the primary antibody. NBT/BCIP solution (Roche) was used for visualization and then the slides were counterstained with Nuclear Fast Red.

Short RNA sequencing

Purified short RNAs were ligated to chimeric-oligonucleotide adaptors and reverse transcribed to cDNA. PCR products with a size of 11–40 nt were eluted from 12% polyacrylamide gels. The PCR products were digested by a restriction enzyme, concatenated, column purified to eliminate short concatemers, and sequenced using an Illumina/Solexa GAIIx Genome Sequencer (Illumina, San Diego, CA, USA). RNAs were aligned to the human genome (NCBI build 35) and were used to search for miRNA sequences in the miRBase 9.1 database. We selected sequences with a single match in the best BLAST hits.

miRNA quantitative PCR

Total RNA was extracted using a mirVana miRNA Isolation Kit (Ambion). RNA (10 ng) was reverse transcribed to cDNA using a TaqMan micro-RNA reverse transcription kit (Applied Biosystems). Quantitative PCR (qPCR) for cDNA was performed using TaqMan microRNA assay primers and a Step One Real-Time PCR System (Applied Biosystems). The relative level of miRNA was calculated by normalizing the target gene signal by the signal for U6B small nuclear RNA.

Plasmid construction

In order to overexpress TET2, we purchased a Halo-tagged expression vector, which included the *TET2* cDNA clone (TET2a: FHC22012 and TET2b: FHC22011) from Promega. A *TET2*-3'-UTR sequence containing the miR-29-binding sites or a subsequent sequence lacking these sites was generated by PCR amplification using the following primers:

TET2-3'-UTR-F: 5'-GGGCTCGAGAGTATTACAGTGACAGGAAT -3',

TET2-3'-UTR-R: 5'-CCCGCGGCCGCATATTTGTAGCAGGCTGAGT-3',

TET2-3'-UTR-NC-F: 5'-GGGCTCGAGATCATAATGTGAGCTAAGAA -3',

TET2-3’-UTR-NC-R: 5’-CCCGCGGCCGCCAGTTTAACAAATGACAGTA-3’.

Amplified sequences were cloned into the psiCHECK-2 vector (Promega). Vectors were designated as *TET2*-3’-UTR-Luc and *TET2*-3’-UTR-NC -Luc, respectively.

Cell culture and reagents

VCaP and 293T cells were grown in DMEM medium supplemented with 10% fetal bovine serum (FBS), 50 U mL^{-1} penicillin, and 50 μg mL^{-1} streptomycin. 22Rv1, DU145, RWPE and LNCaP cells were grown in RPMI medium supplemented with 10% FBS, 50 U mL^{-1} penicillin, and 50 μg mL^{-1} streptomycin. LTAD cells were grown in phenol red free RPMI medium supplemented with 10% charcoal-dextran stripped FBS, 50 U/mL penicillin, and 50 μg mL^{-1} streptomycin. BicR cells were grown in RPMI medium supplemented with 10% FBS, 10 μM bicalutamide, 50 U mL^{-1} penicillin, and 50 μg mL^{-1} streptomycin. LNCaP cells were obtained from ATCC. STR analysis was performed for the authentication of the cell lines which were newly established from LNCaP cells or provided from other laboratories (VCaP, Du145, RWPE). We also checked the expression patterns of AR and its variants to verify the prostate cancer cell lines. Cells were routinely checked for mycoplasma contamination using Mycoplasma Detection Kit (JENA Bioscience GmbH, Jena, Germany). We used cells verified to be mycoplasma free for

experiments. The antibodies used in this study were 5-hmC, 5-mC (Active Motif), TET2 (Abcam), mTOR (Cell Signaling), p-mTOR (Cell Signaling), S6K (Cell Signaling), p-S6K (Cell Signaling), p-AR (Ser81) (Millipore), AR (Santa Cruz Biotechnology), FOXA1 (Abcam), EZH2 (BD Biosciences), RNA pol II (Millipore), AcH3 (Millipore), H3K4me3, H3K4me1, H3K9me2 (Abcam), Halo (Promega) and β-actin (Sigma).

ChIP and quantitative PCR (qPCR)

For ChIP using AR, FOXA1 and TET2 antibody, cells were crosslinked with 1% formaldehyde for 10 minutes and stopped by adding 0.2 M glycine. Cells were lysed by lysis buffer[48, 49] and chromatin DNA was sheared by sonication. Sonicated lysates were incubated overnight at 4℃ with specific antibodies. Then protein G agarose beads were added and rotated for 2 h. The beads were washed several times and incubated at 65℃ overnight to reverse crosslink. DNA was purified with ethanol precipitation. The fold enrichment relative to the IgG-IP control or % of input was quantified by qPCR using SYBR Green PCR master mix and the ABI StepOne System (Life Technologies, Carlsbad, CA). We used *GAPDH* locus as a negative control (*NC*)[48]. The primer sequences for the detection of ARBSs by qPCR are listed in Supplementary Table 6.

qRT-PCR

Total RNA was isolated using the ISOGEN reagent. First-strand cDNA was generated using a PrimeScript RT reagent kit (Takara, Kyoto, Japan). The primer sequences are listed in Supplementary Table 6. Expression levels were quantified by qPCR[48, 49] using SYBR Green PCR master mix and the ABI StepOne system (Life technologies).

Western blot analysis

Whole cell lysates were prepared using NP40 lysis buffer. Protein concentration was determined by the BCA assay (Pierce, Rockford, IL). Each protein lysate was loaded onto 8 or 10 % SDS-polyacrylamide gels, separated by electrophoresis, and electrotransfered onto Immobilon-P Membranes (Millipore, Billerica, MA). Membranes were incubated with primary antibodies overnight and then incubated with secondary antibodies. Antibody-antigen complexes were detected using ECL Western Blotting Substrate (Pierce). Films were quantified by scanning densitometry using Image J software (NIH). All full scan images of immunoblotting are shown in Supplementary Fig. 21.

Luciferase assay

LNCaP cells were incubated with phenol red-free medium supplemented with 5% dextran

charcoal-stripped fetal bovine serum (FBS) for 24 h before transfection. Cells were transfected with pGL3 vectors including ARBSs and tk-pRL using the FuGENE HD reagent (Promega, Madison, WI). Twenty four hours after transfection, the cells were treated with 10 nM DHT or vehicle for 24 h, and then luciferase activity was determined using luminometer[49].

Migration assay

Cellular migration assays were performed using 24-well plate matrigel-coated invasion chambers (BD Biosciences, San Jose, CA). Briefly, cells (5×10^4 cells) were suspended in serum free RPMI medium then transferred into suspended inserts with 8μm pores. RPMI medium with 10% FBS was placed at the bottom of the wells and the cells were cultured for 24 h. Invading cells were fixed with methanol and stained with Giemsa[51]. The number of invading cells in 5 random fields was counted using a microscope, and the average number of cells per field was calculated.

EMSA

Gel shift assay was performed by using the DIG Gel shift kit (Roche) with DIG labeled oligonucleotides containing FOXA1 binding sites (in the *MTOR* locus) identified by

ChIP-sequence. HA-tagged FOXA1 protein was overexpressed in 293T cells and purified using an anti-HA antibody. After mixing probes with FOXA1 protein at room temperature, samples were analyzed on a 6% polyacrylamide gel electrophoresis (PAGE) gel. After transferring to a positive-charged nylon membrane (Roche), signals were detected by using an anti-DIG antibody (Roche). 5-mC and 5-hmC modified oligonucleotides were purchased from Eurosins Genomics (Tokyo, Japan). The oligonucleotide sequence for preparing the probe was as follows: 5'-CCTAGGTTGTTTACAAACACAGAATGCTTG-3'.

.

3C assay

3C assay was basically performed as previously described[53]. Briefly, cross-linked samples were incubated with HindIII restriction enzyme at 37℃ overnight and then incubated with T4 DNA ligase (Promega) at 16℃ for 4 h. Samples were diluted and immunoprecipitated with AR antibody at 4℃ overnight. Next, the samples were rotated with protein A agarose beads for 2 h at 4℃ The beads were washed with ChIP dilution buffer and de-crosslinked. Primer sequences used for PCR amplifications were as follows. Promoter: 5'-CTTCTCTTATGCCGCGAAACT-3' and

Enhancer: 5'-GTCACTGGGATTCATGCAAA-3'.

siRNA transfection

For siRNA experiments, we purchased Stealth RNAi™ siRNAs (Life Technologies) targeting TET2 (#1: HSS123253, #2:HSS123254), EZH2 (HSS176652)[56], AURKA (HSS186148), HBP1 (HSS178254) and a negative control siRNA. Cells were transfected with siRNAs using siGene (Promega) 48–72 h before each experiment.

miRNA and anti-miRNA transfection

Transfection of small RNAs pre-miRNA 29a/b, anti-miRNA 29a/b, control miRNA (NC) and anti-negative control (anti-NC) (purchased from Life Technologies) were performed using siPort transfection reagent (Life Technologies) according to the manufacturer's protocol with some modifications as described in the Supplementary Table 7 or Figure legends.

Patients and tissue samples

We obtained 102 prostate cancer samples from patients who underwent a radical prostatectomy performed at the University of Tokyo Hospital (Tokyo, Japan). The Tokyo University Ethics Committee approved this study, and informed consent was obtained from

each patient before surgery. The ages of the patients ranged from 52 to 78 years (mean, 67 years), and pretreatment serum prostate-specific antigen (PSA) levels ranged from 1.2 to 136 ng mL^{-1} (mean, 16.9 ng mL^{-1}). The prostate tissue sections submitted for this study contained 95 benign and 102 cancerous foci. The sections were evaluated by two specialized pathologists (T.S and KI.T). Clinicopathological parameters such as Gleason scores, pathological primary tumor (pT) stages, and pathological regional lymph node (pN) stages were summarized in Supplementary Table 2. Thirty-three patients were treated with surgery alone. The remaining patients, who had pT3 cancer and/or experienced a postoperative PSA nadir of >0.2 ng mL^{-1}, received adjuvant androgen deprivation and/or radiation therapy. Patients were followed-up by their surgeons at 3-month intervals for 5 years and yearly thereafter. The mean patient follow-up period was 144 ± 56 months (range: 10–240 months).

Cell proliferation assay

Cells were plated at 3×10^3 cells per well in 96-well plates. For RNAi experiments, cells were transfected with siRNA 24 h after plating. The MTS [3-(4,5-dimethylthiazol-2-yl)-5-(3-carboxymethoxyphenyl)-2-(4-sulfophenyl)-2H-tetrazolium, inner salt] assay was performed using the CellTiter 96® Aqueous MTS reagent

(Promega) according to the manufacturer's instructions. The experiment was performed in quintuplicate.

In vivo tumor formation assay

LNCaP, BicR, 22Rv1 and LTAD (3×10^6) cells were subcutaneously injected into each side of twenty 5-week-old male BALB/C nude mice. For the experiment of LNcaP and BicR xenografts, the mice were randomly divided into three groups when the tumor volumes reached 100 mm^3. Each group was treated with vehicle or bicalutamide (20 mg kg^{-1}; Santa Cruz Biotechnology) orally every other day and an intratumoral injection of anti-miRNA-29b was started. To study the effect of miR-29a/b knockdown on castration-resistant tumor growth, 22Rv1 and LTAD xenografts were grown. Once the tumors reached 100 mm^3, mice were physically castrated and randomly divided into two groups. Each group was treated with an intratumoral injection of anti-miRNA-29a/b or anti-NC. Each tumor was injected with 5 μg of anti-miR-29b, a/b or anti-NC, three times a week using Lipofectamine RNAi MAX Transfection Reagent (Life Technologies). Tumor volume was determined using the following formula: $V = 0.5 \times r1 \times r2 \times r3$ ($r1 < r2 < r3$). Tokyo university animal ethics committee approved these experiments.

Microarray

For expression microarrays, a GeneChip Human Exon 1.0 ST Array (Affymetrix, Santa Clara, CA) was used according to the manufacturer's protocol. Data analysis was performed using the Affymetrix Microarray Suite software. To compare arrays, normalization was performed on data from all probe sets. GO term and Pathway analysis was performed using DAVID[54, 55].

Statistical analyses

For cell line experiments, statistical differences (*P* values) among groups were obtained using the two-sided Student's *t*-test. All experiments were performed at least twice and similar results were obtained. *P* values less than 0.05 were considered statistically significant. Statistical analysis was performed using Graphpad Prism 5 software (GraphPad Software, San Diego, CA) or MS Excel. The association between miRNA expressions and clinicopathological factors was evaluated using the student's *t*-test, Wilcoxon signed rank test, cross-table using the chi square-test, Spearman rank correlation test or the correlation coefficient (*R*) and regression equation. We excluded samples if the obtained values were more than twice the s.d. of the mean. For xenograft experiments, sample sizes were calculated using s.d in the preliminary experiments and the expected difference of two

groups. Other sample sizes were equal or greater than the recommended minimum sample size in the past publications. A cancer-specific survival curve was generated according to the Kaplan-Meier method, and statistical significance was calculated using the log-rank test.

Accession codes

The microarray, CAGE, RNA-seq and ChIP-seq data have been deposited in Gene Expression Omnibus (GSE66039). We also used previously deposited data (GSE62492, GSE58428 and GSE58309 [50, 51, 56]).

References

1. Suganuma T, Workman JL. Chromatin and signaling. Curr Opin Cell Biol. 25(3), 322-326 (2013).

2. Wu H, Zhang Y. Reversing DNA methylation: mechanisms, genomics, and biological functions. Cell. 156(1-2), 45-68 (2014).

3. Wu H, Zhang Y. Mechanisms and functions of Tet protein-mediated 5-methylcytosine oxidation. Genes Dev. 25(23), 2436-2452 (2011).

4. Kohli RM, Zhang Y. TET enzymes, TDG and the dynamics of DNA demethylation. Nature. 502(7472), 472-9 (2013).

5. Solary E, Bernard OA, Tefferi A, Fuks F, Vainchenker W. The Ten-Eleven Translocation-2 (TET2) gene in hematopoiesis and hematopoietic diseases. Leukemia. 28(3), 485-496 (2014).

6. Lian CG, et al. Loss of 5-hydroxymethylcytosine is an epigenetic hallmark of melanoma. Cell. 150(6), 1135-1146 (2012).

7. Ko M, et al. Impaired hydroxylation of 5-methylcytosine in myeloid cancers with mutant TET2. Nature. 468(7325), 839-843 (2010).

8. Yang H, et al. Tumor development is associated with decrease of TET gene expression and 5-methylcytosine hydroxylation. Oncogene. 32(5):663-669 (2013).

9. Chen CD,et al. Molecular determinants of resistance to antiandrogen therapy. Nat Med. 10(1), 33-39 (2004).

10. Wang Q, et al. Androgen receptor regulates a distinct transcription program in androgen-independent prostate cancer. Cell. 138(2), 245-256 (2009).

11. Takayama K, Inoue S. Transcriptional network of androgen receptor in prostate cancer progression. Int J Urol. 20(8), 756-768 (2013).

12. Debes JD, Tindall DJ. Mechanisms of androgen-refractory prostate cancer. N Engl J Med. 351(15), 1488-90 (2004).

13. Karantanos T, Corn PG, Thompson TC. Prostate cancer progression after androgen deprivation therapy: mechanisms of castrate resistance and novel therapeutic approaches. Oncogene. 32(49), 5501-5511 (2013).

14. Lim S, et al. Epigenetic regulation of cancer growth by histone demethylases. Int J Cancer. 127(9), 1991-1998 (2010).

15. Nagy L, et al. Mechanism of the nuclear receptor molecular switch. Trends Biochem Sci. 29(6), 317-324 (2004).

16. Buranapramest M, et al. Chromatin remodeling and nuclear receptor signaling. Prog Mol Biol Transl Sci. 87, 193-234 (2009).

17. Dasgaputa S, Lonard DM, and O'Mally BW. Nuclear receptor coactivators: master regulators of human health and disease. Annu. Rev. Med. 65, 279-292 (2014).

18. Perissi V, Jepsen K, Glass, CK, and Rosenfeld MG. Deconstructing repression: evolving models of co-repressor action. Nat. Rev. Genet. 11, 109-123 (2010).

19. Banerjee T, and Chakravarti D. A peak into the complex realm of histone phosphorylation. Mol. Cell. Biol. 31, 4858-4873 (2011).

20. Metzger E, et al. Phosphorylation of histone H3 at threonine 11 established a novel chromatin mark for transcriptional regulation. Nat. Cell. Biol. 10, 53-60 (2008).

21. Kim JY, et al. A role for WDR5 in integrating threonine 11 phosphorylation to lysine 4 methylation on histone H3 during androgen signaling and in prostate cancer. Mol. Cell. 54, 613-625 (2014).

22. Kanamori-Katayama M, et al. Unamplified cap analysis of gene expression on a single-molecule sequencer. Genome Res. 21(7), 1150-9 (2011).

23. FANTOM Consortium and the RIKEN PMI and CLST (DGT). A promoter-level mammalian expression atlas. Nature. 507(7493), 462-470 (2014).

24. Shi XB, et al. An androgen-regulated miRNA suppresses Bak1 expression and induces androgen-independent growth of prostate cancer cells. Proc Natl Acad Sci U S A. 104(50):19983-19988 (2007).

25. Ribas J, et al. miR-21: an androgen receptor-regulated microRNA that promotes hormone-dependent and hormone-independent prostate cancer growth. Cancer Res. 69(18), 7165-9 (2009).

26. Murata T, et al. miR-148a is an androgen-responsive microRNA that promotes LNCaP prostate cell growth by repressing its target CAND1 expression. Prostate Cancer Prostatic Dis. 13(4), 356-361 (2010).

27. Hu L, et al. Crystal structure of TET2-DNA complex: insight into TET-mediated 5mC oxidation. Cell. 155(7), 1545-1555 (2013).

28. Escamilla-Powers JR, et al. The tumor suppressor protein HBP1 is a novel c-myc-binding protein that negatively regulates c-myc transcriptional activity. J Biol Chem. 285(7), 4847-4858 (2010).

29. Song CX, et al. Selective chemical labeling reveals the genome-wide distribution of 5-hydroxymethylcytosine. Nat Biotechnol. 29(1), 68-72 (2010).

30. Zhang Y, et al. Model-based analysis of ChIP-Seq (MACS). Genome Biol 9, R137 (2008).

31. Jozwik KM, Carroll JS. Pioneer factors in hormone-dependent cancers. Nat Rev Cancer. 12(6), 381-385 (2012).

32. Wang D, et al. Reprogramming transcription by distinct classes of enhancers functionally defined by eRNA. Nature. 474(7351), 390-394 (2011).

33. Tan PY, et al. Integration of regulatory networks by NKX3-1 promotes androgen-dependent prostate cancer survival. Mol Cell Biol. 32(2), 399-414 (2012).

34. Hsieh AC, et al. The translational landscape of mTOR signalling steers cancer initiation and metastasis. Nature. 485(7396), 55-61 (2012).

35. Chen S, et al. Androgen receptor phosphorylation and stabilization in prostate cancer by cyclin-dependent kinase 1. Proc Natl Acad Sci U S A. 103(43):15969-15974 (2006).

36. Phillips R. Prostate cancer: an enzalutamide antiandrogen withdrawal syndrome. Nat Rev Urol. 11(7), 366 (2014).

37. Cao Q, et al. Coordinated regulation of polycomb group complexes through microRNAs in cancer. Cancer Cell. 20(2), 187-199 (2011).

38. Lu J, et al.MicroRNA expression profiles classify human cancers. Nature. 435, 834–838 (2005).

39. Croce CM. Causes and consequences of microRNA dysregulation in cancer. Nat Rev Genet. 10, 704–714 (2009).

40. Thieu W, Tilki D, deVere White RW, Evans CP. The role of microRNA in castration-resistant prostate cancer. Urol Oncol. 32(5), 517-523 (2014).

41. Wang Y, Zhang X, Li H, Yu J, Ren X. The role of miRNA-29 family in cancer. Eur J Cell Biol. 92(3), 123-8 (2013).

42. Jiang H, Zhang G, Wu JH, Jiang CP. Diverse roles of miR-29 in cancer. Oncol Rep. 31(4), 1509-1516 (2014).

43. Wang C, Bian Z, Wei D, Zhang JG. miR-29b regulates migration of human breast cancer cells. Mol Cell Biochem. 352(1-2), 197-207 (2011).

44. Gebeshuber CA, Zatloukal K, Martinez J. miR-29a suppresses tristetraprolin, which is a regulator of epithelial polarity and metastasis. EMBO Rep. 10(4), 400-405 (2009).

45. Kroon P, et al. JAK-STAT blockade inhibits tumor initiation and clonogenic recovery of prostate cancer stem-like cells. Cancer Res. 73(16), 5288-5298 (2013).

46. Wang G, et al. Crosstalk between the androgen receptor and beta-catenin in castrate-resistant prostate cancer. Cancer Res. 68(23):9918-9927 (2008).

47. Burgio SL, et al. Perspective on mTOR inhibitors for castration-refractory prostate cancer. Curr Cancer Drug Targets. 12: 940-949 (2012).

48. Takayama K, et al. Integration of cap analysis of gene expression and chromatin immunoprecipitation analysis on array reveals genome-wide androgen receptor signaling in prostate cancer cells. Oncogene. 30(5), 619-30 (2011).

49. Takayama K,et al. Androgen-responsive long noncoding RNA CTBP1-AS promotes prostate cancer. EMBO J. 32(12), 1665-1680 (2013).

50. Takayama K, et al. Integrative analysis of FOXP1 function reveals a tumor-suppressive effect in prostate cancer. Mol Endocrinol. 28(12), 2012-2024 (2014).

51. Takayama K, et al. CtBP2 modulates the androgen receptor to promote prostate cancer progression. Cancer Res. 74(22), 6542-6553 (2014).

52. Heinz S, et al. Simple combinations of lineage-determining transcription factors prime cis-regulatory elements required for macrophage and B cell identities. Mol Cell 38(4), 576-589 (2010).

53. Hagege H, et al. Quantitative analysis of chromosome conformation capture assays (3C-qPCR). Nat Protoc. 2, 1722-1733 (2007).

54. Huang DW, Sherman BT, Lempicki RA. Systematic and integrative analysis of large gene lists using DAVID Bioinformatics Resources. Nature Protoc. 4(1), 44-57 (2009).

55. Huang DW, Sherman BT, Lempicki RA. Bioinformatics enrichment tools: paths toward the comprehensive functional analysis of large gene lists. Nucleic Acids Res. 37(1), 1-13 (2009).

56. Takayama K, et al. RUNX1, an androgen- and EZH2-regulated gene, has differential roles in AR-dependent and –independent prostate cancer. Oncotarget. 6, 2263-2276 (2015).

Acknowledgements

We thank RIKEN for sequencing our samples and National Institute of Genetics (NIG) for analyzing sequence data. We thank Dr. Hiroyuki Mano (The University of Tokyo) for the bioinformatics analysis of short RNA sequence data. We also thank E. Sakamoto, T. Oishi, K. Kodama, and N. Sasaki for technical assistance (establishment of cell lines, cell proliferation assay, cell culture, xenografts, bioinformatics analysis and microarray). This work was supported by Grants of the Cell Innovation Program (S.I. and YO.H) and the P-Direct (S.I.) from the MEXT, Japan; by Grants (S.I. and KE.T.) from the JSPS, Japan; by Grants-in-Aid (S.I.) from the MHLW, Japan; by the Program for Promotion of Fundamental Studies in Health Sciences (S.I.), NIBIO, Japan; by Grants from Takeda Science Foundation (S.I. and KE.T.), by a Grant from Yamaguchi Endocrine Research Foundation (KE.T.), Japan, by a Grant from Mochida Memorial Research Foundation (KE.T), Japan..

Author contributions

KE.T. designed the study, performed experiments, and analyzed data. A.M. designed the concept, constructed luciferase vectors, and analyzed miRNA sequence data. T.S. and KI.T. performed *in situ* hybridization and immunohistochemistry. YO.H. performed sequence analysis. T.F., YU.H., and S.T. analyzed tumor samples. T.U supervised the study. S.I.

designed, supervised the study, and coordinated collaborative studies. KE.T. and S.I. wrote the manuscript.

Competing financial interests

The authors declare no competing financial interests

Figure legends

Figure 1. TET2 is differentially regulated by androgen in hormone-dependent and hormone-refractory prostate cancer.

(a) To analyze the androgen-regulated transcriptional program, we prepared total RNA extracted from LNCaP cell lines treated with 10 nM R1881 at 7 time points in each biological duplicate. *CTBP1* and *CTBP1-AS* are positive control androgen-regulated genes[49]. (b) *TET2* is repressed by R1881 10 nM treatment in LNCaP cells. Time course of CAGE data (fold induction); duplicate biological samples were evaluated at each time point. Values represent the mean ± S.D. $^{**}P < 0.01$ (two-sided Student's *t*-test). (c) Regulation of *TET2*, as determined by CAGE, in LNCaP and BicR cells treated with vehicle, 10 nM DHT, 10 nM DHT + 1 μM bicalutamide, or 1 μM bicalutamide for 6 or 24 h. *P*-value is determined by Fisher's exact test. (d) Immunoblots of extracts from LNCaP and BicR cells treated with 10 nM DHT or 1 μM bicalutamide for the indicated time. (e) Regulation of *TET2* mRNA expression by bicalutamide in LNCaP and BicR cells. Both cell lines were treated with vehicle or bicalutamide for 6, 12, or 24 h. *TET2* mRNA induction was measured by qRT-PCR ($n = 3$). Values represent the mean ± S.D. $^{*}P < 0.05$, $^{**}P < 0.01$ (two-sided Student's *t*-test).

Figure 2. Mechanism of TET2 repression by androgen-regulated miRNAs and AR in HRPC.

(a) (upper) *TET2* 3′-UTR including miR-29 binding sequences. (lower) A luciferase vector including the *TET2* 3′-UTR and several mimics of androgen-regulated miRNAs were transfected into LNCaP cells; 48 h after transfection, cells were lysed and a luciferase assay was performed (n = 3). Values represent the mean ± S.D. *P < 0.05, **P < 0.01, ***P < 0.001 (two-sided Student's t-test). (b) qRT-PCR of miR-29a/b in LNCaP and BicR cells was performed. Cells were treated with vehicle, 10 nM DHT, and 1 μM bicalutamide for 24 h. (n = 3). Values represent the mean ± S.D. (c) Mapping of AR binding sites in the vicinity of the *miR-29a/b1* locus. The black arrow shows the direction of miRNAs. (d) LNCap and BicR cells were transfected with luciferase vectors TET2-3'-UTR and TET2-3'-UTR-NC, with control miR (NC) or miR-29a/b. (n = 3). Values represent the mean ± S.D. (e) Immunoblot of cell lysates from LNCaP and BicR cells transfected with anti-miRNA-29a/b to detect TET2 protein levels. (f) Immunoblots of cell lysates of LNCaP and BicR cells transfected with miRNA-29a/b to detect TET2 protein levels. (g) Mapping of AR binding sites in the vicinity of the *TET2* locus. The black arrow shows the direction of genes. The red box indicates the TET2 enhancer region. (h) A luciferase vector including the *TET2* enhancer region with or without mutated AREs was transfected into

BicR cells. Cells were treated with vehicle, 10 nM DHT, or 1 μM bicalutamide for 24 h and then a luciferase assay was performed (n = 3). Values represent the mean ± S.D. *P < 0.05 (two-sided Student's t-test). (i) A luciferase vector including TET2 enhancer region was transfected into BicR cells which were treated with siControl or siAR (10 nM) for 48 h. Cells were treated with vehicle, 10 nM DHT, or bicalutamide (1 or 5 μM) for 24 h and then luciferase activity was measured (n = 3). Values represent the mean ± S.D. ***P < 0.001 (two-sided Student's t-test) (j) ChIP analysis of K9me2 and PolII in the *TET2* enhancer region in LNCaP and BicR cells were treated with vehicle, 10 nM DHT, or 1 μM bicalutamide for 24 h. Enrichment over input (% input) was measured by qPCR (n = 3). Values represent the mean ± S.D. **P < 0.01 (two-sided Student's t-test).

Figure 3. Clinical significance of miR-29 family and TET2 protein expression in prostate cancer.

(a) TET2 and 5-hmC are downregulated in a subset of prostate cancer samples. Immunohistochemistry of 5-hmC and TET2 in prostate cancer and benign prostate tissues (n = 102) was performed. Bar: 100 μm. (b, c) Downregulation of TET2 (b) and 5-hmC (c) is a prognostic factor for prostate cancer. Kaplan–Meier analysis using the log-rank test was performed. (d) Positive correlation of TET2 expression with 5-hmC levels. (e) No

significant correlation between 5-mC and TET2 expression levels. Regression analysis was performed to analyze the correlation. N.S: not significant. (f) miR-29 expression levels were analyzed by in situ hybridization (ISH) in prostate cancer samples (n = 101). Bar: 100 μm. (g) High miR-29b expression is a prognostic factor for prostate cancer patients. Kaplan–Meier analysis using the log-rank test was performed. (h) The association of miR-29 a/b with 5-hmC level and TET2 protein level was analyzed by the chi-square test.

Figure 4. Critical role of miR-29a/b and TET2 repression for hormone-refractory prostate cancer cell growth and migration.

(a) Growth of BicR cells in medium with or without 10 μM bicalutamide after transfection of anti-negative control (anti-NC) or anti-miR-29a/b (n = 4). Values represent the mean ± S.D. *P < 0.05, **P < 0.01 (two-sided Student's t-test) (b) Expression levels of TET2 protein level by western blot analysis. VCaP cells were transfected with an empty vector or TET2 expression vector. LNCaP cells were transfected with siControl, si*TET2* #1, or si*TET2* #2 (1 nM). (c) Growth of LNCaP cells transfected with siControl, si*TET2* #1, or si*TET2* #2 (1 nM) (n = 4). Values represent the mean ± S.D. ***P < 0.001 (two-sided Student's t-test) (d) Growth of VCaP cells transfected with TET2 expression vector or control vector (n = 4). Values represent the mean ± S.D. **P < 0.01 (two-sided Student's

t-test) (e) Growth of LNCaP cells transfected with miR-29b with or without rescue of TET2 (n = 4). Values represent the mean ± S.D. *P < 0.05 (two-sided Student's *t*-test) (f) Growth of BicR cells transfected with anti-miR-29b with or without knockdown of TET2 (n = 4). Values represent the mean ± S.D. **P < 0.01 (two-sided Student's *t*-test) (g) LNCaP and BicR cells were seeded onto filters with an 8-μm pore size in a matrigel-coated upper chamber. The average numbers of invading cells per field are shown (n = 5). Cells were treated with miR-29b or anti-miR-29b. Values represent the mean ± S.D. *P < 0.05, **P < 0.01 (two-sided Student's *t*-test).

Figure 5. Hormone-refractory tumor growth is inhibited by modulating miR-29 and TET2 pathway.

(a) Nude mice were inoculated with BicR cells; Tumor growth (b) of xenografted BicR cells in nude mice treated with anti-NC or anti-miR-29b are shown (n = 7). Values represent the mean ± S.D. **P < 0.01 (two-sided Student's *t*-test). Vehicle or bicalutamide was administered orally each day. Representative views of tumors in nude mice are shown. (c) Western blot analysis was performed to evaluate TET2 expression levels in tumors (n = 2). (d) Downregulation of miR-29b in tumor cells injected with anti-miR-29b (n = 4). qRT-PCR was performed to measure the miRNA expression level in those tumors. Values

represent the mean ± S.D. $^{**}P < 0.01$ (two-sided Student's *t*-test).

Figure 6. Global analysis of 5-hmC-regulated pathways in prostate cancer progression.

(a) Global mapping of genomic regions modified with 5-hmC (upper) and 5-mC (lower) in prostate cancer cells. Genomic DNA was extracted from LNCaP cells and from BicR cells treated with anti-NC or anti-miR-29b. Binding regions were determined by MACS. (b) Validation of 5-hmC levels in LNCaP and BicR cells by hMeDIP. Cells were transfected with anti-NC and anti-miR-29b. (c) Overlap of 5-hmC and 5-mC modified regions in LNCaP and BicR cells. (d) The FOXA1 motif was most enriched in 5-hmC regions ($P = 1.0x10^{-1878}$, HOMER[52] was used for motif analysis and calculation of *P*-value). (e) 5-hmC modification in the vicinity of FOXA1 binding regions. FOXA1 binding sites were determined by ChIP-seq in LNCaP cells. 5-hmC signals around FOXA1 peaks are summarized. (f) Interaction of TET2 with FOXA1. (Upper) Immunoprecipitation by anti-TET2 antibody. LNCaP cells were treated with 10 nM DHT or vehicle for 24 h. Lysates were immunoprecipitated by an anti-TET2 antibody. (Lower) Interaction of TET2 with FOXA1 in VCaP cells. VCaP cells were transfected with TET2 expression vector or empty vector for 72 h. Lysates were immunoprecipitated by an anti-FOXA1 antibody or

normal IgG. (g) Representative mapping of 5-hmC, FOXA1, AR, K4me1, and K4me3 binding regions in a representative 5-hmC target gene, *NKX3.1*. (h) FOXA1 enhancer activity is regulated by miR-29 and TET2 pathway. ChIP analysis of AR, K4me1, and FOXA1 in the 3′-UTR enhancer region (ARBS) of *NKX3.1*. ChIP qPCR was performed to evaluate the enrichment (n = 3). Values represent the mean ± S.D. *P < 0.05, **P < 0.01 (two-sided Student's t-test).

Figure 7. Identification of prostate cancer-related genes such as *mTOR* as 5-hmC targets.

(a) *NKX3.1* is up-regulated in BicR cells. The RNA-seq view of *NKX3.1* locus is shown. Arrows indicate the direction of transcription. (b) Regulation of expression levels of 5-hmC target genes in BicR cells. 5-hmC binding genes only in LNCaP cells were selected and changes in their expression levels in BicR cells compared with LNCaP cells are summarized. *P*-value is obtained by chi-square test. N.S: not significant. (c) Pathway analysis of 5-hmC-regulated genes. The top 10 pathways are shown. (d) Epigenetic regulation of ARBS in the enhancer region of *MTOR*. Mapping of 5-hmC, FOXA1, AR, K4me1, and K4me3 binding regions is shown. (e) LNCaP and BicR cells treated with anti-NC or anti-29a/b were treated with vehicle or 10 nM DHT for 24 h. mRNA levels of

NKX3.1 and *MTOR* were analyzed by qRT-PCR (n = 3). Values represent the mean ± S.D. $^{**}P < 0.01$, $^{***}P < 0.001$ (two-sided Student's *t*-test). (f) Two days before androgen stimulation, BicR cells were transfected with anti-NC, anti-miR-29a/b, or anti-miR-29a/b + si*TET2* #1 (1 nM). BicR cells were treated with 10 nM DHT or vehicle for 24 h. ChIP analysis was performed using anti-AcH3K9, polII, FOXA1, and AR antibodies. Enrichments were measured by qPCR and normalized by an IgG control (n = 3). Values represent the mean ± S.D. $^{*}P < 0.05$, $^{**}P < 0.01$ (two-sided Student's *t*-test). (g) Lysates from LNCaP and BicR cells transfected with anti-NC or anti-miR-29a/b were analyzed by western blot analysis to detect *mTOR* signals in prostate cancer.

Figure 8. Critical role of TET2 in regulating androgen signaling and AR.

(a) Knockdown of *TET2* induced gene transcription. Microarray analysis was performed to explore the effect of TET2 on gene expression profiles. LNCaP cells were treated with siControl or si*TET2* #1 (1 nM) for 48 h. (b) AR transcriptional activity is enhanced by *TET2* knockdown. LNCaP cells were treated with siControl, si*TET2* #1, or si*TET2* #2 (1 nM) for 48 h. Cells were treated with vehicle or 10 nM DHT for 24 h. mRNA expression levels were measured by qRT-PCR (n = 3). Values represent the mean ± S.D. $^{**}P < 0.01$ (two-sided Student's *t*-test). (c) AR transcriptional activity is repressed by TET2

overexpression. VCaP cells were transfected with a TET2 expression vector (Halo-TET2) or empty vector. After 48 h incubation, cells were treated with vehicle or 10 nM DHT for 24 h. Expression levels of mRNAs were measured by qPCR (n = 3). Values represent the mean ± S.D. $^{**}P < 0.01$ (two-sided Student's t-test). (d) Reduced expression of miR-29a/b repressed androgen-mediated gene induction. BicR cells were transfected with control, anti-miR-29a/b, or anti-miR-29a/b + si*TET2* #1 (1 nM) (n = 3). Values represent the mean ± S.D. $^{**}P < 0.01$ (two-sided Student's t-test). (e) VCaP cells were transfected with anti-NC, anti-miR-29a/b, or anti-miR-29a/b + si*TET2* #1 (1 nM). After incubation for 72 h, cells were treated with DHT or vehicle for 24 h. Expression levels of androgen-regulated genes were analyzed by qRT-PCR (n = 3). Values represent the mean ± S.D. $^{**}P < 0.01$ (two-sided Student's t-test). (f) Up-regulation of p-AR (ser81) in BicR cells in the absence of 10 nM DHT or 10 μM bicalutamide treatment compared with LNCaP cells. LNCaP, BicR, cells were treated with vehicle, 10 nM DHT, or 10 μM bicalutamide for 24 h. Western blot analysis was performed to evaluate the protein levels of p-AR. (g) BicR cells were treated with anti-NC or anti-miR-29a/b for 48 h. Cells were treated with vehicle, 10 nM DHT, or 10 μM bicalutamide for 24 h. Western blot analysis was performed to evaluate the protein levels of p-AR. (h) Expression level of phosphorylated AR (Ser81) in tumors derived from BicR cells by western blot analysis. (i) Working model of TET2 repression

by AR-regulated miRNAs or antagonist-bound AR to control the genome-wide 5-hmC status for prostate cancer progression.

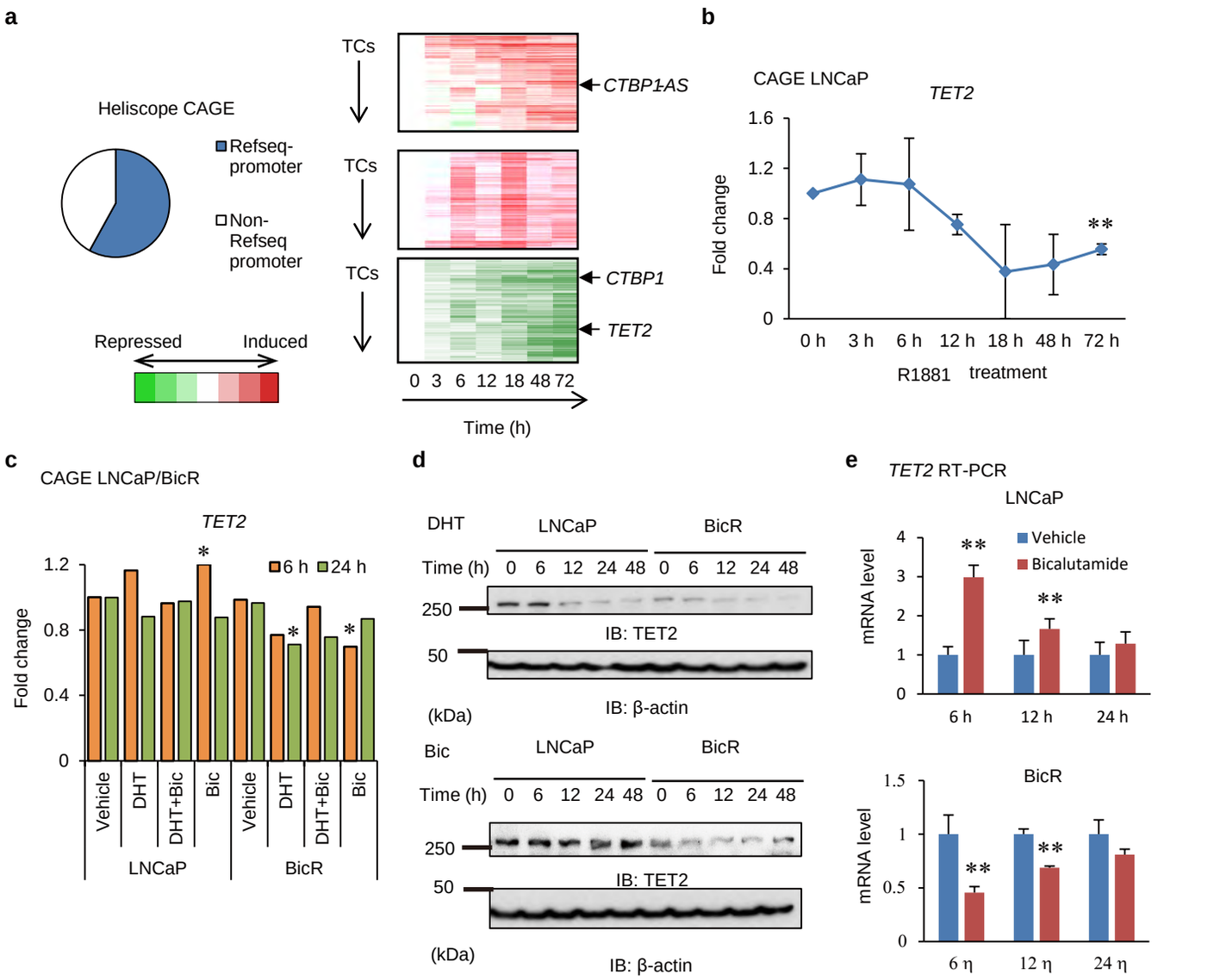

Figure 1 (Inoue)

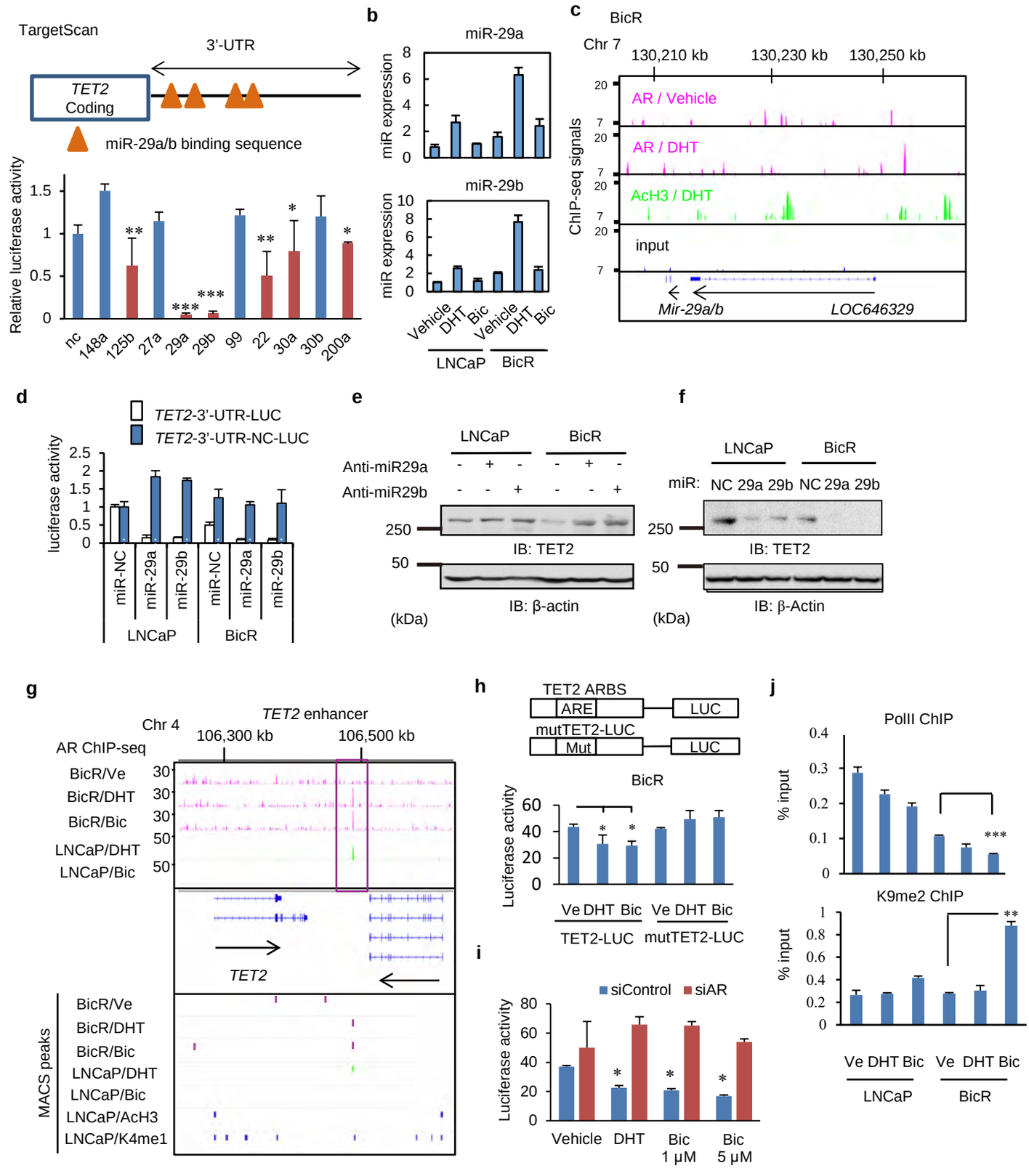

Figure 2 (Inoue)

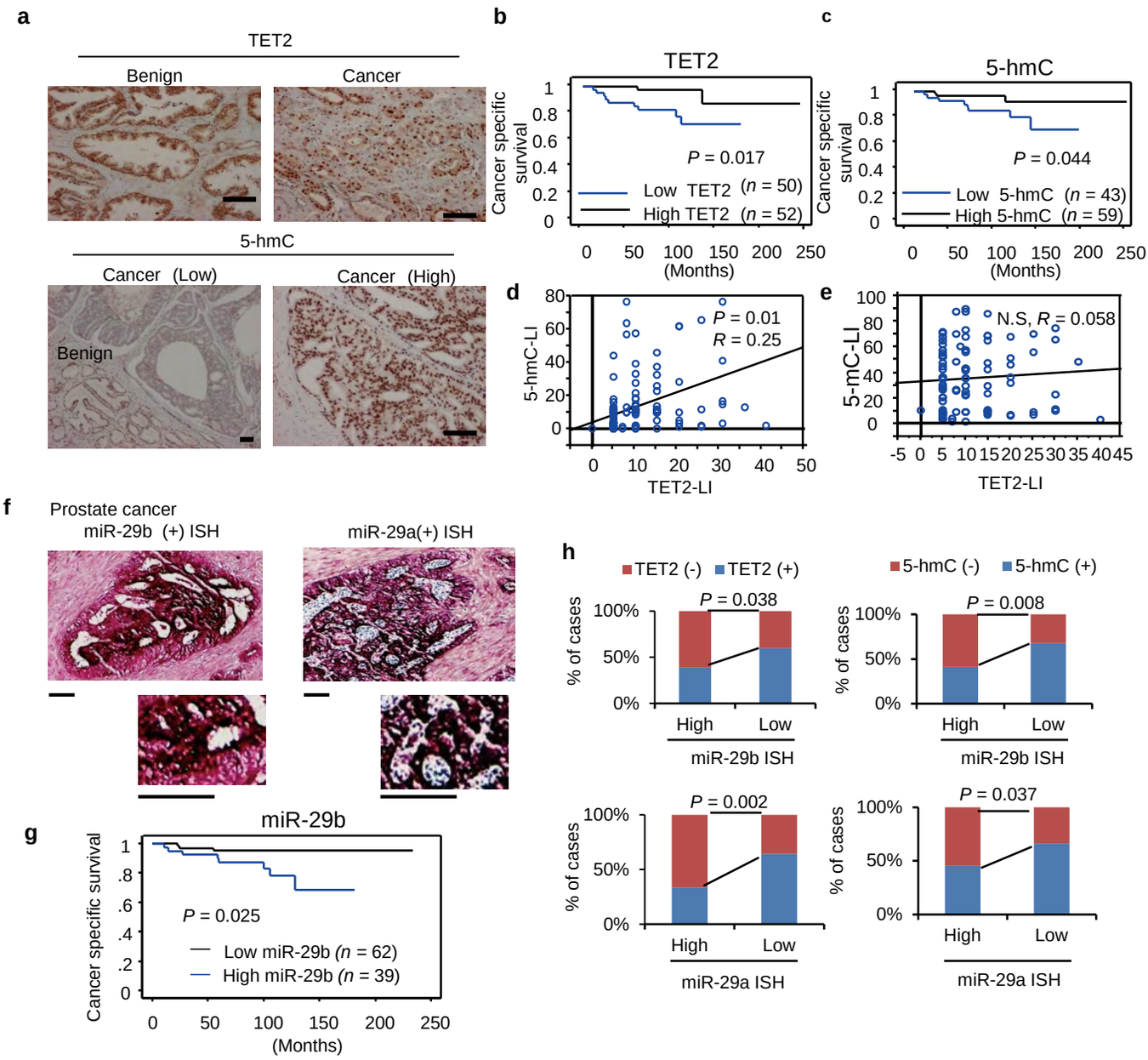

Figure 3 (Inoue)

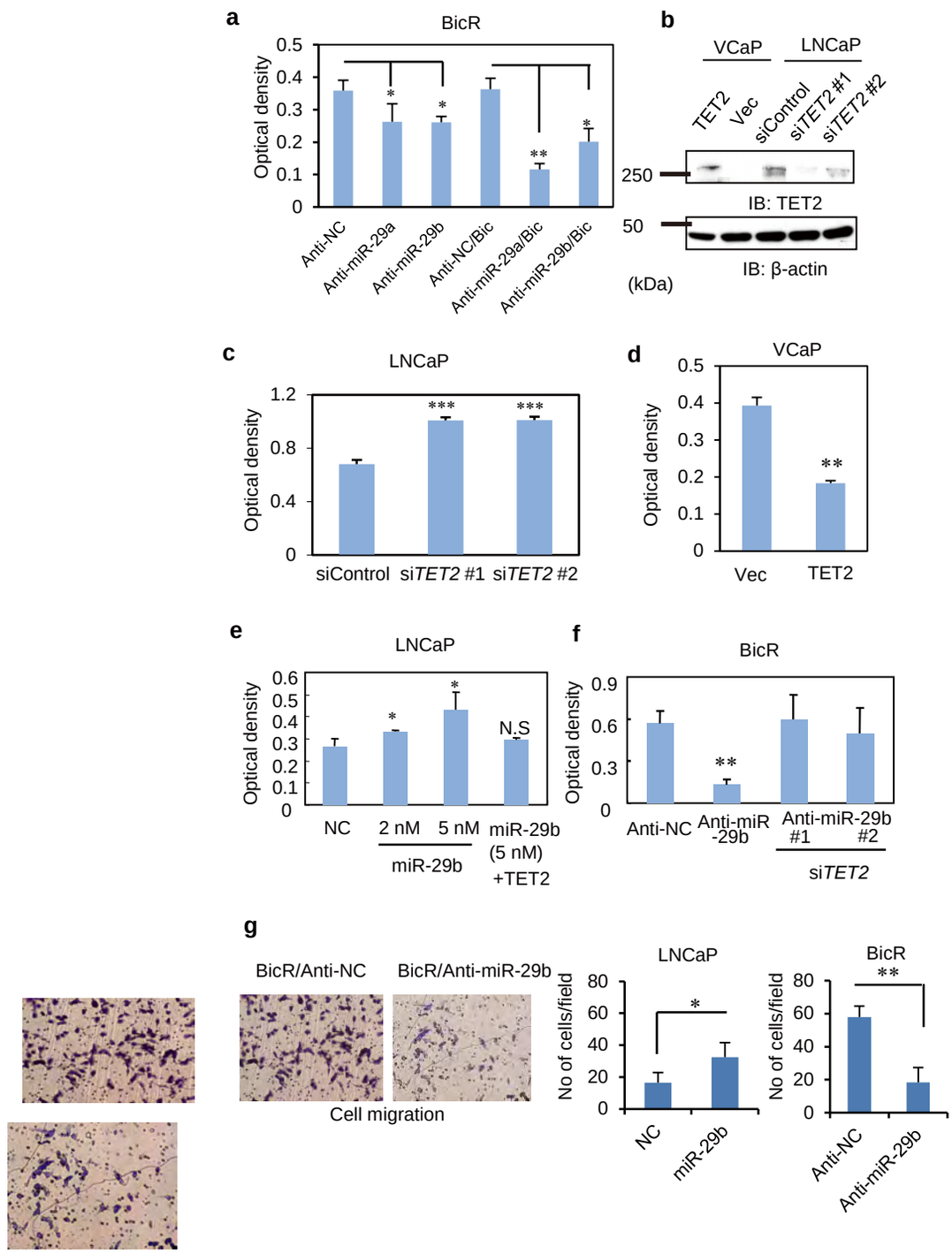

Figure 4 (Inoue)

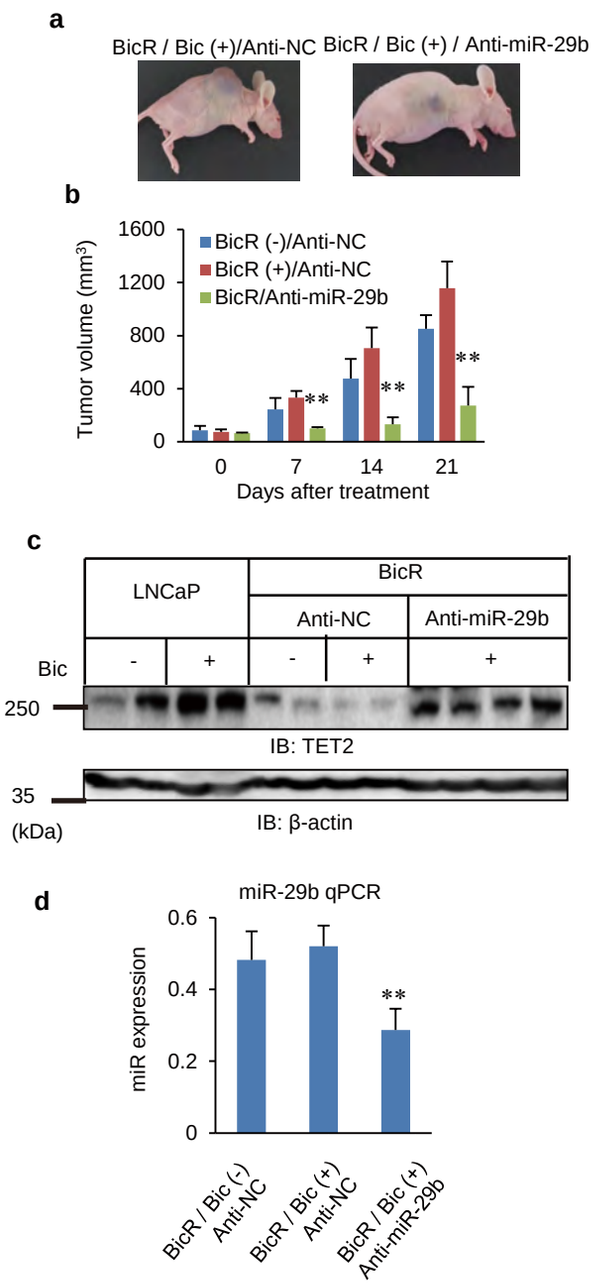

Figure 5 (Inoue)

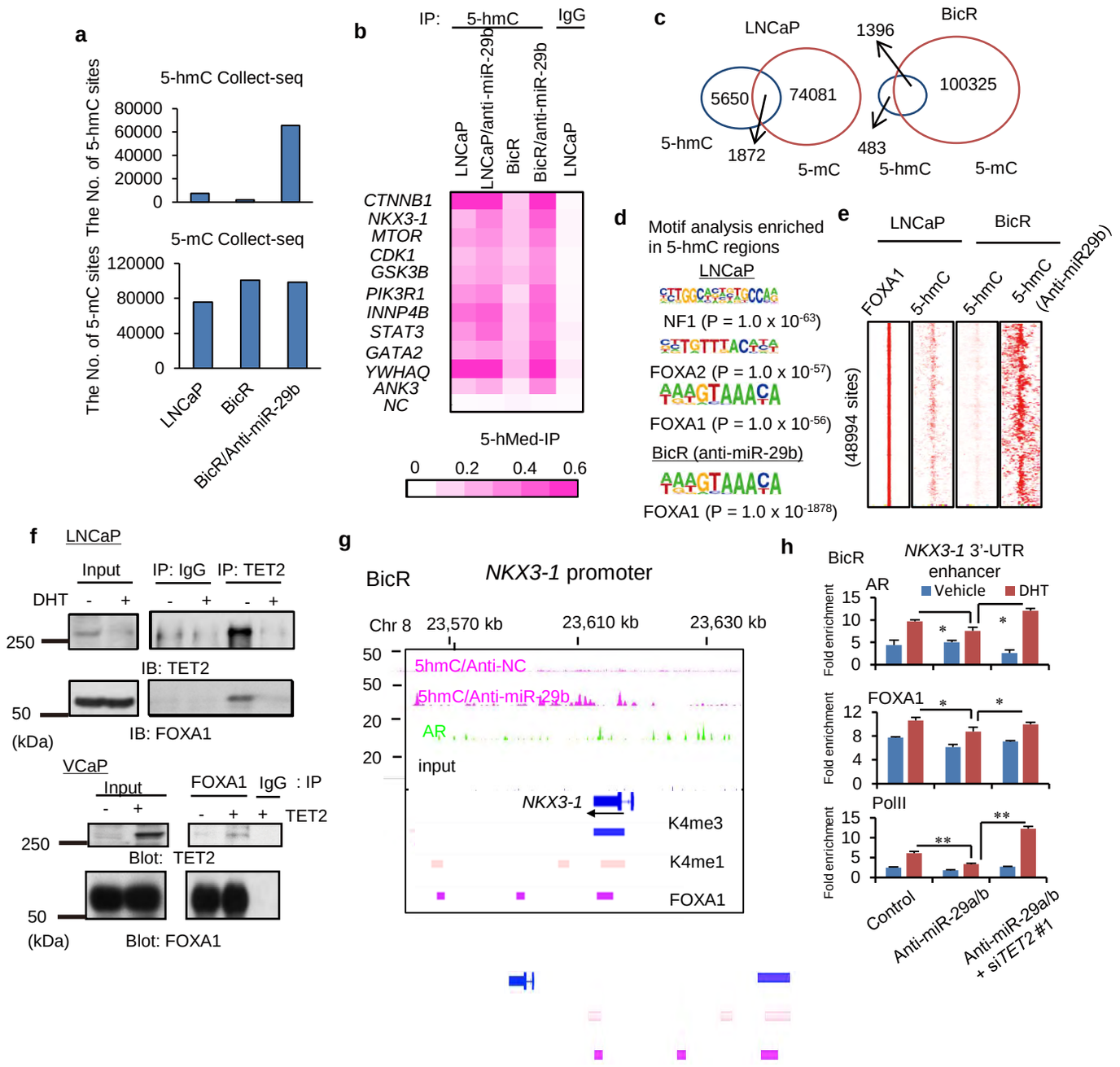

Figure 6 (Inoue)

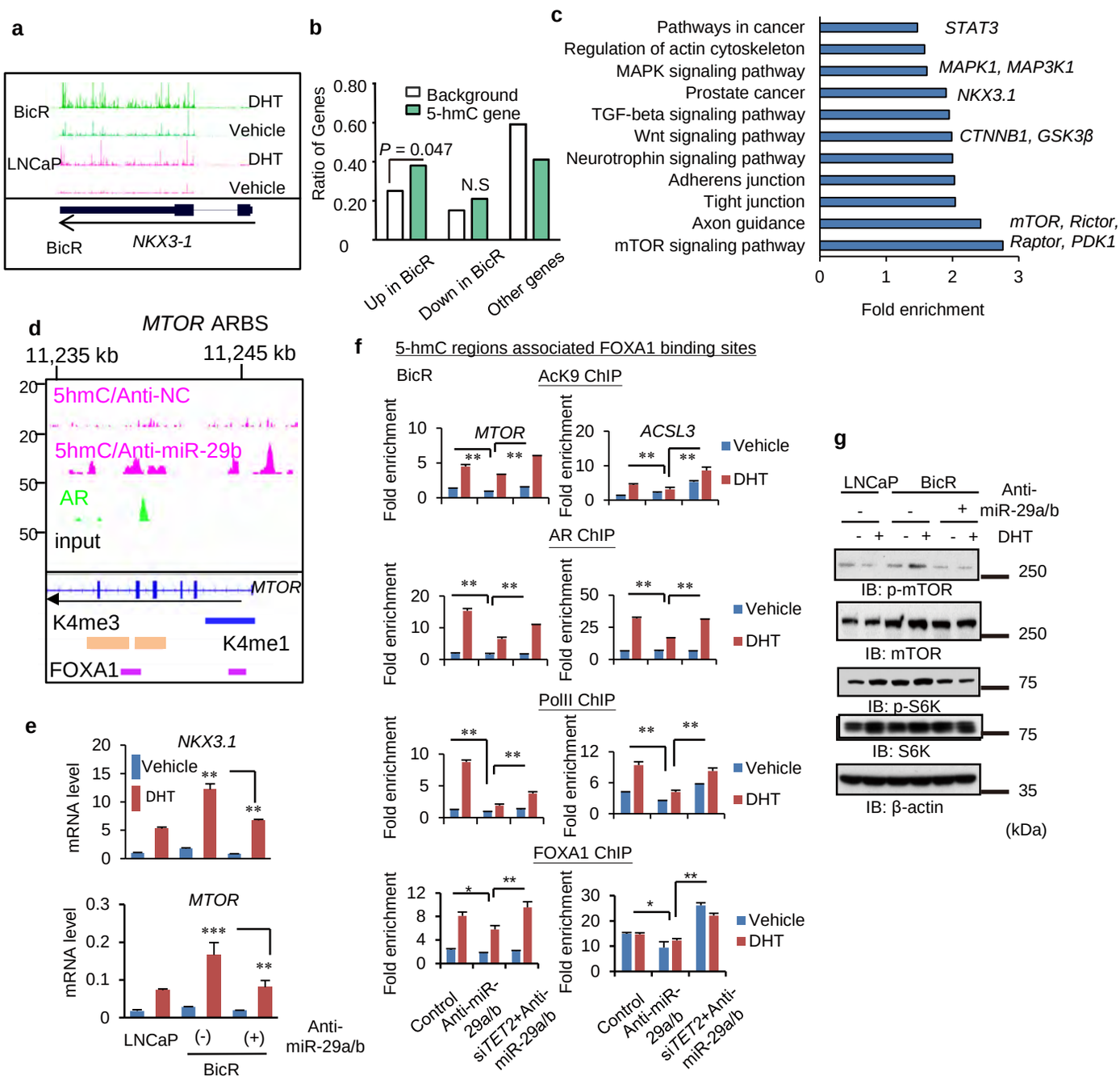

Figure 7 (Inoue)

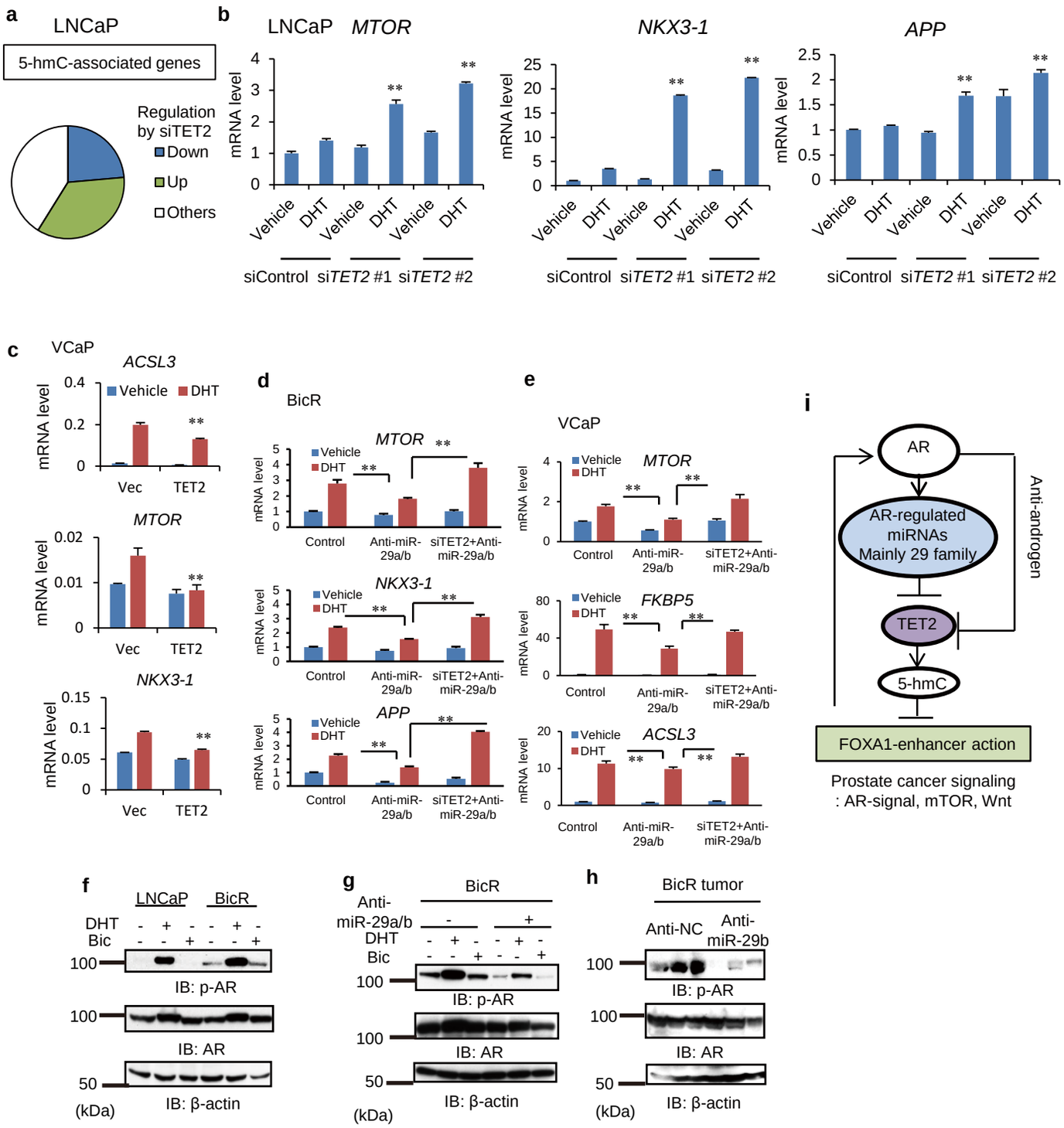

Figure 8 (Inoue)

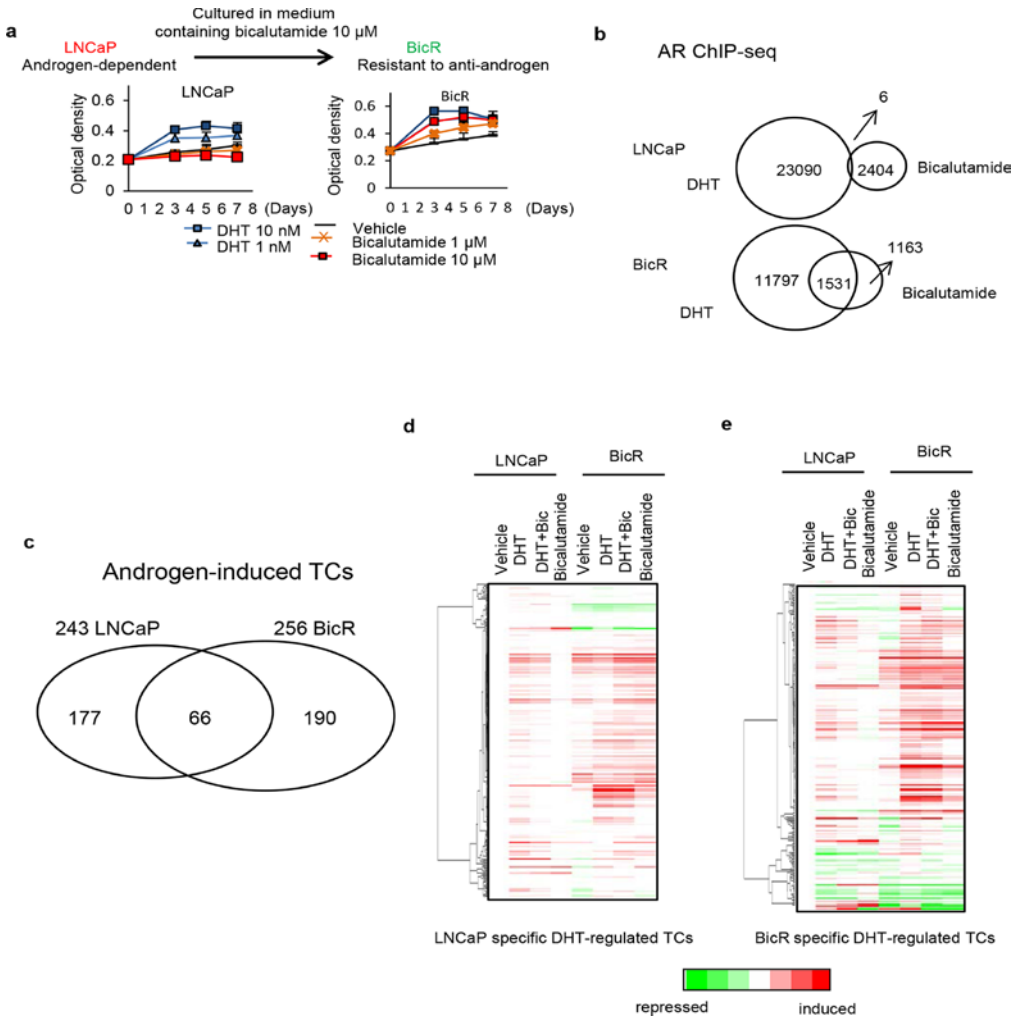

Supplementary Figure 1. HeliScope CAGE revealed androgen-regulated signaling and differentially regulated promoters in hormone-refractory prostate cancer cells.

(a) Cell proliferation of BicR cells in the presence of bicalutamide. We established bicalutamide-resistant (BicR) cell lines by cultivating LNCaP cells in media containing 10 μM bicalutamide for more than three months. We used parental LNCaP cells cultured without bicalutamide as the control. MTS assay was performed in both LNCaP and BicR cells. Cells were treated with vehicle, DHT (1, 10 nM), or bicalutamide (1, 10μM). Cell proliferation was enhanced in BicR cells compared with parental LNCaP cells (n = 4). We confirmed that the cell proliferation of BicR cells was not inhibited by bicalutamide treatment, although LNCaP cell proliferation was inhibited.

(b) AR ChIP-seq analysis in LNCaP and BicR cells. Both cell lines were treated with vehicle, DHT 10 nM, or Bicalutamide 1 μM) for 24 h. AR ChIP analysis was

performed and sequenced. Significant AR binding sites were determined by MACS.

(c) Identification of differentially regulated-promoters in hormone refractory prostate cancer cells. Both LNCaP and BicR cells were treated with vehicle, 10 nM DHT, 10 nM DHT + 1μM bicalutamide, or 1μM bicalutamide for 24 h. Heliscope CAGE analysis was performed on these 8 samples. We identified 243 promoters that were upregulated by more than 2-fold by DHT in LNCaP cells and 256 in BicR cells. Although 66 were commonly regulated in both cells, others were cell-type specific.

(d) Androgen-regulated promoters in LNCaP cells. They were up-regulated in the absence of DHT in BicR cells, suggesting androgen hypersensitivity in BicR cells.

(e) Androgen-regulated promoters in BicR cells. Enhancement of androgen-responsiveness in BicR cells was observed.

a Short-RNA sequence

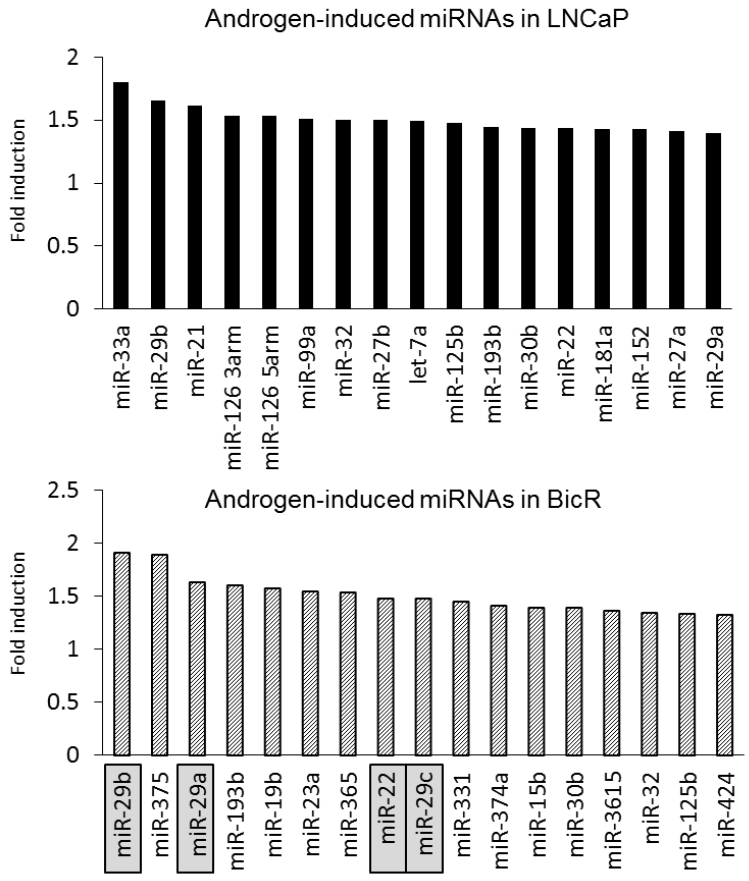

b

miR-22 target scan		miR-29 target scan	
FUT9	−0.84	ATAD2B	−1.3
CCDC67	−0.76	COL3A1	−0.93
CBL	−0.65	ELN	−0.81
TET2	−0.63	HBP1	−0.8
H3F3B	−0.6	COL4A4	−0.77
DDIT4	−0.56	SUV420H2	−0.75
MUM1L1	−0.56	HIF3A	−0.74
NET1	−0.55	***TET2***	−0.73
LAMC1	−0.55	COL5A3	−0.73
PLCXD3	−0.54	ADAMTS2	−0.71

Supplementary Figure 2. Identification of androgen-regulated miRNAs by short RNA-sequence in LNCaP and BicR cells.

(a) Top 17 androgen-regulated miRNAs in each cell line are summarized. Fold inductions by 10 nM DHT treatment for 24 h are presented.

(b) TargetScan analysis of miR-22 and miR-29 family showed that TET2 is a common target of both miRNAs. The context of the sites within the UTR (total context score) is shown.

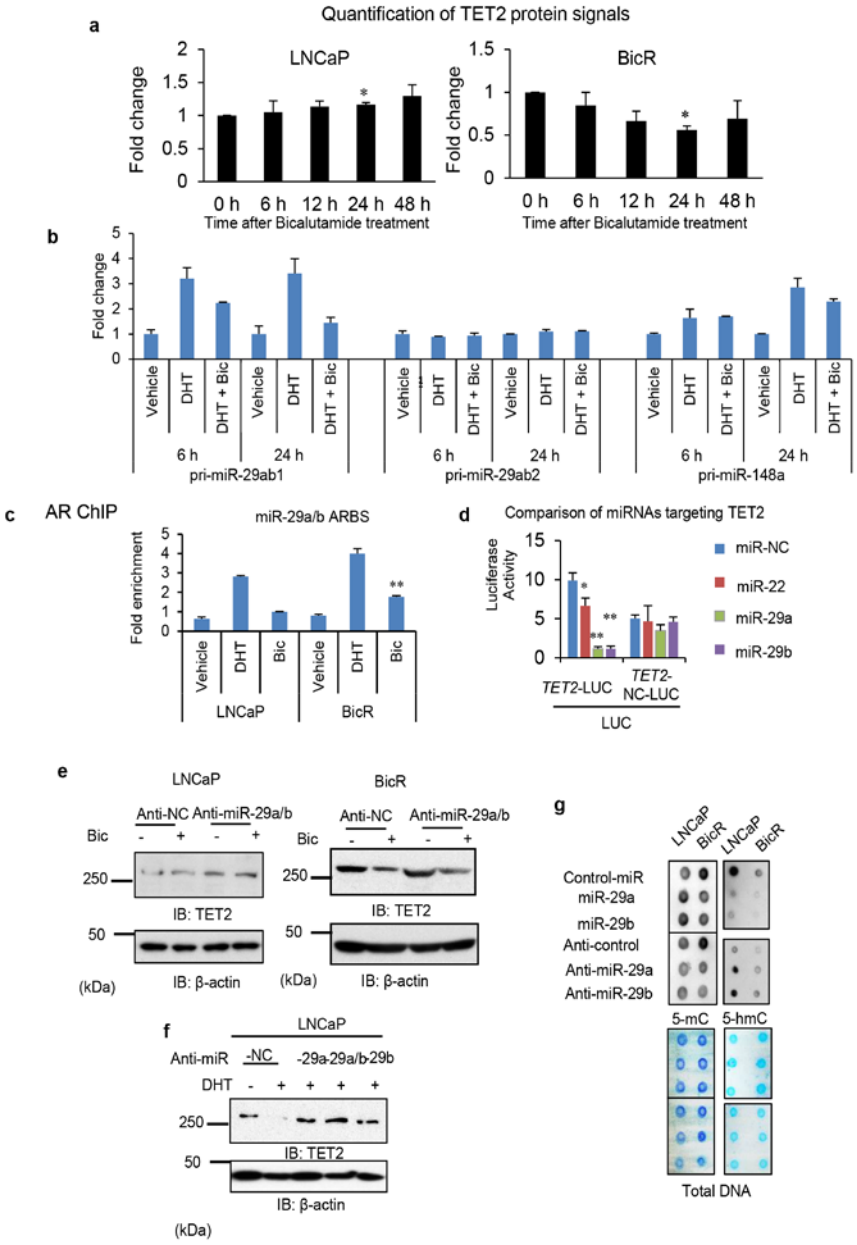

Supplementary Figure 3. TET2 repression is dependent on miR-29a/b expression in prostate cancer cells.

(a) Quantification of Western blotting in Figure 1d. We measured the signals of bands, normalized by β-actin and fold change relative to 0 h was calculated (n = 3). Values represent the mean ± S.D. *P < 0.05 (two-sided Student's t-test).

(b) Cells were treated with vehicle, DHT (100 nM), or DHT with 10 μM bicalutamide for 6 h or 24 h. Expression levels of primary miRNAs miR-29b1, miR-29b2, and positive control miR (miR-148a) were analyzed by qRT-PCR (n = 3). Values

represent the mean ± S.D. We found pri-miR-29ab1 to be the dominant primary transcript regulated by androgen.

(c) Validation of AR ChIP-seq analysis in LNCaP and BicR cells. After 72 h of hormone depletion, both cell lines were treated with vehicle, DHT, or bicalutamide for 24 h, and then AR ChIP analysis was performed. Enrichment of the ARBS regions (miR-29a/b ARBSs shown in Figure 2) were quantified using qPCR (n = 3). Values represent the mean ± S.D. $^{**}P < 0.01$ (two-sided Student's t-test).

(d) Luciferase analysis of TET2 repression by androgen-regulated miRNAs. Luciferase vectors *TET2*-3'-UTR or *TET2*-3'-UTR-NC with control miR (NC), miR-22 or 29a/b were transfected into LNCaP cells. Cells were lysed after 48 h transfection and luciferase assay was performed (n = 3). Values represent the mean ± S.D. $^{*}P < 0.05$, $^{**}P < 0.01$ (two-sided Student's t-test).

(e) LNCaP and BicR cells were treated with vehicle or 1 μM bicalutamide for 24 h. Cells were transfected with anti-negative control (anti-NC) or anti-miR29a/b. TET2 protein levels were analyzed by western blot analysis.

(f) LNCaP cells were treated with 10 nM DHT for 24 h. Cells were transfected with anti-NC, anti-miR-29a, b or a/b. TET2 protein levels were analyzed by western blot analysis.

(g) Genomic DNA from LNCaP and BicR cells transfected with anti-miR-29a/b or miR-29a/b was analyzed for 5-mC and 5-hmC levels using dot blot analysis.

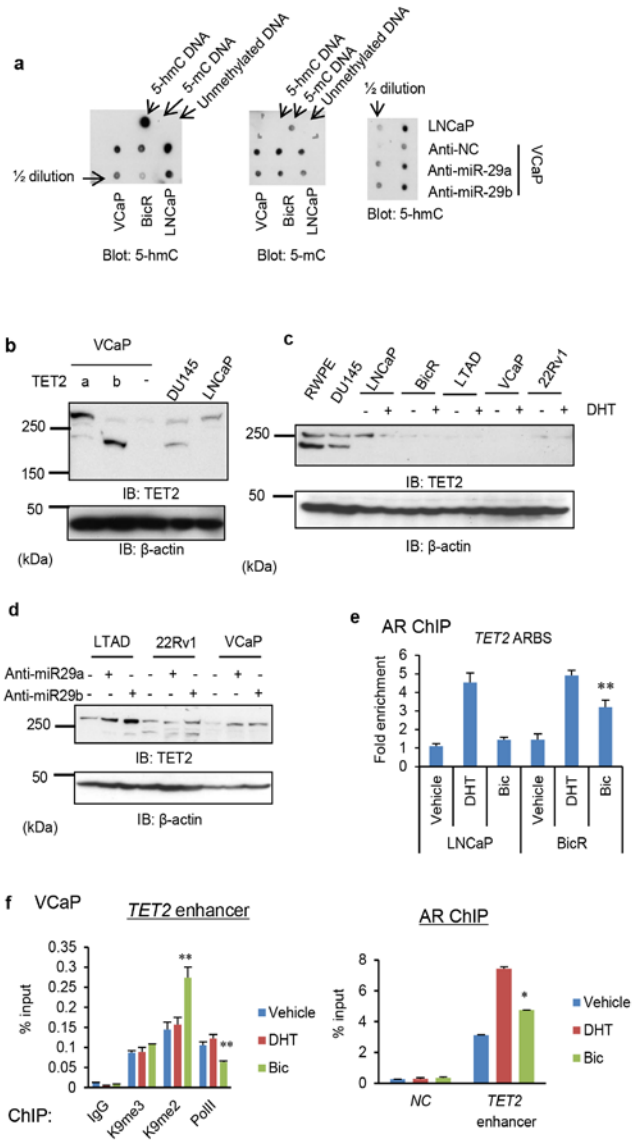

Supplementary Figure 4. Regulation of TET2 expression in other prostate cancer cell lines

(a) Comparison of 5-hmC and 5-mC in three cell lines (LNCaP, BicR, and VCaP cells) by dot blot analysis. 5-mC was increased in all three cell lines. However, 5-hmC was reduced in BicR and VCaP cells. We also validated the induction of 5-hmC by anti-miR-29a/b. These results are consistent with the TET2 western blot analysis presented in Supplementary Fig. 4c. No cross reaction of the antibody with 5-mC was observed.

(b) Analysis of TET2 variants in prostate cancer cells. 293T cells were transfected with Halo-TET2a or Halo-TET2b. After 48 h, the cells were lysed. TET2 protein levels were analyzed by western blot analysis. Prostate cancer cell extracts (DU145 and LNCaP cells) were also analyzed.

(c) TET2 is repressed in AR positive hormone-refractory prostate cancer cell lines. TET2 protein levels were analyzed by western blot analysis in RWPE, DU145, LNCaP, BicR, long term androgen deprivation (LTAD), VCaP, and 22RV1 cells with or without 10 nM DHT treatment.

(d) LTAD, 22RV1 and VCaP cells were transfected with anti-NC, anti-miR29a, or anti-miR-29b for 48 h. TET2 protein levels were analyzed by western blot analysis.

(e) Recruitment of AR to *TET2* ARBS is responsible for repression of *TET2* enhancer. AR ChIP analysis was performed. Enrichment of the ARBS regions (miR-29a/b ARBSs shown in Figure 2) were quantified using qPCR (n = 3). Values represent the mean ± S.D. $^{**}P < 0.01$ (two-sided Student's t-test).

(f) ChIP analysis of AR, H3K9me2, H3K9me3 and RNA polII were performed in VCaP cells. Enrichment in the *TET2* ARBS was analyzed by qPCR (n = 3). Values represent the mean ± S.D. $^{*}P < 0.05$, $^{**}P < 0.01$ (two-sided Student's t-test).

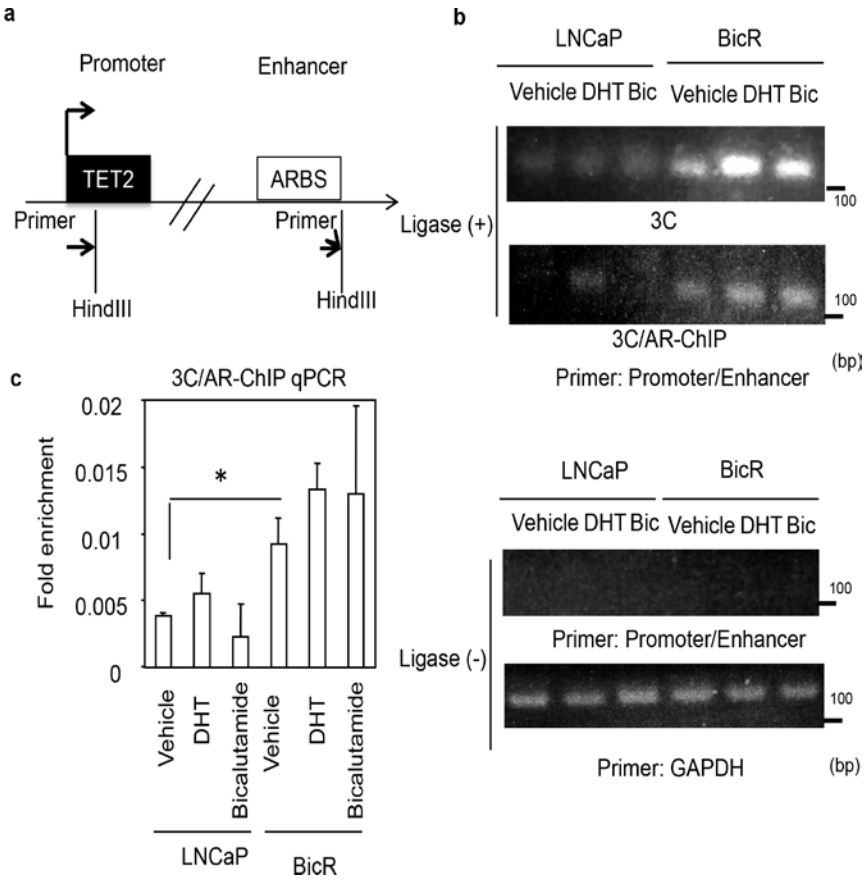

Supplementary Figure 5. AR binding to distal enhancer plays a role in the chromatin conformational change.

(a) Long-range interactions between the TET2 promoter and enhancer, determined using 3C/ChIP assay. The vertical black bars represent each HindIII fragment in the corresponding regions.

(b) 3C products were amplified by primers specific for *TET2* locus. *GAPDH* was used as a positive control for PCR amplification. Ligase (-) samples were used as negative controls.

(c) Frequency quantification by qPCR analysis. Relative amplification to *GAPDH* locus is shown (n = 3). Values represent the mean ± S.D. *P < 0.05 (two-sided Student's t-test).

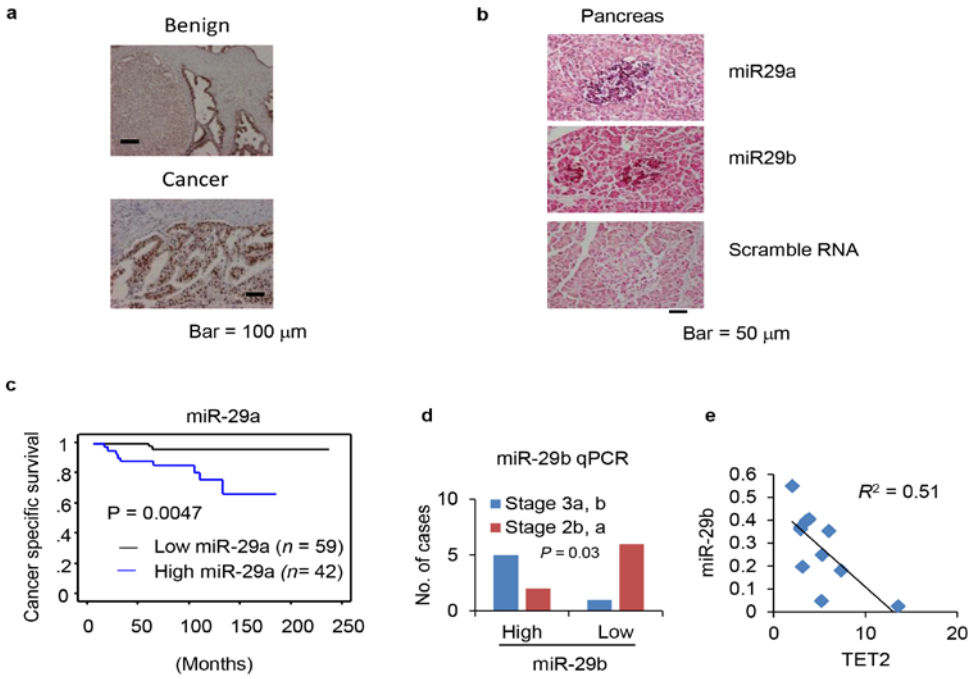

Supplementary Figure 6. Analysis of TET2 and miR-29a/b expression in prostate cancer tissues.

(a) Immunohistochemistry of 5-mC in prostate cancer and benign prostate tissues (*n* = 102).

(b) Positive and negative controls for miRNA-29a/b ISH analysis. Specimens from the pancreas (islets of Langerhans) were probed with miRNA-29a/b or negative control (Scramble RNAs). We detected ISH signals in the islets with miRNA probes. However, no signal was detected with scramble RNAs.

(c) High miR-29a expression is a prognostic factor for prostate cancer patients. Kaplan–Meier analysis using the log-rank test was performed.

(d) Analysis of miR-29b in prostate cancer samples. Total RNA was extracted from prostate cancer tissues by laser capture microdissection (LCM) (*n* = 14). Expression levels of miR-29b were measured by miRNA qRT-PCR. A significant association of miR-29b with pathological stages was observed. Chi-square test was performed to obtain *P*- value.

(e) Expression levels of miR-29b are negatively associated with *TET2* expression. Expression levels of *TET2* were measured by qRT-PCR (*n* = 12). Regression analysis was performed.

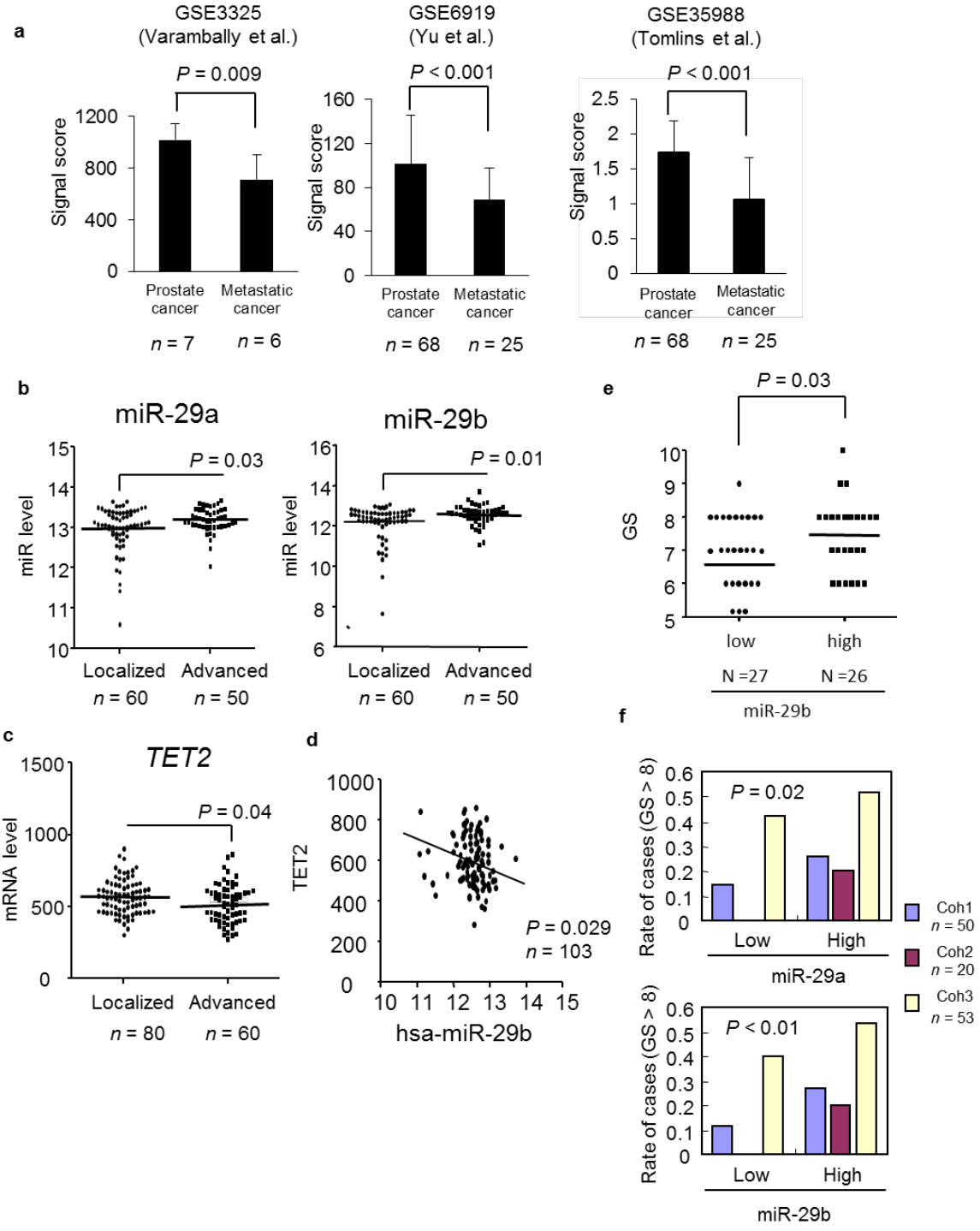

Supplementary Figure 7. Analysis of miR-29a/b expression and TET2 in other cohorts.

(a) TET2 expression is repressed in metastatic prostate cancer tissues. Three datasets of microarray (GSE3325, GSE6919 and GSE35988, Supplementary ref. 1-3) were

downloaded from GEO datasets. Significant repression of TET2 was determined by Student's t-test. Values represent the mean ± S.D.

(b) Upregulation of miR-29a/b in advanced prostate cancer tissues. Cases (Taylor et al. GSE21036, Supplementary ref. 4) were classified to advanced (clinical stage ≧ T2 or pathological stage ≧ T3C) or localized. Significance was determined by Wilcoxon signed-rank test.

(c) Downregulation of TET2 in advanced prostate cancer tissues. Cases (Taylor et al. GSE21034) were classified to advanced (clinical stage ≧ T2 or pathological stage ≧ T3A) or localized. Significance was determined by Wilcoxon signed-rank test.

(d) Expression levels of miR-29b are negatively associated with TET2 expression. Cases commonly included in GSE21034 and GSE21036 were selected. Significance was determined using Spearman rank correlation test (R = -0.18).

(e) MiR-29a/b expression was significantly associated with high Gleason scores in prostate cancer tissues. Three datasets of microarray (Cohort1: GSE45604, Cohort2: GSE23022 and Cohort3: GSE46738; Supplementary ref. 5, 6) were downloaded from GEO datasets. In cohort3, Gleason scores were divided into high or low miR-29b expression groups. Wilcoxon signed-rank test was performed to obtain a P-value.

(f) In all three cohorts, cases with high Gleason score (GS >8) were enriched in the high miR-29a/b expressed group. Chi-square tests were performed combining the data to obtain a P-value.

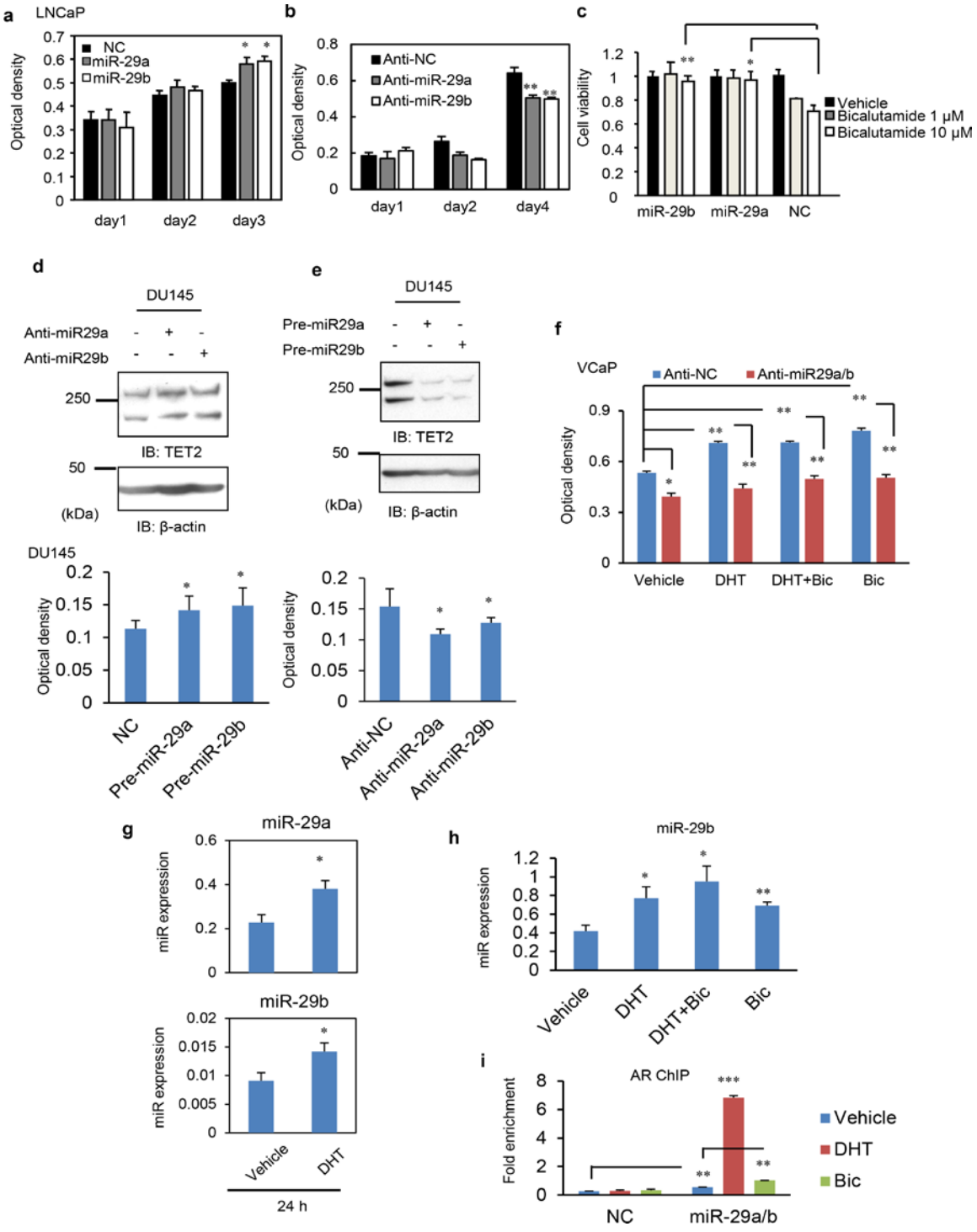

Supplementary Figure 8. Overexpression of miR-29a/b promotes prostate cancer cell proliferation and resistance to bicalutamide.

(a) miR-29a and miR-29b overexpression promotes cell proliferation. An MTS assay was performed in LNCaP cells transfected with control miR (NC), miR-29a or

miR-29b on days 0, 3 and 5 (n = 4). Transfection condition is shown in Supplementary Table 7. Values represent the mean ± S.D. *P < 0.05 (two-sided Student's t-test).

(b) Knockdown of miR-29a and miR-29b repressed cell proliferation. An MTS assay was performed in LNCaP cells transfected with anti-miR-29a, anti-miR-29b, or anti-NC on day 5 (n = 4). Bar: s.d. **P < 0.01 (two-sided Student's t-test).

(c) An MTS assay was performed in LNCaP cells transfected with control miR, miR-29a or miR-29b on day 5. Cells were treated with vehicle or bicalutamide (1 or 10 μM). Repression of cell proliferation by bicalutamide was relieved by miR-29a and miR-29b transfection (n = 4). Values represent the mean ± S.D. *P < 0.05, **P < 0.01 (two-sided Student's t-test).

(d) Knockdown of miR-29a/b in DU145 cells. DU145 cells were transfected with anti-NC, anti-miR-29a, or anti-miR-29b. TET2 protein levels were analyzed by western blot analysis. Anti-NC, anti-miR-29a, or anti-miR-29b was transfected into DU145 cells. An MTS assay was performed on day 5 (n = 4). Values represent the mean ± S.D. *P < 0.05 (two-sided Student's t-test).

(e) DU145 cells were transfected with control miR, miR-29a, or miR-29b. TET2 protein levels were analyzed by western blot analysis. Control miR, miR-29a, or miR-29b was transfected into DU145 cells. An MTS assay was performed on day 5 (n = 4). Values represent the mean ± S.D. *P < 0.05 (two-sided Student's t-test).

(f) Knockdown of miR-29a/b in VCaP cells. Anti-NC or anti-miR-29a/b was transfected into VCaP cells and then incubated for 48 h. Cells were treated with vehicle, 10 nM DHT, 10 nM DHT + 10 μM bicalutamide, or 10 μM bicalutamide for 3 days. An MTS assay was performed to evaluate cell viability. VCaP cells were originally established from metastatic tissues of hormone-refractory prostate cancer. We observed that this cell line could proliferate in the presence of bicalutamide. Values represent the mean ± S.D. *P < 0.05, **P < 0.01 (two-sided Student's t-test).

(g) Induction of miR-29a and miR29b in VCaP cells in response to DHT. VCaP cells were treated with 10 nM DHT for 24 h. miRNA qPCR was performed to measure the expression level of miR-29a/b (n = 3). Values represent the mean ± S.D. *P < 0.05 (two-sided Student's t-test).

(h) miR-29b is also induced by bicalutamide treatment in VCaP cells. VCaP cells were treated with vehicle, 10 nM DHT, DHT + 10 μM bicalutamide, or 10 μM bicalutamide for 24 h. miRNA qPCR was performed to measure the expression level of miR-29b (n = 3). Values represent the mean ± S.D. *P < 0.05, **P < 0.01 (two-sided Student's t-test).

(i) AR binding in miR-29a/b ARBS in VCaP cells. AR ChIP assay was performed in VCaP cells treated with vehicle, 10 nM DHT, or 10 μM bicalutamide for 24 h. Enrichment was measured by qPCR. Enrichment was observed in the vehicle condition and enhanced by both DHT and bicalutamide (n = 3). Values represent the mean ± S.D. $^{**}P < 0.01$, $^{***}P < 0.001$ (two-sided Student's t-test).

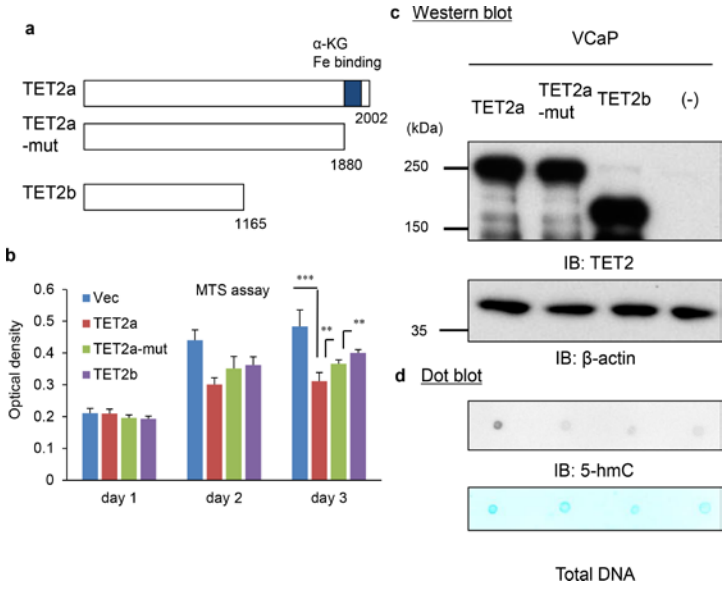

Supplementary Figure 9. Inhibition of the oxidative activity of TET2 alleviates the growth inhibitory activity.

(a) Deletion mutant of TET2 lacking the critically required domain for the catalytic function, Fe- and α-ketoglutarate (KG)-binding sites, was constructed. Another variant TET2b lacking the domain is also shown.

(b) VCaP cells were transfected with TET2a, TET2a-mutants or TET2b. MTS assay was performed at the indicated time points to evaluate cell growth (n = 4). Values represent the mean ± S.D. *P < 0.05, **P < 0.01 (two-sided Student's t-test).

(c) Western blot analysis was performed to analyze the expression of exogenous TET2.

(d) DNA dot blot analysis was performed to analyze the 5-hmC levels.

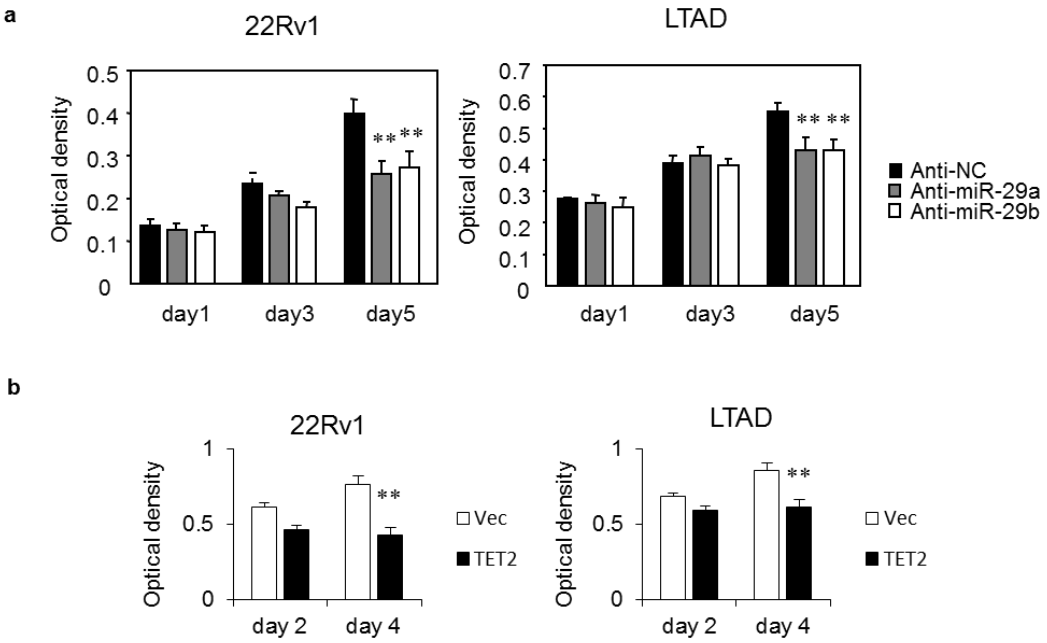

Supplementary Figure 10. Role of miR-29a/b in castration-resistant prostate cancer cell proliferation.

(a) LTAD and 22Rv1 cells were transfected with anti-NC or anti-miR-29a/b.

(b) LTAD and 22Rv1 cells were transfected with TET2 expression vector. MTS assay was performed to analyze castration-resistant cell growth (n = 4). Values represent the mean ± S.D. **P < 0.01 (two-sided Student's t-test).

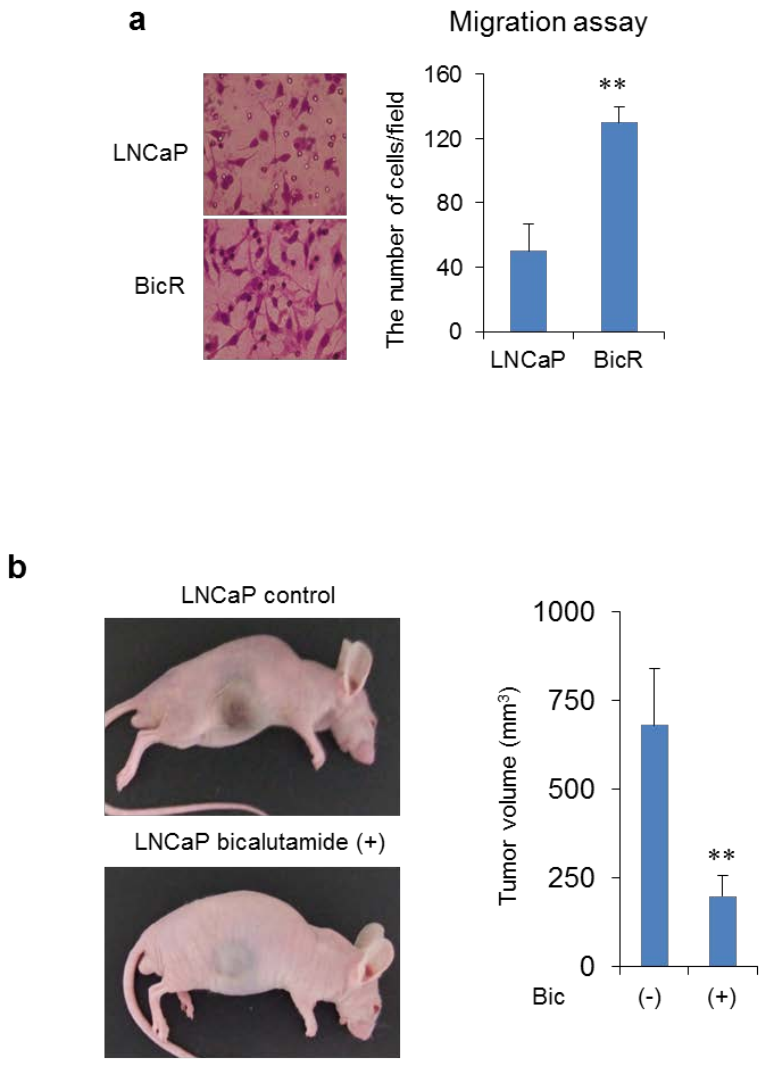

Supplementary Figure 11. Enhancement of cell migration in BicR cells and bicalutamide treatment inhibits the growth of tumours derived from LNCaP cells.

(a) Cell migration assay using LNCaP and BicR cells. We observed an increase in cell migration in BicR cells (n = 5). Values represent the mean ± S.D. $^{**}P < 0.01$ (two-sided Student's t-test).

(b) Nude mice were inoculated with LNCaP cells. Vehicle (n = 6) or bicalutamide (n = 6) was orally administered each day for 4 weeks after tumor formation. Representative views of tumors in nude mice (left). Tumor volume of each group (right). Values represent the mean ± S.D. $^{**}P < 0.01$ (two-sided Student's t-test).

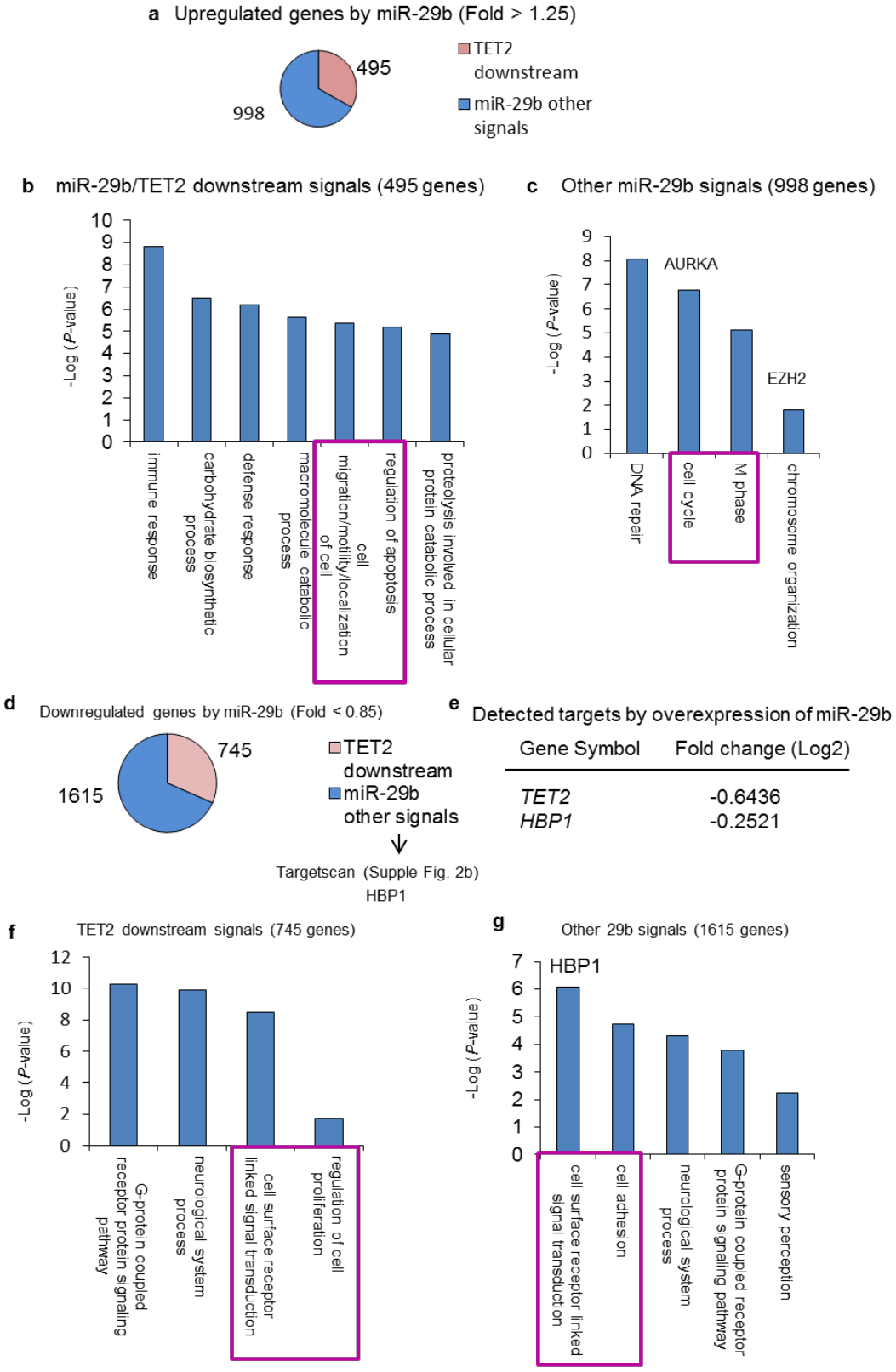

Supplementary Figure 12. Analysis of miR-29b target genes by microarray.

(a) Investigation of TET2 and miR-29b target genes in LNCaP cells. We treated LNCaP

cells with siControl, si*TET2* #1 (1nM), control miR, or miR-29b for 72 h. Total RNA was extracted and microarray analysis was performed. Upregulated genes between cells transfected with miR-29b or si*TET2* #1 were identified. Among 1493 gene upregulated (>1.25-fold relative to control) by miR-29b, 495 genes were also upreguated by TET2 repression, indicating that these genes are TET2 downstream signals. The other 998 genes were considered as additional genes regulated by miR-29b.

(b) GO term analysis of miR-29b and TET2 downstream signaling. *P*-value was obtained by using DAVID.

(c) GO terms for the other miR-29b-regulated genes are summarized. *EZH2* and *AURKA* were representative targets upregulated by miR-29b. *P*-value was obtained by using DAVID.

(d) Downregulated genes by miR-29b and si*TET2* #1 were also identified. MiR-29b target gene candidates were investigated by searching for putative binding sequences using TargetScan. Only *TET2* and *HBP1* were repressed by miR-29b overexpression in our microarray analysis.

(e) TET2 is the primary target gene in LNCaP cells. The reesults indicating the repression of HBP1 and TET2 by miR-29b in microarray are shown.

(f) GO term analysis of miR-29b and si*TET2*-mediated repressive pathways. *P*-value was obtained by using DAVID.

(g) GO term analysis of other miR-29b-mediated repressive pathways. *P*-value was obtained by using DAVID.

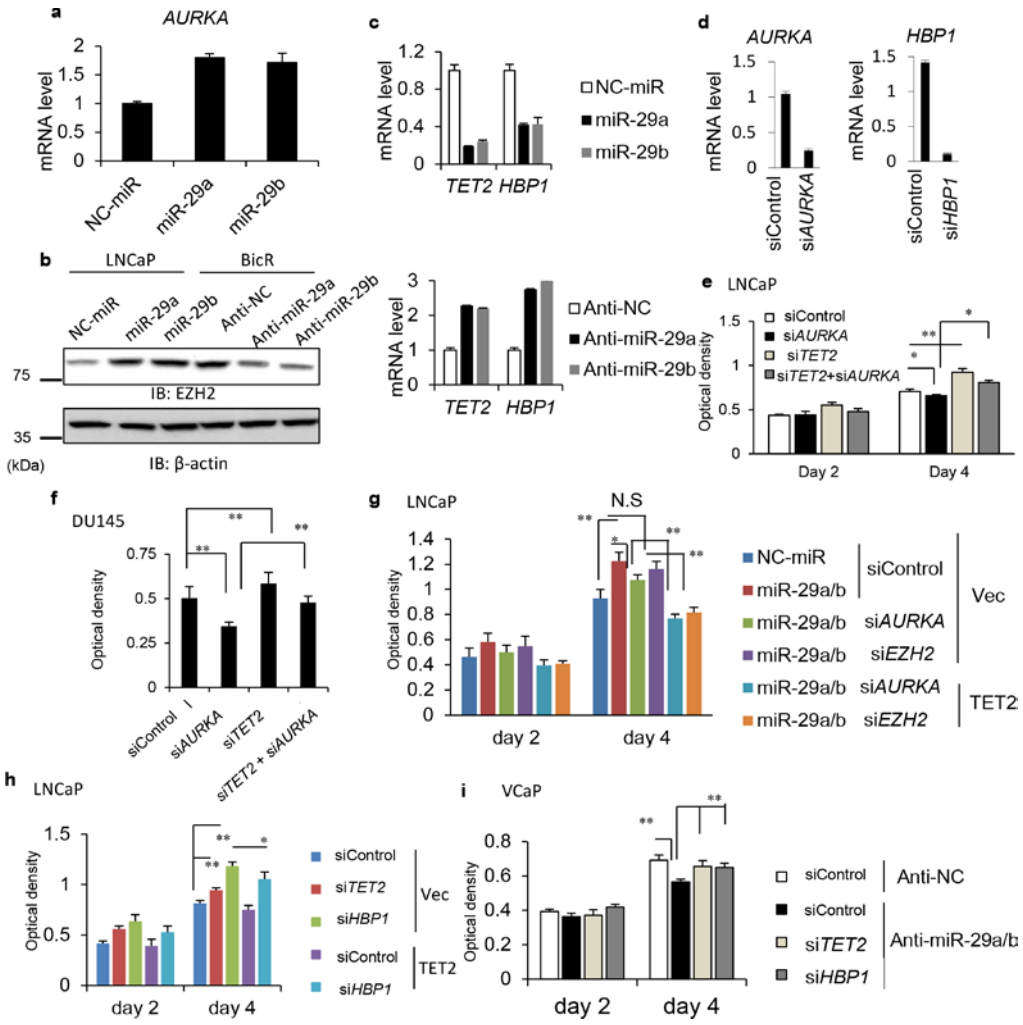

Supplementary Figure 13. Analysis of additional miR-29a/b target genes in prostate cancer.

(a) Upregulation of *AURKA* by miR-29a/b. LNCaP cells were transfected with control (NC) miR, miR-29a/b or anti-miR-29a/b. qRT-PCR analysis was performed to measure the expression level of *AURKA* (n = 3). Values represent the mean ± S.D.

(b) Upregulation of EZH2 by miR-29a/b. LNCaP cells were transfected with miR-29a/b or anti-miR-29a/b. Western blot analysis was performed to measure the expression level of EZH2.

(c) Downregulation of *TET2* and *HBP1* by miR-29a/b. LNCaP cells were transfected with miR-29a/b or anti-miR-29a/b. qRT-PCR analysis was performed to measure the expression level of HBP1 and TET2 (n = 3). Values represent the mean ± S.D.

(d) Knockdown of *AURKA* and *HBP1* by siRNA. LNCaP cells were transfected with siRNAs (10 nM) targeting *AURKA* and *HBP1*. mRNA levels were measured by qRT-PCR analysis (n = 3). Values represent the mean ± S.D.

(e) (f) Knockdown of *AURKA* inhibits cell growth. However, this effect is reversed by *TET2* knockdown. MTS assay was performed in LNCaP cells (e) or DU145 (f) cells to evaluate cell growth (n = 5). Values represent the mean ± S.D. *P < 0.05, **P < 0.01 (two-sided Student's t-test).

(g) miR-29a/b dependent cell growth promotion is inhibited by *AURKA* knockdown and completely rescued by TET2 overexpression. MTS assay was performed in LNCaP cells to evaluate the cell growth (n = 5). Values represent the mean ± S.D. *P < 0.05, **P < 0.01 (two-sided Student's t-test).

(h) Knockdown of *HBP1* and *TET2* promote cell growth. However, TET2 overexpression inhibits this effect. MTS assay was performed in LNCaP cells to evaluate cell growth (n = 5). Values represent the mean ± S.D. *P < 0.05, **P < 0.01 (two-sided Student's t-test).

(i) Growth inhibition by anti-miR-29a/b is rescued by *TET2* or *HBP1* knockdown. MTS assay was performed in VCaP cells to evaluate cell growth (n = 5). Values represent the mean ± S.D. **P < 0.01 (two-sided Student's t-test).

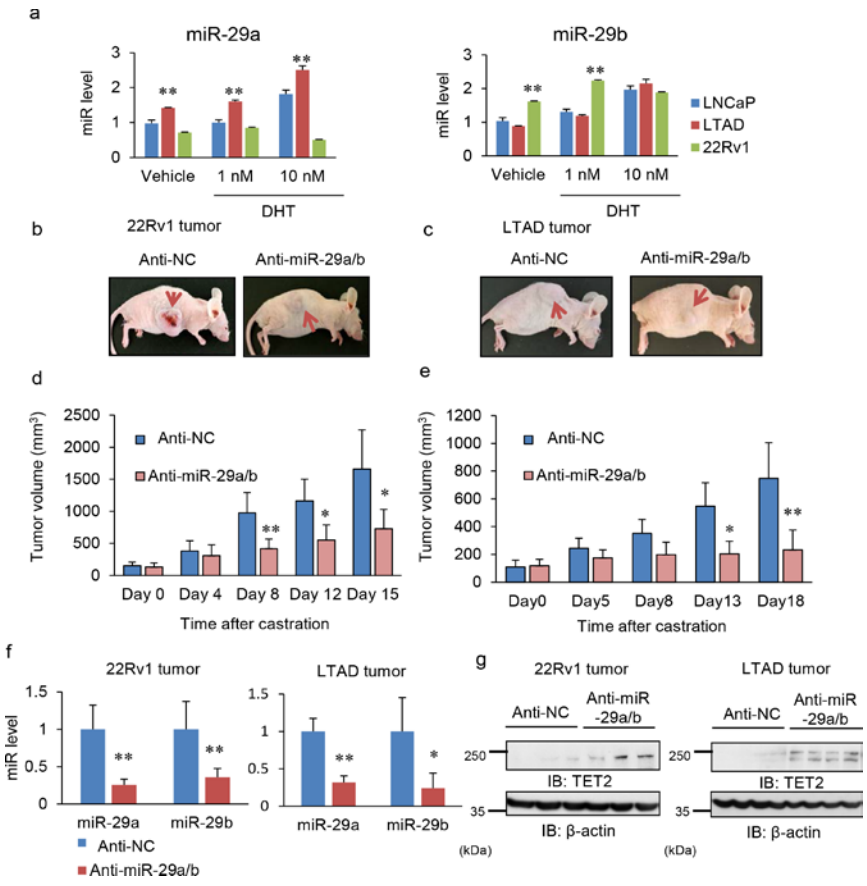

Supplementary Figure 14. Inhibition of tumor growth in castration-resistant prostate cancer xenograft models by repression of miR-29a/b.

(a) MiR-29a/b expression in 22Rv1 and LTAD cells compared with LNCaP cells. Cells were treated with vehicle, DHT 1 nM and 10 nM for 24 h. miRNA expression levels were analyzed by miRNA qPCR (n = 3). Values represent the mean ± S.D. *P < 0.05, **P < 0.01 (two-sided Student's t-test).

(b) Nude mice were inoculated with 22Rv1 cells. After tumor development, mice were castrated. Castrated mice were randomized and treated with anti-NC or anti-miR-29a/b. Representative views of tumors in nude mice are shown.

(c) Nude mice were inoculated with LTAD cells. After tumor development, mice were castrated. Castrated mice were randomized and treated with anti-NC or anti-miR-29a/b. Representative views of tumors in nude mice are shown.

(d) Tumor growth of 22Rv1 xenografts treated with anti-NC or anti-miR-29b are shown (n = 8). Values represent the mean ± S.D. *P < 0.05, **P < 0.01 (two-sided Student's t-test).

(e) Tumor growth of LTAD xenografts treated with anti-NC or anti-miR-29b are shown

(n = 6). Values represent the mean ± S.D. *P < 0.05, **P < 0.01 (two-sided Student's t-test).

(f) qRT-PCR was performed to measure the miRNA expression level in those tumors. Values represent the mean ± S.D (n = 4). *P < 0.05, **P < 0.01 (two-sided Student's t-test).

(g) Western blot analysis was performed to evaluate TET2 expression levels in tumors (22Rv1: n = 3, LTAD: n = 4)

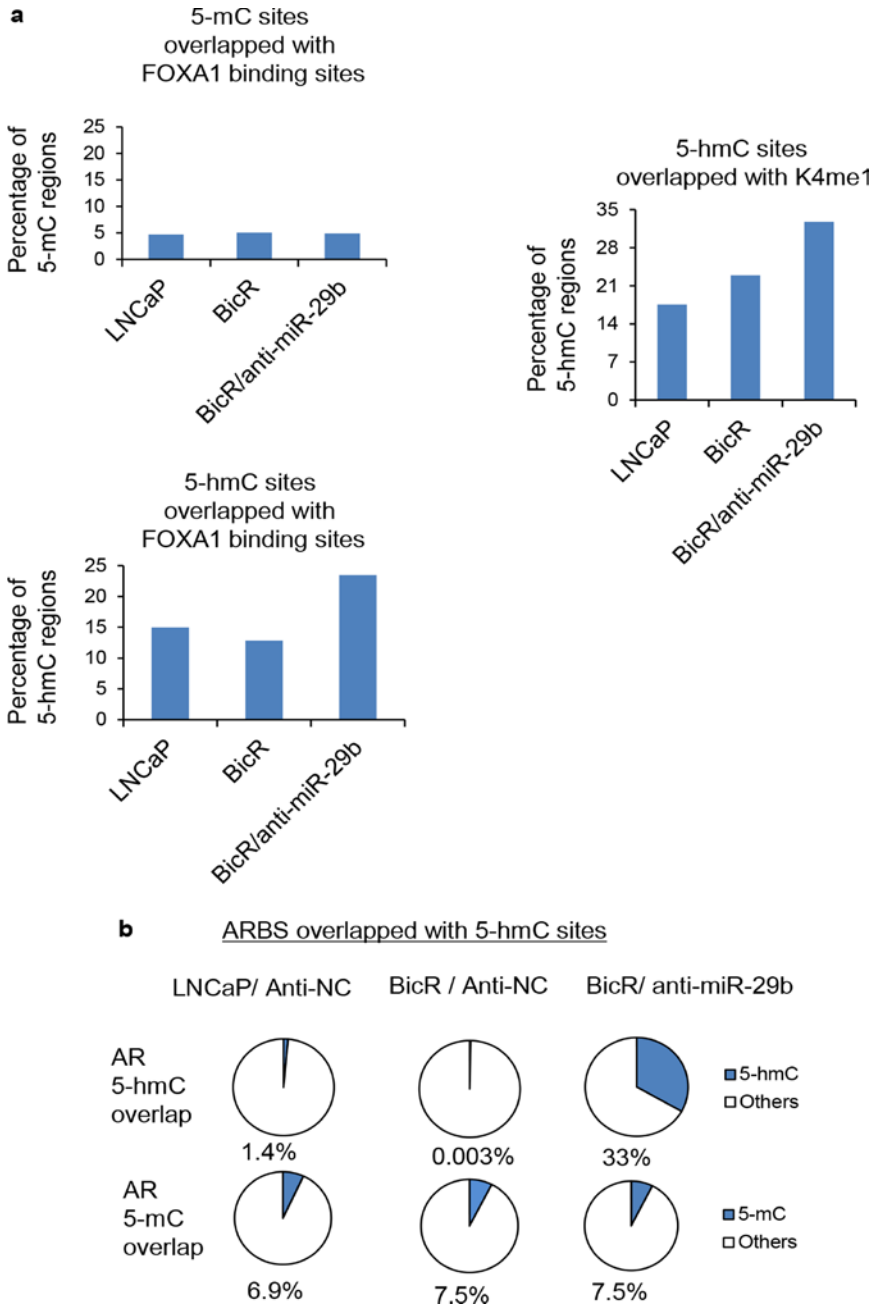

Supplementary Figure 15. Overlap of 5-hmC regions with FOXA1 and AR binding sites.

(a) 5-mC and 5-hmC regions overlapping with FOXA1 binding sites and their regulation by anti-miR-29b. (right) Overlap of 5-hmC regions with K4me1 modified regions.

(b) Overlap of ARBSs with 5-hmC and 5-mC associated sites. AR binding sites were determined by ChIP-seq. The percentage of ARBSs that significantly overlap with 5-mC and 5-hmC are shown.

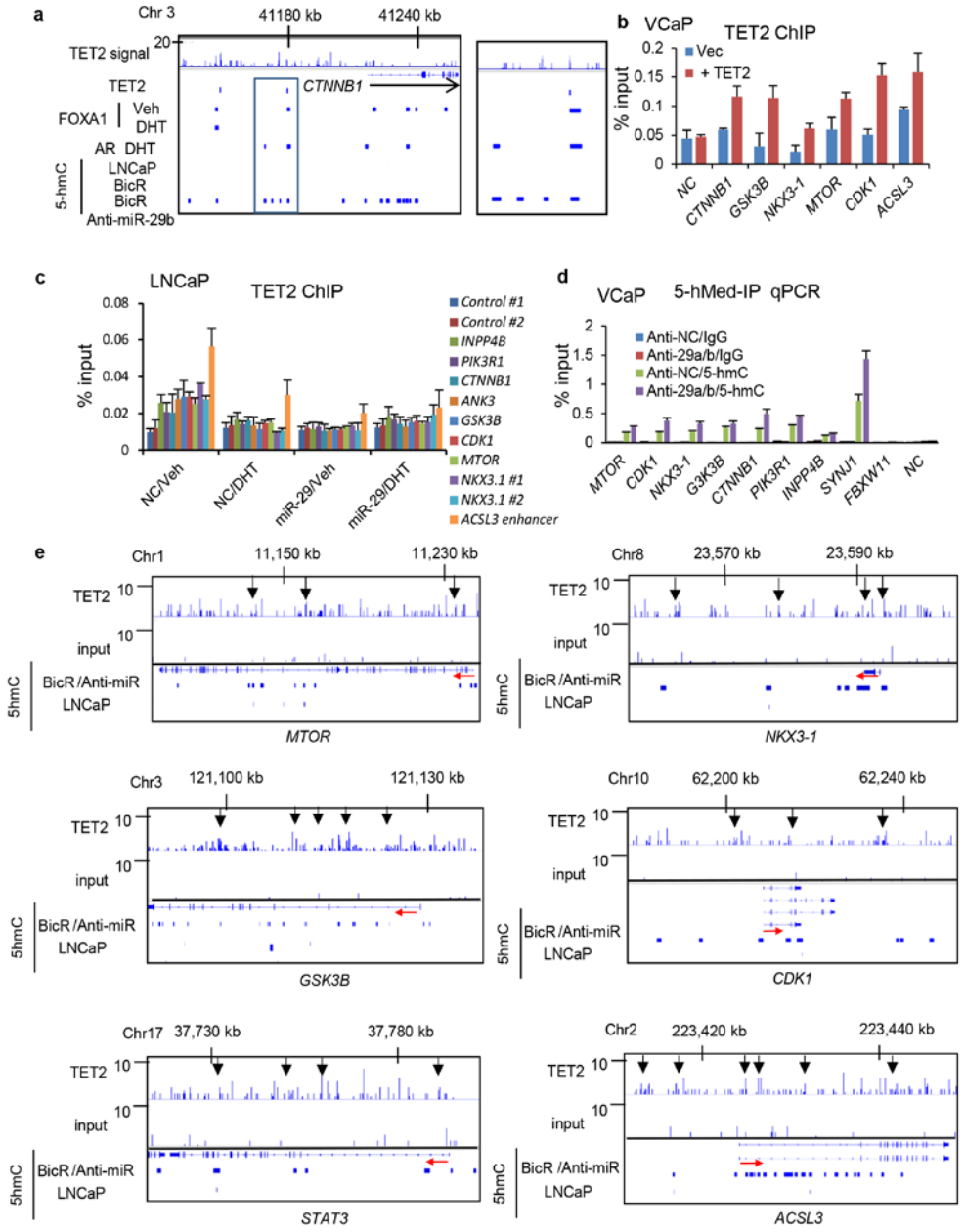

Supplementary Figure 16. Validation of 5-hmC modification and overlap of 5-hmC regions with TET2 or FOXA1 binding sites.

(a) Overlap of 5-hmC modified regions with FOXA1 binding sites in representative TET2 target genes. Mapping of significant TET2, FOXA1, AR, and 5-hmC modified regions determined by MACS. We used untreated LNCaP cells for TET2 ChIP analysis. Significant TET2 sites were determined by MACS ($P < 10^{-4}$, Poisson distribution) and 8153 binding sites were found. TET2 ChIP-seq signals were observed in the vicinity of FOXA1 binding regions. Arrows indicate the direction of

gene transcription. A representative 5-hmC regulated gene, *CTNNB1* is shown.

(b) VCaP cells were transfected with a TET2 expression vector or empty vector. After 48 h incubation, ChIP was performed using a TET2 antibody. Enrichment of the TET2 binding sites was analyzed by qPCR (n = 3). *NC*: negative control (*Myoglobin*) locus. Values represent the mean ± S.D.

(c) LNCaP cells were transfected with control miR (NC) or miR-29a/b. After 72 h incubation, cells were treated with vehicle or DHT for 24 h. ChIP analysis was performed using a TET2 antibody. Enrichment of the TET2 binding sites was analyzed by qPCR (n = 3). We selected TET2 binding sites identified by ChIP-seq in the enhancer regions of ten 5-hmC regulated genes. Control #1: *GAPDH*, Control #2: *Myoglobin* locus. Values represent the mean ± S.D.

(d) 5-hmC levels in VCaP cells were analyzed by 5-hMed-IP. Genomic DNA was extracted from VCaP cells treated with anti-NC or anti-miR-29a/b for 72 h. hMed-IP was performed using a specific antibody to 5-hydroxymethylated cytosine. Values represent the mean ± S.D.

(e) TET2 binding signals could be detected in the vicinity of 5-hmC modified regions. Representative views of TET2 ChIP-seq signal in the vicinity of several 5-hmC targeted gene loci.

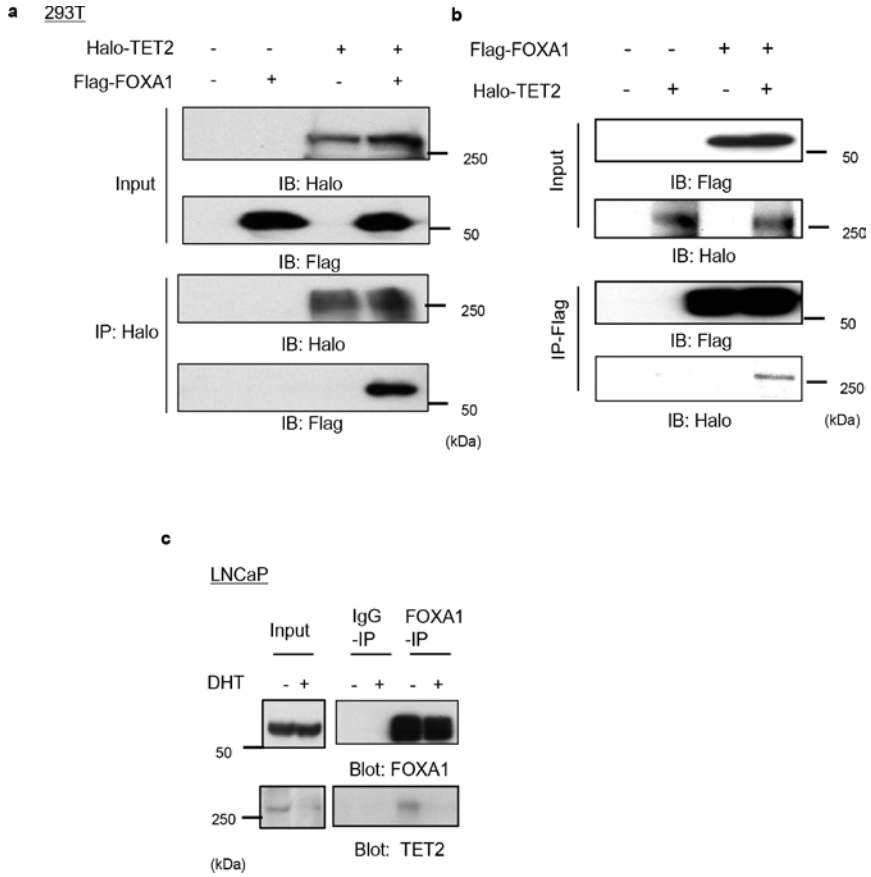

Supplementary Figure 17. Exogenous interaction of FOXA1 with TET2.

(a, b) 293T cells were transfected with Flag-FOXA1, Halo-TET2, or empty vector. After 48 h incubation, cells were harvested and lysed. The lysates were immunoprecipitated using anti-Halo (a) or anti-Flag (b) antibodies. Eluted proteins were analyzed by western blotting. (c) Immunoprecipitation by an anti-FOXA1 antibody. LNCaP cells were treated with 10 nM DHT or vehicle for 24 h. Lysates were immunoprecipitated by an anti-FOXA1 antibody.

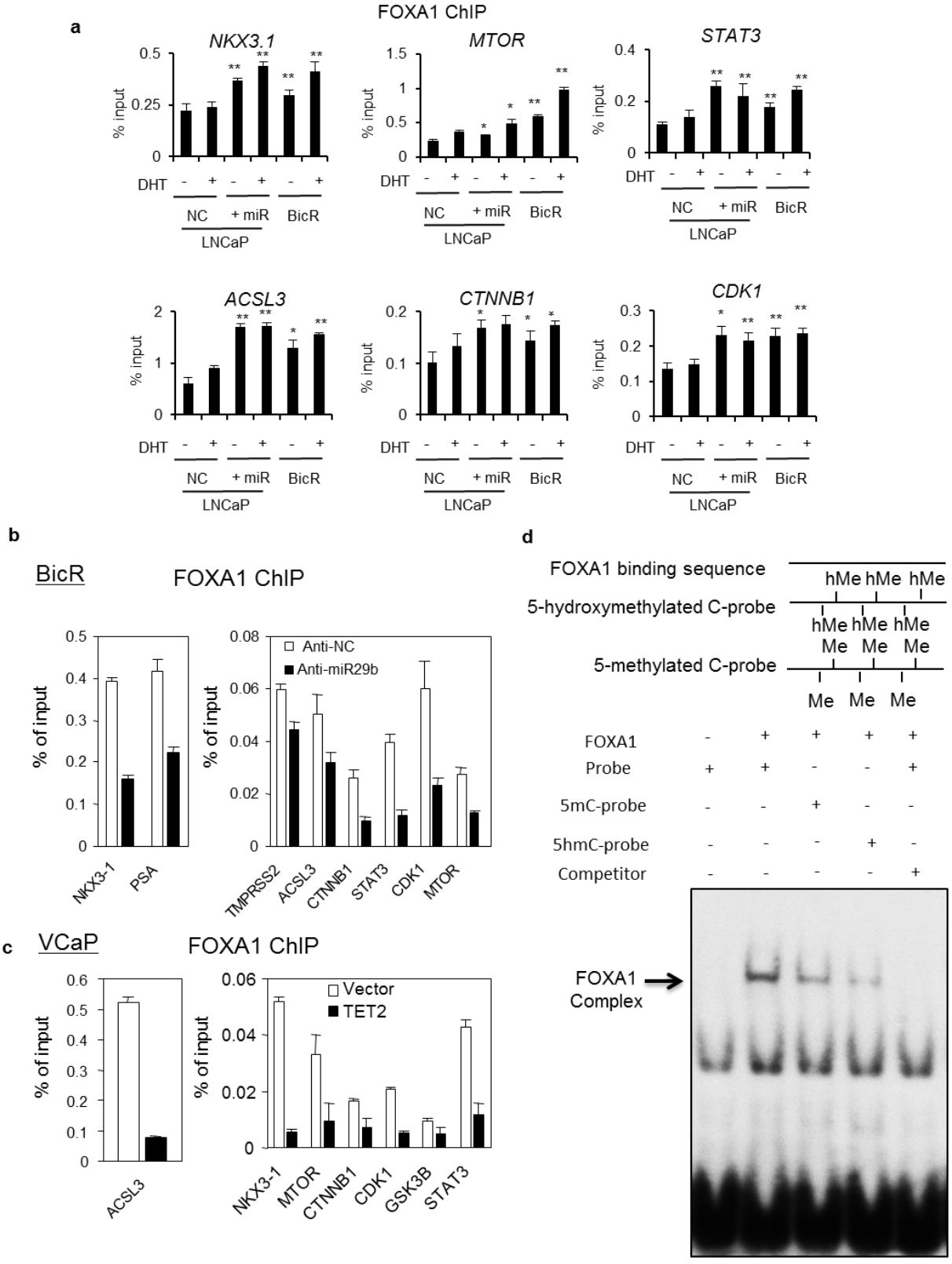

Supplementary Figure 18. Loss of 5-hmC by miR-29a/b-mediated TET2 depletion promotes FOXA1 binding.

(a) LNCaP and BicR cells were transfected with control miR (NC) or miR-29a/b. After 72 h incubation, cells were treated with 10 nM DHT or vehicle for 24 h. ChIP analysis was performed using an anti-FOXA1 antibody. Enrichment was measured by qPCR (n = 3). Values represent the mean ± S.D. *P < 0.05, **P < 0.01 (two-sided Student's t-test).

(b) BicR cells were transfected with anti-NC or anti-miR-29a/b. ChIP analysis was performed using an anti-FOXA1 antibody. Enrichment was measured by qPCR (n = 3). Values represent the mean ± S.D.

(c) VCaP cells were transfected with TET2 or control vectors. ChIP analysis was performed using an anti-FOXA1 antibody. Enrichment was measured by qPCR (n = 3). Values represent the mean ± S.D.

(d) 293T cells were transfected with HA-FOXA1 and FOXA1 protein was purified by an anti-HA antibody. FOXA1 binding sequence identified by ChIP-seq in the *MTOR* locus was used for EMSA. 5-mC and 5-hmC modified DNA oligos were also used. Non-labeled oligos were used as competitors.

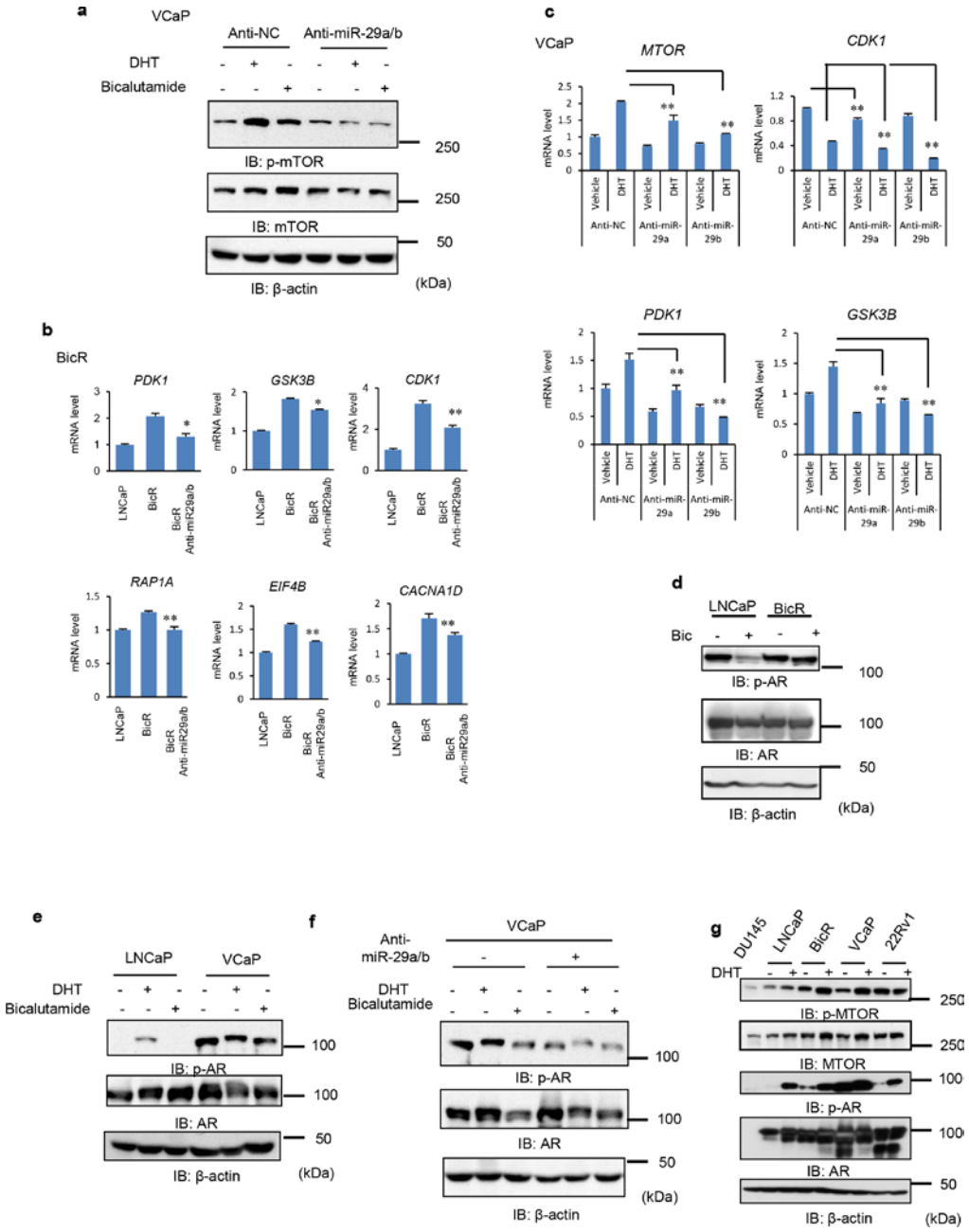

Supplementary Figure 19. Positive effects of miR-29a/b on the phosphorylation of mTOR and AR (ser81).

(a) Knockdown of miR-29a/b in VCaP cells inhibits mTOR induction. VCaP cells were treated with anti-NC and anti-miR-29a/b for 48 h, then treated with vehicle, 10 nM DHT, or 10 μM bicalutamide for 24 h. p-mTOR and mTOR protein levels were analyzed by western blot analysis.

(b) LNCaP and BicR cells were treated with anti-NC or anti-miR-29a/b for 48 h. Expression levels of some 5-hmC related genes were analyzed by real-time

RT-PCR (n = 3). Values represent the mean ± S.D. $*P < 0.05$, $**P < 0.01$ (two-sided Student's t-test).

(c) VCaP cells were treated with anti-NC and anti-miR-29a/b for 48 h, then treated with vehicle or DHT for 24 h. Expression levels of some 5-hmC related genes were analyzed by real-time RT-PCR (n = 3). Values represent the mean ± S.D. $*P < 0.05$, $**P < 0.01$ (two-sided Student's t-test).

(d) Expression levels of phosphorylated AR (ser81) in LNCaP and BicR cells with or without 10 μM bicalutamide treatment were examined by western blot analysis.

(e) Up-regulation of p-AR (ser81) in VCaP cells in the absence of 10 nM DHT or 10 μM bicalutamide treatment compared with LNCaP cells. LNCaP and VCaP cells were treated with vehicle, 10 nM DHT, or 10 μM bicalutamide for 24 h. Western blot analysis was performed to evaluate the protein levels of p-AR.

(f) VCaP cells were treated with anti-NC or anti-miR-29a/b for 48 h. Cells were treated with vehicle, 10 nM DHT, or 10 μM bicalutamide for 24 h. Western blot analysis was performed to evaluate the protein levels of p-AR.

(g) AR positive prostate cancer cell lines were treated with vehicle or 10 nM DHT for 24 h. p-mTOR, m-TOR, p-AR (ser81), and AR protein levels were analyzed by western blot analysis. p-mTOR is up-regulated in BicR, VCaP, and 22RV1 cells compared with LNCaP cells or AR-negative DU145 cells. Phosphorylation in the absence of DHT was observed in BicR, VCaP, and 22RV1 cells. The protein level induction of mTOR in BicR and VCaP cells after DHT treatment was observed.

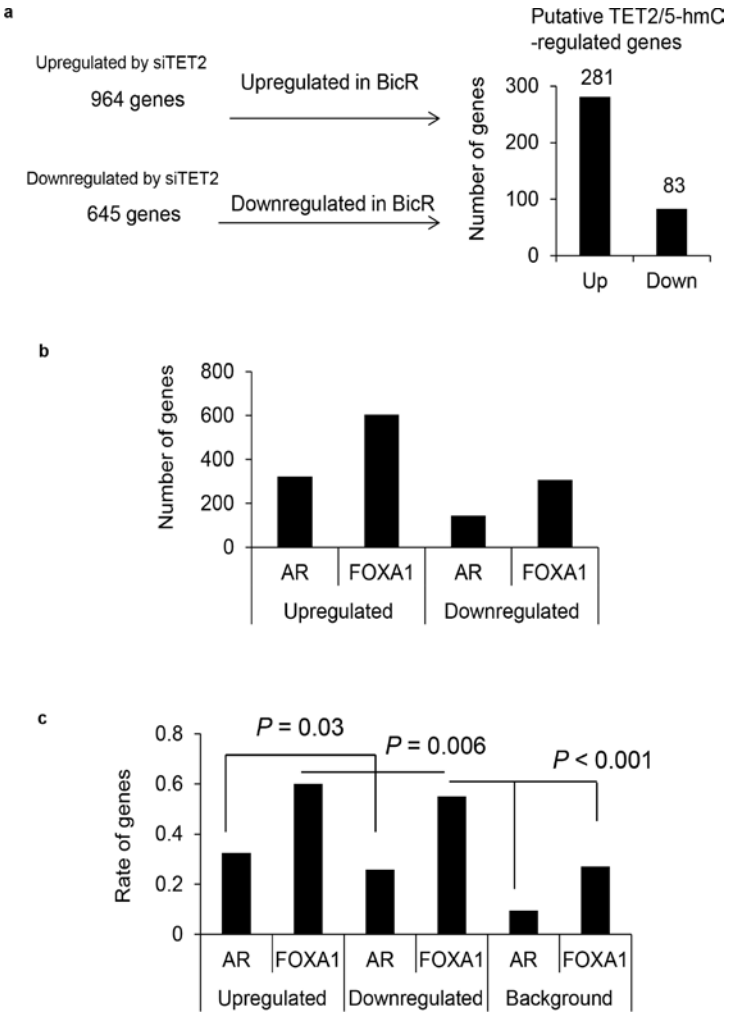

Supplementary Figure 20. Loss of 5-hmC is associated with gene induction regulated by FOXA1 and AR.

(a) TET2 repression is more associated with gene induction rather than repression. We combined microarray and RNA-seq data to determine the number of genes associated with the repression of TET2 and 5-hmC.

(b) 5-hmC binding genes were selected in LNCaP cells and changes in their expression levels in BicR cells were compared with those of LNCaP cells. The numbers of upregulated or downregulated genes in BicR cells that are in the vicinity of AR- or FOXA1-binding sites are summarized.

(c) AR and FOXA1 binding genes were enriched among 5-hmC target genes. Rate of genes with AR- or FOXA1- binding sites among upregulated and downregulated 5-hmC targeted genes. *P*-value was calculated by chi-square test.

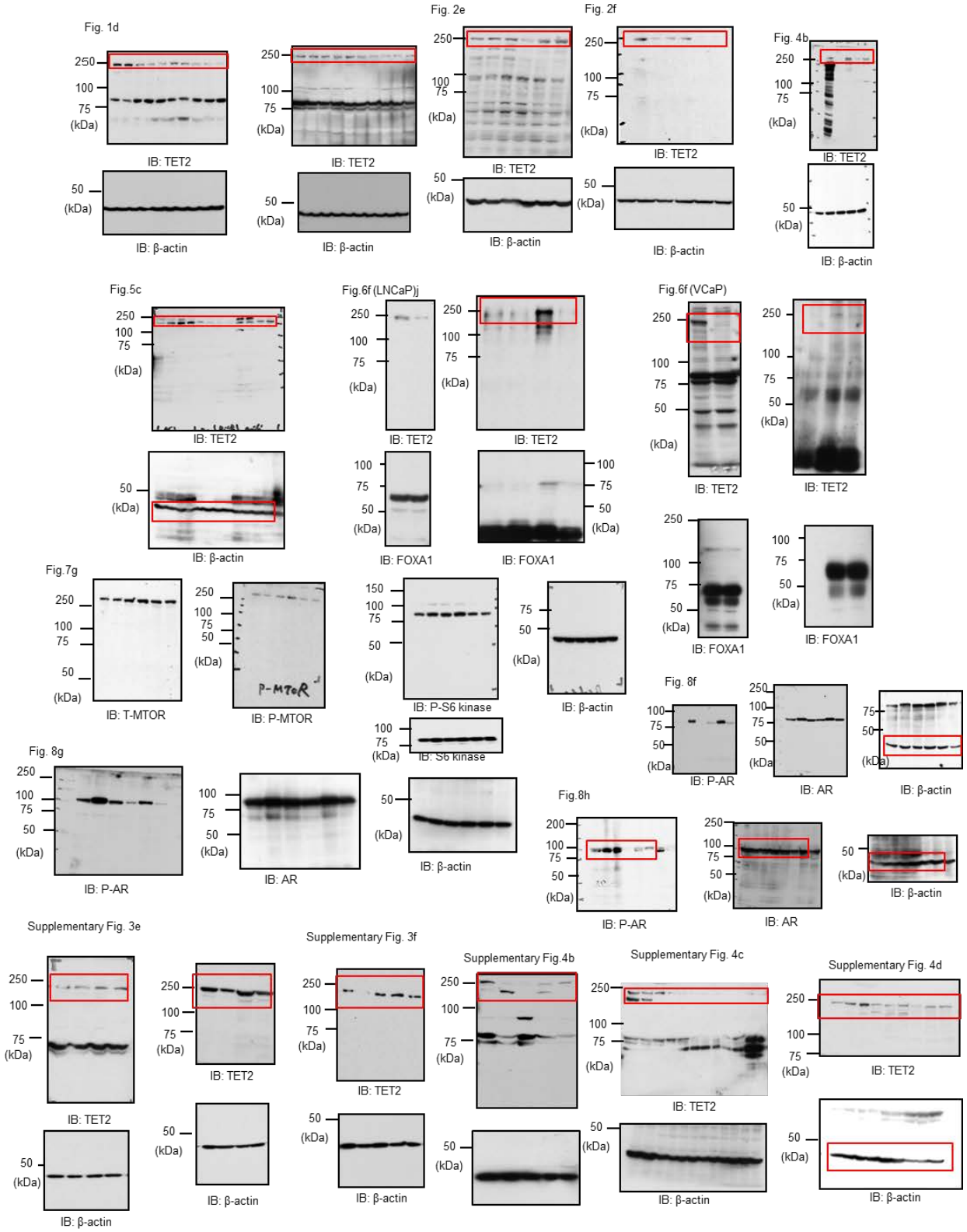

Supplementary Figure 21. Full scan images of gel electrophoresis.

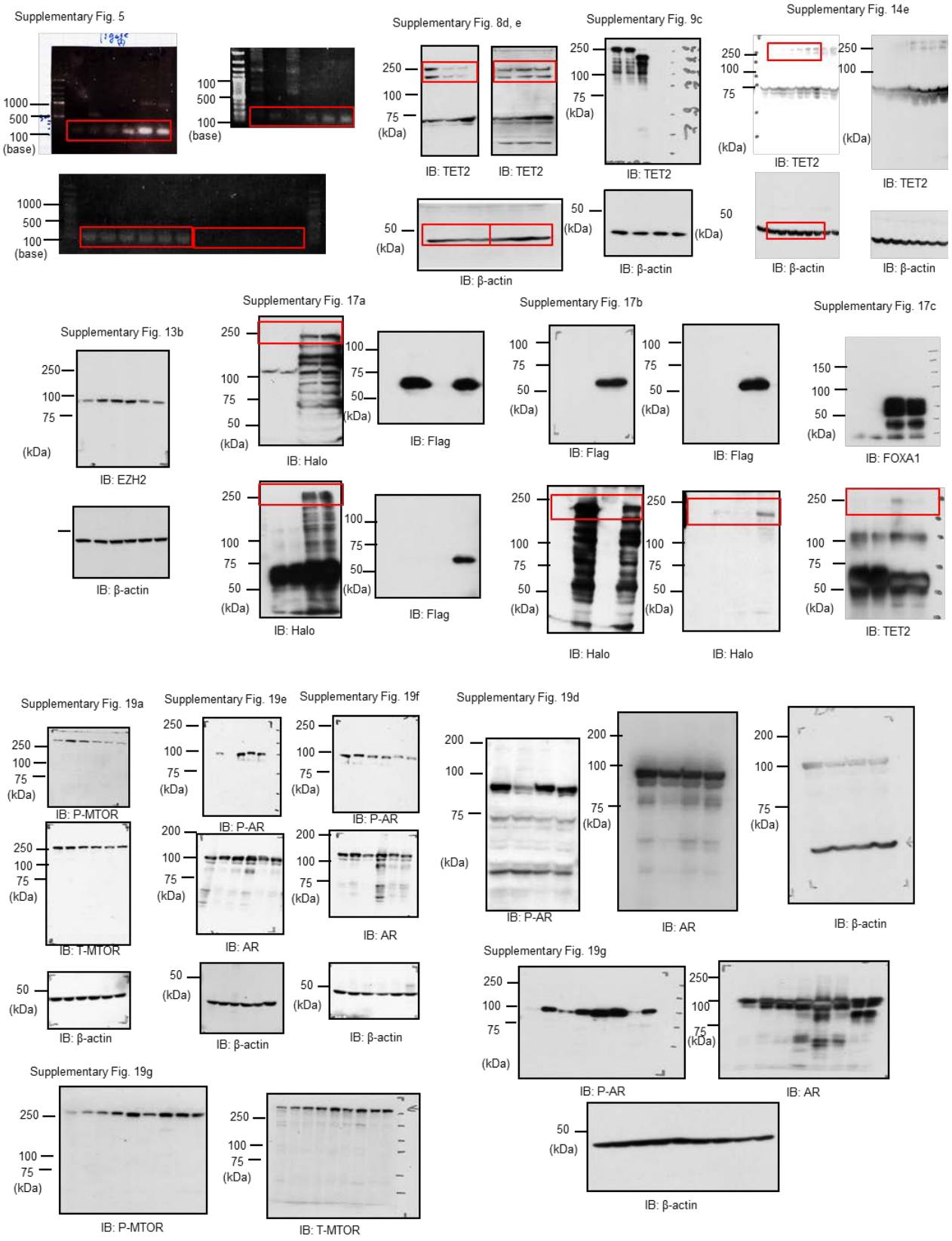

Supplementary Figure 21. Full scan images of gel electrophoresis (continued).

Supplementary Table 1. Comprehensive short RNA sequencing reveals androgen-regulated miRNA cluster and up-regulated miRNAs in hormone refractory prostate cancer cells.

	LNCaP	Fold change	BicR	Fold change
1	hsa-mir-33a 5arm	1.806158638	hsa-mir-29b 3arm	1.911094294
2	hsa-mir-29b 3arm	1.657083803	hsa-mir-375 3arm	1.895071171
3	hsa-mir-21 3arm	1.618654398	hsa-mir-29a 3arm	1.634833805
4	hsa-mir-126 3arm	1.535826547	hsa-mir-193b 3arm	1.61074087
5	hsa-mir-126 5arm	1.532115114	hsa-mir-19b 3arm	1.578422255
6	hsa-mir-99a 5arm	1.516221197	hsa-mir-23a 3arm	1.547784738
7	hsa-mir-32 5arm	1.506364799	hsa-mir-365 3arm	1.538973339
8	hsa-mir-27b 3arm	1.50099665	hsa-mir-22 3arm	1.484779491
9	hsa-let-7a 3arm	1.492255369	hsa-mir-29c 3arm	1.482937789
10	hsa-mir-125b 5arm	1.476654707	hsa-mir-331 3arm	1.450538516
11	hsa-mir-193b 3arm	1.448734642	hsa-mir-374a 5arm	1.414823074
12	hsa-mir-30b 5arm	1.441943507	hsa-mir-15b 3arm	1.399766213
13	hsa-mir-22 3arm	1.438985528	hsa-mir-30b 5arm	1.394924481
14	hsa-mir-181a 5arm	1.434137813	hsa-mir-3615 3arm	1.363928883
15	hsa-mir-152 3arm	1.430103608	hsa-mir-32 5arm	1.345707008
16	hsa-mir-27a 3arm	1.418643321	hsa-mir-125b 5arm	1.342608342
17	hsa-mir-29a 3arm	1.409594807	hsa-mir-424 5arm	1.324076404
18	hsa-mir-197 3arm	1.402151742	hsa-mir-128 3arm	1.28787325
19	hsa-mir-195 5arm	1.383039161	hsa-mir-361 3arm	1.286408713
20	hsa-mir-29c 3arm	1.346444545	hsa-mir-186 5arm	1.277755436
21	hsa-mir-26a 5arm	1.341944432	hsa-mir-99a 5arm	1.276228938
22	hsa-mir-28 5arm	1.336219972	hsa-mir-181a 5arm	1.274752965
23	hsa-mir-30c 5arm	1.327806013	hsa-mir-200b 5arm	1.240796719
24	hsa-mir-148a 5arm	1.308740247	block288666 3arm	1.239009411
25	hsa-let-7b 3arm	1.306123333	hsa-mir-96 5arm	1.235628735
26	hsa-mir-99a 3arm	1.299172159	hsa-mir-125a 5arm	1.232946052
27	hsa-mir-24 3arm	1.286036015	hsa-mir-30c 5arm	1.226431431
28	hsa-mir-1307 5arm	1.279055735	hsa-mir-126 5arm	1.219145513

29	hsa-mir-561 5arm	1.277986675	hsa-mir-99a 3arm	1.214704917
30	hsa-mir-125a 5arm	1.273602853	hsa-mir-28 3arm	1.20854682
31	hsa-mir-16 5arm	1.269974576		
32	hsa-mir-30e 5arm	1.25479111		
33	hsa-mir-374a 5arm	1.254707614		
34	hsa-mir-96 5arm	1.253113621		
35	hsa-mir-192 5arm	1.245187218		
36	hsa-mir-17 3arm	1.235012835		
37	block288666 3arm	1.234283717		
38	hsa-mir-99b 5arm	1.231100405		
39	hsa-let-7c 3arm	1.230835196		
40	hsa-mir-340 5arm	1.217390145		
41	hsa-mir-148b 3arm	1.210909987		
42	hsa-mir-148a 3arm	1.210899271		
43	hsa-mir-101 3arm	1.210432238		
44	hsa-mir-532 5arm	1.200674078		

Short RNA sequencing in LNCaP and BicR cells. Both cells were treated with 10 nM DHT and then total RNA was extracted. After short RNA sequencing by a Illumina Genome Analyzer, the total number of readings were normalized with mapped reads in each sample. We also extracted RNA from cells at 0 h for comparison. For LNCaP cells, up-regulated (Fold >1.2) miRNAs included miR-125b, 21, 148a, 30 family, 27a, and 99a, which were previously reported as androgen-regulated miRNAs[7-9]. For BicR cells, enhanced androgen-responsiveness was observed in five miRNAs (underlined).

Supplementary Table 2. Association of TET2 expression with clinicopathological parameters in prostate cancer tissues.

Value		TET2		*P* value
		+ (*n* = 52)	- (*n* = 50)	
Age* (years)		65.9 ± 0.9	67.5 ± 0.8	0.20
PSA* (ng ml^{-1})		18.3 ± 3.2	15.4 ± 2.0	0.45
Stage (Jewett Staging Sysyem)				
	B	18	15	
	C	32	24	
	D1	2	11	**0.016**
pT				
	pT1-2	19	14	
	pT3-4	33	36	036
pN				
	pN0	50	39	
	N1	2	11	**0.0042**
Gleason score (GS3)				
	2-6	18	19	
	7-8	24	23	
	9-10	10	8	0.8907
AR				
	+	40	47	
	-	12	3	**0.015**
5-mC				
	+	38	31	
	-	14	19	023
5-hmC				
	+	37	22	
	-	15	28	**0.0052**
5-mC/5-hmC status				
	+/+	30	17	
	+/-	8	14	
	-/+	7	5	
	-/-	7	14	**0.0465**

*; Data are presented as mean ± 95% confidence interval (CI). All other values represent the number of cases.

Supplementary Table 3. Univariate and multivariate analysis of prognostic factors in prostate cancer.

	Univariate	Multivariate	
Variable	*P* value	*P* value	Relative risk (95% CI)
Gleason score (8-10 / 2-7)	**0.0034**†	**0.0076**	6.190 (1.623-23.613)
pN (pN1 / pN0)	**0.0245**†	0.4040	
TET2 (-/+)	**0.0338**†	**0.0085**	9.405 (1.770-49.975)
5-hmC (-/+)	0.0605†	**0.0249**	4.913 (1.222-19.754)
5-mC (+/-)	0.0792†	**0.0182**	13.678 (1.560-119.932)
pT (pT3-4 / pT2)	0.1106		
AR status (+/-)	0.9107		

†: Significant ($P < 0.05$) and borderline-significant ($0.05 \leq P < 0.10$) values were examined by multivariate analyses.

Univariate and multivariate analyses were evaluated using Cox's proportional hazard model with PROC PHREG in SAS software (V9.2; Cary, NC).

Supplementary Table 4. Association of miR-29a expression with clinicopathological parameters in prostate cancer tissues.

Value		miR-29a status		*P* value
		+ (*n* = 42)	- (*n* = 59)	
Age* (years)		67.4±1.0	66.1±0.8	0.30
PSA* (ng ml^{-1})		20.8±4.1	13.8±1.6	0.073
Stage (Jewett Staging Sysyem)				
	B	8	24	
	C	26	31	
	D1	8	4	**0.029**
pT				
	pT1-2	9	23	
	pT3-4	33	36	0.058
pN				
	pN0	34	55	
	N1	8	4	0.060
Gleason score (GS)				
	2-6	9	28	
	7	11	19	
	8-10	22	12	**0.0021**
5-mC				
	+	29	38	
	-	13	21	0.63
miR-29b (ISH)				
	+	29	10	
	-	13	49	**<0.0001**

Supplementary Table 5. Association of miR-29b expression with clinicopathological parameters in prostate cancer tissues.

Value		miR-29b status		*P* value
		+ (*n* = 39)	- (*n* = 62)	
Age* (years)		67.0±1.2	66.5±0.7	0.67
PSA* (ng ml^{-1})		21.5±4.1	13.7±1.8	**0.049**
Stage (Jewett Staging Sysyem)				
	B	11	21	
	C	19	38	
	D1	9	3	**0.022**
pT				
	pT1-2	10	22	
	pT3-4	29	40	0.30
pN				
	pN0	30	59	
	N1	9	3	**0.0058**
Gleason score (GS)				
	2-6	9	28	
	7	9	21	
	8-10	21	13	**0.0027**
5-mC				
	+	29	38	
	-	10	24	0.18

Supplementary Table 6. A list of primer sequences used in this study.

LUC-TET2/Mlu Xho

ACACGCGTCATCTGAGATATATGCTAGGTTCAG

TGCTCGAGGTATAGCTAAGGTACAGAAGTGAGTC

RT-PCR

Pri-miR-29ab1

F: ATGGTGCTCTTCCCCAATCA

R: TCCCAACCCTCACGACCTT

Pri-miR-29b2

F: CTTGGCTGTGCTGCAATTCT

R: CTTCATTGAGATCCTCTTCTTCTGG

TET2

CAAGGCTGAGGGACGAGAAC

ATCCACAAGGCTGCCCTCTA

NKX3-1

F: CCAGAGCCAGAGCCAGAG

R: CGCCTGAAGTGTTTTCAGAG

MTOR

F: CACAATGCAGCCAACAAGAT

R: AAACATGCCTTTCACGTTCC

CDK1

F: GGTCAAGTGGTAGCCATGAAA

R: CCAGGAGGGATAGAATCCAA

CACNA1D

F: TGTGGGCTTTGTCATCGTTA

R: GAAAGGCGAAGAGTTCACCA

RAP1A

F: GCCAACAGTGTATGCTCGAA

R: CCCTCAGGTCCTGTAAGTCG

PIK3R1

F: AAAGGTGTTCGGCAAAAGAA

R: CGCAACAGGTTTTCAGCTTT

GSK3B

F: ATTACGGGACCCAAATGTCA

R: TGCAGAAGCAGCATTATTGG

Rictor

F: CTAGCAGCACCAAAAGCACA

R: AGCAAATGGGAAACCTCAGA

Raptor

F: GTGAGTGTGAGCGTCAATGG

R: TGTAGATGGCGGTGAACTGA

PDK1

F: GCTCTTTTTCCACGGTTGTC

R: AACAAAGAAGGGGTGATCCA

EIF4B

F: ACTGGTGGAGGAAGCACCTA

R: GTGGAGCAGTGGGAAGGAT

HBP1

F: CCTCCACCAGTGTCCTCTTC

R: ATTGCACCATCCCAAATCAT

AURKA

F: GTCACAAGCCGGTTCAGAAT

R: TTTGATGCCAGTTCCTCCTC

APP

F: TCCTGACAAGTGCAAATTCTTACAC

R: TCTTCTCACTGCATGTCTCTTTGG

FKBP5

F: CTGCAGAGATGTGGCATTCACT

R: TCCAGAGCTTTGTCAATTCCAA

ACSL3

F: TGTAACATTTGCCACCCTCAGA

R: GCGAGAATCTTCCTCGATCAA

GAPDH

F: GGTGGTCTCCTCTGACTTCAACA

R: GTGGTCGTTGAGGGCAATG

Myoglobin

F: AAGTTTGACAAGTTCAAGCACCTG

R: TGGCACCATGCTTCTTTTAAGTC

ChIP or hMed-IP

NKX3-1 #1/5-hmC and TET2

F: TGTGACTGGACTGGACGGTA

R: AATCGAGGCTGCAGTGAGTT

NKX3-1 #2/FOXA1 site

F: GGAGCAGCAGAGATGGGTAG

R: CAAACCAAGGAGGGAACAAA

MTOR/5-hmC, TET2, FOXA1 binding

F: ATGGAGCCATCTCCTTACCC

R: TCTTCTTCCAGCAAGTGCAA

CDK1/5-hmC

F: TGGAGCCTAGGAGTTGGAGA

R: TCTGTCTTCATTGCCATCCA

YWHAQ/5-hmC

F: TGCTGGTATTACAGGCGTGA

R: CCGGAACCAGAAAGTCATGT

INPP4B/5-hmC

F: CCCAGTTGAGAGCTTTCCTG

R: CTGTCATACCGTGGCTGCT

PIK3R1/5-hmC

F: TAGAGATGGCCCAAGGTCAC

R: GAAGTCAGCAGCATCAAGCA

FBXW11/5-hmC

F: TTGCTAATGCCAATGAGCTG

R: TTTTGCCTTGATTGGGTCTT

KEAP1/5-hmC

F: TGATTGGTCATGGGGTTGTA

R: CTACTTCCGACAGTCGCTCA

SYNJ1/5-hmC

F: TGGAGCTCTTTGTGCAACTG

R: TGAACAAAAGGCAGCACAAG

CTNNB1/5-hmC

F: ATTCCATCCCCTCTTGCTCT

R: CAGGGGTTCAAAAGAAAACG

GATA2/5-hmC

F: GAAGAGGGACGAGAGGGTCT

R: CAGGTTGAGCTGGGTGACTC

STAT3/5-hmC and TET2

F: TCTCGAACTCCTGACCTCGT

R: AAATCCTTGGCATCCCATCT

ANK3/5-hmC

F: GGAGCTACCATTCACATCCAA

R: GATGGCTATCGGTATGATCCA

SPATA13/5-hmC

F: TTTGCATGTTGAGGTGCATT

R: TTGGGTTTGATGGTGGTTTT

TET2/ARBS

F: GGTGGATGTGAGCAGTGAGA

R: TGGCAATGGAAAGTTGTTTG

miR-29ab1/ARBS

F: CTTAGCCGTTCAAATAGCTCCA

R: GCGTAAGACTGCTTTAGGAGGA

INPP4B/TET2

F: TGGACAATGGATTCTTGCTG

R: ATTTCCATGGCTGCATTTTC

PIK3R1/TET2

F: GCATGGTTCCCTTCTTCAAA

R: AACCCGTTGTTGGTACATGC

CTNNB1/TET2

F: CTGGAATAAAACGGCAGCAT

R: GCAAATGAAGGGAGATGGAG

ANK3/TET2

F: GTTTAAAGCCATGGGCACAG

R: TTGGAAATTGACCAACAATCA

GSK3B/TET2 and 5-hmC

F: GGAGGCACATTCTCAGGCTA

R: ACATACCCTGGGGCGAATTA

CDK1/TET2 and FOXA1

F: ATTGAGGCTGGGTTCAAGTG

R: GGGGAAGAACAGGGATAAGG

ACSL3/ARBS

F:TCCTGCTGTACTCATTGTTACTAGAATAAA

R: GCTTTTCATTTGTCAGAGTGCTAAGTAT

Supplementary Table 7. Overexpression and knockdown of miR-29a and miR-29b in prostate cancer cell lines.

(a) Overexpression of miRNA by pre-miRNA (Expression level relative to control)

	miR-29a		miR-29b	
	Ave.	S.D.	Ave.	S.D.
LNCaP	7.975892186	0.576349554	14.7511985	1.281622978
DU145	4.362108255	0.193143861	2.799192049	1.110942325

(b) Inhibition of miRNA by anti-miRNA (Expression level relative to control)

	miR-29a		miR-29b	
	Ave.	S.D.	Ave.	S.D.
BicR	0.205611349	0.027145695	0.10873707	0.054870064
LTAD	0.386353468	0.072525607	0.148726815	0.03821419
VCaP	0.137429256	0.069244538	0.235777242	0.073630444
DU145	0.319535728	0.128028447	0.315493213	0.045398745

For overexpression analysis in cell growth assay, we treated cells with 5 nM miRNAs (control miR (NC), miR-29a, or miR-29b pre-miR). As a modification of the manufacturer`s protocol, reduced concentration is important to avoid off-target effect. For knockdown analysis, we treated cells with 10 nM anti-miRNAs (anti-negative control (anti-NC), 29a, or 29b) according to the manufacturer's instructions. After 48 h incubation, miRNA expression levels were measured by qPCR (n = 3). We performed overexpression in DU145 and LNCaP cells, and knockdown in DU145, BicR, VCaP and LTAD cells.

Supplementary references

1. Varambally S, Yu J, Laxman B, Rhodes DR et al. Integrative genomic and proteomic analysis of prostate cancer reveals signatures of metastatic progression. Cancer Cell 8(5), 393-406 (2005).

2. Yu YP, Landsittel D, Jing L, Nelson J et al. Gene expression alterations in prostate cancer predicting tumor aggression and preceding development of malignancy. J Clin Oncol 22(14), 2790-2799 (2004).

3. Grasso CS, Wu YM, Robinson DR, Cao X et al. The mutational landscape of lethal castration-resistant prostate cancer. Nature. 487(7406), 239-243 (2012).

4. Taylor BS, Schultz N, Hieronymus H, Gopalan A et al. Integrative genomic profiling of human prostate cancer. Cancer Cell. 18(1),11-22 (2010)..

5. Casanova-Salas I, Rubio-Briones J, Calatrava A, Mancarella C et al. Identification of miR-187 and miR-182 as biomarkers of early diagnosis and prognosis in patients with prostate cancer treated with radical prostatectomy. J Urol 192(1):252-259 (2014).

6. Wach S, Nolte E, Szczyrba J, Stöhr R et al. MicroRNA profiles of prostate carcinoma detected by multiplatform microRNA screening. Int J Cancer 130(3), 611-621 (2012).

7. Shi XB, et al. An androgen-regulated miRNA suppresses Bak1 expression and induces androgen-independent growth of prostate cancer cells. Proc Natl Acad Sci U S A. 104(50):19983-19988 (2007).
8. Ribas J, et al. miR-21: an androgen receptor-regulated microRNA that promotes hormone-dependent and hormone-independent prostate cancer growth. Cancer Res. 69(18), 7165-9 (2009).
9. Murata T, et al. miR-148a is an androgen-responsive microRNA that promotes LNCaP prostate cell growth by repressing its target CAND1 expression. Prostate Cancer Prostatic Dis. 13(4), 356-361 (2010).